NBS-GCR-85-493

Experimental Study of Environment and Heat Transfer in A Room Fire. Mixing in Doorway Flows and Entrainment in Fire Plumes

---

E.E. Zukoski, T. Kubota,
and C.S. Lim

May 1985

Sponsored by
U.S. DEPARTMENT OF COMMERCE
National Bureau of Standards
Center for Fire Research
Washington, DC 20234

NBS-GCR-85-493

Experimental Study of Environment and Heat Transfer in A Room Fire. Mixing in Doorway Flows and Entrainment in Fire Plumes

---

E.E. Zukoski, T. Kubota,
and C.S. Lim

California Institute of Technology
Div. Of Engineering & Applied Science
Pasadena, CA 91125

May 1985

NBS Grant Number NB82NADA3033

Sponsored by
U.S. DEPARTMENT OF COMMERCE
National Bureau of Standards
Center for Fire Research
Washington, DC 20234

Notice

This report was prepared for the Center for Fire Research of the National Engineering Laboratory, National Bureau of Standards under Grant Number NB82NADA3033. The statements and conclusions contained in this report are those of the authors and do not necessarily reflect the views of the National Bureau of Standards or the Center for Fire Research.

TABLE OF CONTENTS

I. INTRODUCTION

This final report is written in three sections. The first two draw attention to work reported in detail in the Third Quarterly Progress Report and the third Section describes ongoing work which has not been previously discussed in a Progress Report.

II. DOORWAY MIXING

During the past year we have completed work concerned with mixing, between the two layers within a room, which is caused by the currents flowing into and out of a doorway. The currents in our experiments modeled those that would be produced by a fire of constant heat release rate located within the room. The mixing process was more complex than we had expected and the work discussed in our Progress Report for the Third Quarter may be more closely restricted to the geometry of the room used in the experiments than we would like. However, we believe that the correlation presented in the Third Quarterly Report will give a useful estimate for this mixing process.

This investigation is completed and no further experimental work along these lines is planned for the coming year. We will continue to examine the data and will develop a computer model for use in Room-Fire Codes.

III. FIRE IN CEILING LAYER

The Progress Report for the Third Quarter also included a description of our work, accomplished in the 1983-84 contract period, on the heat release in the ceiling layer when a flame extends far into that layer. The results presented there are not as accurate as we want because our tools for chemical analysis were not accurate enough or complete enough to give us an accurate picture of the chemical composition within the upper layer under the conditions of interest. These problems arose when the fuel air ratio of the gases entering the ceiling layer was above the stoichiometric value. The most serious problems resulted because we did not have the capability of making measurements of hydrogen gas and water vapor concentrations.

In the current year we will continue this work and will have a new instrument, a gas chromatograph, which will allow us to make measurements of all of the principal species. (The major cost of this instrument was supplied by Caltech.) We anticipate that this instrument will allow us to make the accurate determinations of composition required to develop a model for this heat release process. Work in this area will be continued in the current contract year.

IV. GRAVITY CURRENTS - INITIAL FLOW IN A CEILING LAYER

A. INTRODUCTION

We are interested in modeling the initial motion of smoke and hot gas in a hallway or large room when hot gas is introduced into the space either through an opening such as a door or from a fire located within the space.

To have a concrete example in mind consider the development of the ceiling layers produced by a fire in the two-dimensional structure shown in the sketches of Figure 1. The building consists of a small room with an open door which leads to a long hall. The only opening to the outside world is a vent located on the wall of the hall and near the floor.

A fire starts in the small room and smoke rises to form a layer of hot gas near the ceiling, see Figure 1a. Several minutes later, see (1b), when the fire has reached a large size, the hot gas in the room begins to spill out under the door soffit into the adjoining hallway. The rate of flow of the hot gas which enters the hall increases rapidly and quickly rises to a roughly constant value.

The outflowing gas forms a buoyant plume, see (1b), which impinges on the ceiling of the hall and produces a thin wall jet or gravity current which flows at high speed along the ceiling.

The flow in this wall-jet is supercritical, i.e., its velocity is larger than the speed of a gravity wave on the interface between the hot gas and the cooler ambient fluid. The interaction of the head of this current with the ambient fluid produces a hydraulic jump in the supercritical layer, shown in (1c), which entrains a substantial flow of ambient fluid.

The velocity of the gas in the gravity current which forms downstream of the jump is slower than that in the supercritical layer and it contains a larger mass flow rate due to the entrainment process. The current has a definite head and some mixing occurs just behind the head which results in the formation of a mixed region between the current and the ambient flow.

The current formed by this process flows across the ceiling of the hall, see (1c and 1d), with a constant velocity and depth. The mass flow rate and depth of fluid at a point just downstream of the jump are fixed by the properties of the jump, the conditions in the flow upstream of the jump, and the properties of the gravity current formed by the jump.

A short time later, the front of this current impinges on the far wall of the hall, (1e), and reflects as a group of waves on the interface which propagate back toward the jump, (1f). Mixing occurs during the impingement process but the reflected waves do not break and hence do not cause any further entrainment of ambient fluid into the current. When the waves reach the hydraulic jump located near the left hand side of the hall, the jump is submerged in the hot gas, (1g), and no further entrainment of ambient fluid occurs there.

After several reflections, the wave train dies out and a uniform ceiling layer is produced in the hall. The layer slowly grows deeper as the hot gas continues to be supplied to the hall from the fire room.

Heat transfer from the hot gas to the wall occurs throughout this flow by a convective heat transfer process. The magnitude of the heat transfer rate will affect the motion of the current, since the buoyancy of the flow will be reduced.

During the process described above, the pressure within the two rooms will rise due to the the addition of heat and the production of hot gas by the fire. This pressure rise will cause a flow of ambient fluid out of the vent and will set up a velocity field in the ambient fluid remaining in the two rooms. Other motion in the ambient fluid is caused by the passage of the gravity current down the hall. Although the velocities in the ambient fluid are usually small, under some circumstances they may have important effects on the motion of the current due to the development of a boundary layer on the ceiling in front of the head of the current.

The flow described above contains many of the novel features which we wish to examine in this research program. Those which do not fit neatly into the two-layer fire models are the three-dimensional and unsteady geometry of the current, the entrainment in the hydraulic jump, and the mass loss into the mixing region at the head of the current. Heat transfer associated with the motion of the current will affect each of these processes. However, once the initial hydraulic jump is submerged, the layer of hot gas within the hall has approximately a uniform depth and density, and can be treated by the simple two-layer model.

Entrainment at the hydraulic jump can be important. The total mass entrained into the current depends on the entrainment rate at the hydraulic jump and on the period during which it will act. The period is fixed by the geometry of the room, and the velocity of the front of the current and of the reflected waves which eventually submerge the jump. These features must be included in any accurate model of the flow.

Finally, there are situations in which the motion of the layer could be important. For example, if the gravity current is deep enough to submerge an automatic sprinkler head, the motion of the front will determine when the sprinkler can be set off. Or, if the vent on the right hand wall of Figure 1 had been located at ceiling level, the motion of the front will determine the time at which smoke would first leave the hall.

To summarize, the use of the simple two layer model to describe this flow is inappropriate because the layer thickness is not uniform in the hall, because considerable mass may be exchanged between the hot and cooler fluid due to entrainment at the jump and at the head of the gravity current, and because heat transfer from the layer to the wall depends on and influences the motion of the front. In rooms with a height to length ratio of 1 or 2, these effects are usually small enough and are completed in so short a time that they can be ignored. However, in a space such as a long hallway or large room, for which the length to height ratios can be 20 to 50, the time required for the development of the ceiling layer may be long compared with other processes of interest and the effects of heat transfer, and entrainment may not be minor.

The features of the flow which must be included in a fire-model are:

(1) the rate of spread of the gravity current in a variety of geometric configurations and for a range of Reynolds numbers, and the

corresponding motion of reflected waves which eventually submerge the jump,

(2) the geometry of the current while it is spreading throughout the space,

(3) the exchange (in both directions) of material between the current and the cooler ambient fluid which may occur at the head of the current, at any hydraulic jumps which occur in the flow, and at the impact of the head on a side wall, and

(4) the heat transfer from the current to the ceiling during the whole history of the fire and the influence of this heat transfer on the other three processes.

The aim of the present research work is to obtain a good physical understanding of these features of the flow and to develop an analytic model for application in multi-room fire codes.

A considerable body of information concerning items 1 and 2 is available for adiabatic conditions and for flows in simple two-dimensional and axisymmetric geometries. This information will be reviewed in Section IV B. In this review, we will restrict our attention to the motion of the front of a gravity current such as that illustrated in Figures 1c and 1d, and also in Figure 2, and will discuss the initial hydraulic jump, shown in Figures 1c to 1f, and other features of the flow in a later report.

Little data are available for more complex geometric conditions of interest to us and less, concerning the effects of mixing and heat transfer. An experimental program has been started to investigate these problem areas and it will be described in Sections IV C and D. This program has two parts: in the first, salt-water/water modeling techniques are being used to study the effects of geometry and Reynolds number on the flow. This part of the experimental program and preliminary experimental results are presented in Section IV C.

An important part of our experimental work will be to obtain data for non-adiabatic flows in which heat and mass transfer from the gravity flow may substantially affect the flow. Experiments, which make use of hot air currents, have been started to investigate these processes and they are described here in Section IV D.

B. REVIEW OF INFORMATION CONCERNING GRAVITY CURRENTS

A body of experimental and theoretical work is available concerning gravity currents moving over horizontal surfaces because of interest in flows such as those present in estuaries, where salt water from the ocean flows upstream under fresh water outflowing from a river, in cooling water outfall flows from power plants, where hot water discharged from a power plant flows out over cooler river or ocean water, and in the atmosphere, where cold fronts may intrude beneath warmer air.

This work is reviewed by J. E. Simpson (1982) and two of the key papers mentioned in this review are Benjamin (1968) and Simpson and Britter (1979). A third paper by Wilkinson (1982) contains an important addition to our understanding of these flows. Other important papers are included in the reference list.

Much of the information in these papers may not be directly applicable to our problems because, the effects of heat transfer between the intruding gravity current and the wall have usually been ignored, and because the boundary conditions on the flow of the ambient fluid may be different in our case than in those studied previously. The most commonly investigated flow is one in which the fluid which forms the gravity current is injected from the same end of the corridor as that from which ambient fluid, displaced by the current, is withdrawn. Other boundary conditions for the withdrawal of the ambient fluid can be easily modeled in an inviscid flow by making a Galilean transformation.

However, in a real fluid, viscous effects will change the velocity profile near the wall and have been observed to have a large effect on the geometry and velocity of the current. Clearly, the simple Galilean transformation will not allow us to account for these effects.

Finally, the work by Simpson and Britter involved measurements made on the head of a gravity current in which head of the current is held fixed and for which the distance from the source to the head was very small. These data do not give a complete picture of the motion of the front when the front has moved out a large distance from the source because the effects of viscosity on the current are not present in their experimental work.

Thus, there may be substantial quantitative differences between modeling results and the motion of full scale gravity currents produced by fires but large qualitative differences are not expected.

1. Classification of Inviscid Flows

Many types of flow can be produced when hot gas is introduced into a room or hallway and several of these are illustrated in Figure 1. In this report we will concentrate on the flow in the gravity current illustrated in Figures 1c,and 1d, and in more detail in Figure 2.

The exact nature of the flow will depend strongly on parameters of the flow as well as the boundary conditions. For example, mixing and entrainment between the injected flow and the ambient fluid will be controlled in part by the Froude number of the current when it enters the

hall. Viscous effects will be important when the Reynolds number for the flow are small enough or when the current moves far enough down the hallway that the effects of boundary and mixing layers become important, and the end of the hall used to withdraw the ambient fluid displaced by the current will also influence the flow field.

We will describe a few special cases of these flows in a general manner and then will concentrate on the most simple. The nomenclature used here to describe the flows is based on the analysis discussed in the following section but the observations are based largely on flows of salt water moving into ducts filled with fresh water.

(i) Subcritical Source

As an example of the problems we wish to study, consider the inviscid flow illustrated in Figure 2 which is produced when a steady stream of hot gas is introduced at one end of a long hallway at time zero and an equal volumetric flow of the ambient fluid is withdrawn from the same end of the hall. The material is injected so that we can ignore mixing at the inlet between the hot gas and the cooler air present in the hall.

With a subcritical source, the gravity current forms a thin layer which moves away from the source with a constant velocity and with a well defined front. The flow described here is similar to that described in Figure 1 in the region to the right of the hydraulic jump except that the boundary condition on the ambient flow is different.

This source is equivalent to the subcritical flow encountered in open channel flows of water in which the Froude number is less than one and for which sudden changes in the depth of the flow are not possible. However, the flow is more complex here because two streams are involved, the gravity current and the return flow in the lower layer. These differences will be discussed below.

Mixing between the current and the ambient flow occurs in a hydraulic jump associated with the supercritical flow of material in the lighter ambient fluid and, depending on the flow rates, this jump may occur either just behind the head of the current, as is suggested in Figure 2, or closer to the source as shown in Figures 1 and 4.

In the hydraulic jump, material is entrained from the gravity current into the ambient flow and this process produces a mixed layer between the current and the ambient fluid which is primarily made up of ambient fluid. The bottom of this layer is roughly level with the bottom of the head of the current as is suggested in the sketch. Little mixing occurs in the shear layer which forms between the current and the ambient fluid.

Viscous effects produce a boundary layer between the current and the wall, and a shear layer between the lower edge of this current and the ambient fluid. When the thickness of these layers becomes appreciable compared to that of the current, they will affect the flow. In addition, when the Reynolds number for the flow is small, viscous effects can have a large influence on the flow at the nose of the front and will cause a substantial reduction in the speed of the front. For

very small Reynolds numbers, the head of the current disappears entirely.

We can identify three regimes of flow here: an inertial regime in which the effects of viscosity are small; a very low Reynolds number regime in which viscous effects dominate the whole flow and in particular the head of the current; and an intermediate viscous regime in which the development of boundary and shear layers affects the flow. In the latter regime, the velocity of the front and the thickness of the layer behind the head decrease with increasing distance from the source, e.g., see the review in Chen (1980), and other material in Chen and List (1976) and Didden and Maxworthy (1982). The viscous regime will always be reached if the flow is allowed to propagate far enough from the source.

(ii) Supercritical source:

From an analogy with open channel flows, we expect that, when the Froude number of the source is greater than one, rapid changes in the depth of the current are possible and that changes in depth will occur through a process similar to that which occurs in a hydraulic jump such as that shown in Figures 1 and 3.

In the present flow, the hydraulic jump will be accompanied by entrainment of ambient fluid into the gravity current because the fluids are miscible. Downstream of the jump, the depth of the current will be greater than at the start; there will be a smooth change in the velocity and density profiles from the ambient values at the lower edge of the current to larger velocities and smaller densities at the wall; and the average Froude number will be less than one. In addition, the mass flow and density in the current will be increased by entrainment of ambient fluid at the jump. The jump process has been examined experimentally by D. L. Wilkinson and I. R. Wood (1971).

For the situation shown in Figure 1, the strength of the jump is determined by a coupling between the jump process and the motion of the gravity current which it produces. We will discuss the modeling of this process in a later Report.

The entrainment of ambient fluid into the current at the hydraulic jump also causes a return flow in the ambient fluid. When the inlet flow rate is increased still further, this return flow can cause a gross mixing between the current and the ambient fluid. This mixing and the recirculation of the hot gas can lead to the more complex flow field sketched in Figure 3b in which the hot gas from the fire is entrained into the recirculating flow which feeds the jump.

(iii) Plume source:

Finally, when the source of the hot gas is a plume from a fire, flows may be produced which behave like any one of those discussed above. Experiments are required to determine which will occur under a given set of circumstances. The sketch of Figure 3c illustrates one of these flows and other possibilities are described in Lee, Jirka and

Harleman (1974).

Our initial experiments will be concentrated on the subcritical flow of Figure 2, for which no mixing occurs due to the injection of the gravity current into the hall. The more complex cases will be examined later and will not be discussed further in this report.

We turn now to examine in detail the gravity current produced by a subcritical source in an inviscid flow.

2. Description of Subcritical Gravity Currents

The theoretical problem is most conveniently posed as follows: Given the flow of a light fluid into a two-dimensional rectangular channel filled with an initially stationary ambient fluid, whose density is greater than that of the injected fluid, find the velocity and shape of the current produced in the duct when the displaced heavy fluid is withdrawn from the end of the duct used to supply the lighter material.

Benjamin (1968) has analyzed a simplified version of the gravity current under a set of assumptions which makes the flow resemble a gravity current in the inertial regime. The effects of viscosity, mixing, and breaking waves observed at the head of the current are ignored. However, he does include losses as a parameter, and determines the depth of the current and the velocity of the front in terms of this parameter. The loss mechanism is not discussed and is not included in the physical picture of the model.

In a later paper, Wilkinson (1982) clarified the model of Benjamin (1968) by investigating in detail the loss mechanism. He was interested in flow of air into a channel filled with water. Because no mixing can occur between these two fluids and because viscous effects are often negligible in the air, this flow is particularly well modeled by the calculation. In the model used by Wilkinson, losses are allowed to occur in a bore or hydraulic jump which is assumed to lie between the head of the current and the source. The flow is assumed to be energy conserving except for the bore and the affects of mixing at the head and of viscosity throughout the flow are ignored.

In the following paragraphs, the analysis of Wilkinson is used to discuss the idealized flow shown in Figure 4.

Both Wilkinson and Benjamin investigated gravity currents which move into an initially quiescent fluid and we will restrict our analysis to this case too. However, under some circumstances, the development of a boundary layer on the wall upstream of the current can have a large effect on the shape of the head of the current and on its velocity.

(i) Constant Energy Flow

To illustrate the different flow subcritical flow regimes, we first examine the flow produced when a closed duct, initially filled with a heavy fluid, is opened at one end and a lighter fluid which surrounds the duct is allowed to replace the heavier fluid. This replacement occurs when the heavier fluid flows out of the bottom side of the open end and the lighter fluid flows into the top. This process, has been

investigated experimentally by Zukoski (1966) and is illustrated in Figure 4a.

Benjamin (1968) showed that only one depth is allowed for the current when the energy in the flow is conserved. For this constant energy case, see Figure 4a, the current occupies the top half of the duct, and the flow in the lower layer is critical with respect to a coordinate system fixed in the duct wall. This limiting case is called the Constant Energy regime.

(ii) Non-steady Flow Regime

We next consider the flow described above except that now the downstream end of the duct has been slightly blocked on the bottom side. A bore is produced in the outflowing stream by this obstacle which intrudes into the critical flow of the heavier fluid. The bore propagates upstream from the blockage with a velocity which depends on the depth of the fluid, the density ratio, and the velocity in the lower layer upstream of the bore.

For small blockage, Wilkinson shows that the bore moves upstream with a lower speed than the front. Consequently, it can not catch up with the front and the resulting flow is unsteady. The motion in this regime is shown in the sketches of Figure 4b and 4c. In this regime, because the bore moves slower than the front, the motion of the front is unaffected by the bore and the velocity of the front has the same value it had in the flow described above in (i). The depth of the current in the constant energy region behind the head is still half of the duct height. However, the current depth is reduced by the bore and, consequently, the volume flow rate of material in the current is less for this case than that in the constant energy regime.

The presence of the bore is a modification suggested by Wilkinson (1982). This regime is called the Unsteady Flow regime because the distance between the bore and the front increases with time.

(iii) Steady Flow Regime

The depth of the layer of ambient fluid downstream of the blockage, h2, and, consequently, the speed of the bore, v , increase as the blockage is increased. When the depth of the layer rises to about 78% of the duct height, Wilkinson (1982) shows that speed of the bore becomes equal to the speed of the front and for any deeper current the bore is able to catch up with the front. This leads to the formation of a steady flow, shown in Figure 4d, in which the front and the bore move as a unit and with a constant velocity. In this regime, the depth of the current, the volumetric flow rate of lighter material and the velocity of the front decrease as the blockage is increased.

This Steady Flow regime is identical to that described by Benjamin (1968) with the exception that Wilkinson has included an explicit description of the loss mechanism.

(iv) Coflowing Ambient Stream

In the above flow regimes, we assumed that the velocity of the more dense fluid upstream of the front was zero. Because we are dealing here with an inviscid approximation, we can relax this condition by using a Galilean transformation in which the coordinate axis is translated parallel to the duct wall with a constant velocity. This technique will allow us to describe the flow field when we impose any velocity we choose on the flow upstream of the front.

However, in an experimental situation, the flow is viscous, and this procedure can lead to an incorrect prediction of the flow field due to boundary layer effects on the head of the current.

3. Analytic Description of Subcritical Sources

Consider the flows shown in the sketches of Figure 4 and the notation defined there. We assume that flows in the gravity current and the ambient fluid are uniform and parallel to the walls except near the front of the current and the hydraulic jump. We will assume that the fluids are incompressible because, in the fire situation of interest to us, the pressure will remain so close to atmospheric that the density of the gas will not be affected by changes in it. Of course, density variations due to temperature are allowed.

Mass transfer at hydraulic jumps is not allowed and the velocity far upstream of the current is zero.

The flow rate per unit width and density of the light fluid in the current are u and ρ_c, and the density of the heavier fluid is ρ_a. In the following discussion, velocities are given in the coordinate system fixed in the wall of the duct and in defining dimensionless parameters, absolute values of the velocities are used.

In general, the volumetric flow rate per unit width supplied by the source is given by continuity argument as the product of the velocity in the current v and the depth of the current h, evaluated near the source, or

$$u = vh = v(ho-h2), \qquad (1)$$

where ho and h2 are the depth of the duct and depth of the ambient fluid near the source. Thus, either v or h can be taken as unknown when u is specified.

The velocity in the current beneath the source, v2, must be large enough to withdraw a volumetric flow rate from the duct equal to that of the source because we have assumed that no flow occurs in the duct far upstream of the front. Then,

$$v2 = vh/(ho-h) = u/(h2)$$

or

$$F2 = v2/\sqrt{g'ho} = U/H2$$

where

$$H2 = h2/ho \quad \text{amd} \quad U = u/\sqrt{g'ho^3}$$

To simplify the algebra of the problem, the ratio h2/ho defined as H2 is used as one of the independent variables for the problem and we will solve for a dimensionless value of u defined above as U rather than use u as the independent variable which it often will be in experimental work.

(i) Constant Energy Flow

In this limiting case, Benjamin (1968) showed theoretically that the layer thickness h is half of the duct height and that this is the maximum value for the layer thickness which is possible . Thus,

$$h1 = h2 = h)max = (1/2)ho$$

or if we use capital letters to denote dimensionless parameters,

$$H2 = h2/ho = 1/2 \qquad (2)$$

In this case, the velocity of the front and that of the fluid in the current are equal and are:

$$vf = v = 1/2\ \sqrt{g'ho} \qquad (3)$$

This is the maximum velocity that the current can have. The Froude number for the front and the current are defined as:

$$Ff = F = v/\sqrt{g'ho} = 1/2 \qquad (4)$$

The volumetric flow rate per unit width also takes on a maximum for this case. It is given by:

$$u = u)max = 1/4\ \sqrt{g'ho^3} \qquad (5)$$

and the dimensionless value is

$$U = u/\sqrt{g'ho^3} = 1/4 \qquad (6)$$

for the Constant Energy regime.

(ii) Unsteady Flow Regime

In this regime, Wilkinson (1982) showed that the region near the front of the current behaves exactly like the constant energy flow described above. The dimensionless velocity of the front and depth of the current in this region are still given by equations 2 and 4, and the velocity of the bore vb was found to be less than that of the front.

The Froude number for the bore can be written in terms of H2 as

$$Fb = vb/\sqrt{g'ho} = \{((1/2)H2(2H2 + 1))^{1/2} - 1/2\} \qquad (8)$$

and the volumetric flow rate at the source, is found by a continuity argument to be

$$U = u/\sqrt{g'ho^3} = 1/4 - Fb(H2 - 1/2) \qquad (9)$$

From Equation 1, the velocity in the current near the source is

$$v = u/(1-H2)ho$$

or

$$F = v/\sqrt{g'ho} = (U)/(1-H2) \qquad (10)$$

(iii) Steady Flow regime

In this regime, the bore moves with a higher velocity than the front and catches up with the head of the current. A steady flow is produced which is identical to that analyzed by Benjamin (1966).

The flow parameters of interest can be obtained from the equations:

$$F = Ff = Fb = v/\sqrt{g'ho} = (H2(1-H2^2)/(2-H2))^{1/2} \qquad (11)$$

Using the continuity of flow, equation 1, we find that:

$$U = F(1-H2) \qquad (12)$$

Thus, given a value for H2, we can find F and U or conversely, given U we can find F and H or H2.

Finally, consider the limiting flow as ho becomes very large compared with the depth of the current, h. Examination of equation (11) shows that in limit when the layer thickness h is held constant and ho becomes very large:

$$v)o = \sqrt{2g'h}$$

$$u)o = \sqrt{2g'h^3} \qquad (13)$$

For most fire problems, this limit will not be interesting but it does give a limiting value for the velocity of the front.

(iv) Numerical Results for Standard Boundary Conditions

Numerical results for the problem described above are given in Table 1 and Figure 5 where values of U, Ff, Fb and H are presented as functions of H2. In addition, the value for the velocity of the current, normalized of $\sqrt{g'h}$ is given as V in this table. For a given problem, if we assume that values are given for the reduced gravitational acceleration g', the duct height ho, and volumetric flow rate u, then values of U can be calculated and used to obtain values for the other dimensionless and dimensional parameters of the system. Examples will be given in the next section.

(v) Coflowing Ambient Stream

We are interested here in examining a variation on the problem discussed above which involves the relaxation of the condition that the fluid velocity upstream of the front is zero. For example, a second interesting limit is to require that ambient fluid enters the lower

layer at the source end of the duct with an arbitrary velocity, v2′, which can take on positive or negative values. See Figure 6.

For the standard solution, the boundary condition applied to the problem was that the fluid velocity far upstream of the head of the front was zero. The velocity in the flow beneath the source is fixed by the continuity equation and is

$$v2 = - v(ho-h2)/h2 = - u/h2 \qquad (14)$$

If we ignore the effects of viscosity, we can solve for the velocities of the source, bore and front in the new system by making a Galilean transformation which makes the value of the velocity in the ambient fluid beneath the source equal to an arbitrary value, say v2′. We will use primes to distinguish the solutions for this second problem from the solutions to the standard problem.

If the origin for the y axis, shown in Figure 6a for the standard solution, is translated to the left with a constant velocity equal to (v2′ + u/h2), the velocity of the ambient fluid seen by an observer in this new coordinate system, see Figure 6b, will be v2′. Of course, the geometry of the flow will be unaffected by this transformation and, for example, h = h′.

To obtain the velocities in this new coordinate system we must add the quantity, (v2′ + u/h2) to each of the velocities obtained for the standard problem. The results are summarized in Table 2:

TABLE 2: ARBITRARY VALUE FOR V2′ OR F2′

Parameters for:	Constant Energy	Unsteady Flow	Steady Flow
$F' = v'/\sqrt{g'ho}$	1.0 + F2′	F/H2 + F2′	F/H2 + F2′
$Ff' = vf'/\sqrt{g'ho}$	1.0 + F2′	Ff+F2′+ F(1-H2)/H2	F/H2 + F2′
$Fb' = vb'/\sqrt{g'ho}$	---	Fb+F2′+ F(1-H2)/H2	---
$U' = u'/\sqrt{gho^3}$	U/H2 + (1-H2)F2′	for all regimes	

Here, $F2' = v2'/\sqrt{g'ho}$ is specified.

In this table, we use a prime to denote the velocities in the coordinate system in which the ambient velocity beneath the source is v2′ and the unprimed quantities are those obtained in the standard problem and with numerical values listed in Table 1.

As an example for the application of these results, let the velocity v2′ be zero, and select values for g′ and ho. Then F2′ is zero, and when we pick a value for u, we can immediately obtain values for U and, consequently, all the unprimed parameters from Table 1. Then using Table 2, the primed quantities can be found. If we use a more reasonable definition for the problem and select a value for u′ rather than u, an iterative method must be used to find the appropriate value for U and U′.

Numerical Values for the primed quantities are shown in Table 3 for the special case that the velocity in the ambient stream at the origin is zero, i.e., for F2′=0. Values for the standard problem are also given in this table for purposes of comparison.

TABLE 3. Parameters for F2′=0

H2 h2/ho	U $u/\sqrt{g'ho^3}$	U′ $u'/\sqrt{g'ho^3}$	Ff′ $vf'/\sqrt{g'ho}$	U′/U vf′/vf	$\left(\frac{(vf'-vf)}{vf}\right)$
0.98	.0039	.0040	199	1.020	.020
0.94	.0193	.0115	.333	1.036	.036
0.90	.0394	.044	.438	1.11	.11
0.80	.098	.123	.613	1.25	.25
0.70	.167	.238	.738	1.47	.47
0.60	.219	.365	.865	1.73	.73
0.50	.250	.500	1.000	2.00	1.00

Although, the ratio of the velocities of the front of the wave for the two cases are not very sensitive to the transformation for H2 greater than 0.90, the differences are large for H2 near 0.5. However, the comparison made in this table is for flows with the same value for H2; if we compare flows with the same value for the volumetric flow rate of the source, i.e., for U′ = U, the velocity difference ratio, (vf′-vf)/vf is decreased. A few comparisons of this type are made in Table 4 in which the solution for the standard problem is listed as the upper line in each pair of data. For flow rates corresponding to values of U less than 0.05, the influence of the position at which material is withdrawn from the hall is small.

TABLE 4. Parameters for U′ = U and F2′ = 0

$u/\sqrt{g'ho^3}$ or $u'/\sqrt{g'ho^3}$	H2 h2/ho	Ff′ $vf'/\sqrt{g'ho}$	$\left(\frac{(vf'-vf)}{vf}\right)$
U = .044	0.89	.408	
U′ = .044	0.90	.438	0.07
U = .123	0.76	.500	
U′ = .123	0.80	.613	0.23
U = .238	0.55	.500	
U′ = .238	0.70	.738	0.48

4. Effects of Mixing at the Front and of Viscosity

The effects of mixing between the current and ambient fluid at the hydraulic jump or bore and the effects of viscosity are ignored in the analysis discussed above. Experimental data concerning these effects is briefly reviewed here.

(i) Mixing at the Front

Note that in these calculations, no mixing is allowed in the hydraulic jump or bore so that a precise comparison with the velocity of the front determined in experiments is not possible. When fluid is lost from the head, the velocity of the current must be larger than that in the head to supply this loss. Simpson and Britter were able to measure this difference. They found that the velocity in the front v_f is only slightly smaller than that of the current v and that the ratio of the two is approximately given by:

$$(v_f/v) = 1/(1.16 \pm 0.04) \qquad (15)$$

Because the two velocities are so nearly equal, we believe that values of the velocity of the current made for the inviscid case can be used as a first approximation to the velocity of the front or current when viscous effects are negligible.

The results expressed in equation 15 are also interesting because they contain information on the flow of gas into the mixed region. The magnitude of the velocity ratio indicates that there is a net flow of material from the current into the head and that this flow is then entrained from the head into the mixing layer shown in Figure 2. The net flow into and out of the head is about 16% of the flow in the current. This result is important to us since this means that 16% of the flow in the current mixes with and contaminates the ambient fluid.

(ii) Transition to Viscous Regime

Transition between inertial and viscous regimes occurs because of either the effect of viscosity on the flow over the front or because the displacement thickness of the boundary layer between the current and the wall grows to a value which is an appreciable fraction of the depth of the current. Simpson and Britter (1979) found that viscous effects on the flow over the front of the current were negligible when the Reynolds number for the front, based on layer depth and front velocity are greater than 500. We will be interested in this regime.

However, regardless of the Reynolds number for the front, the influence of the boundary layer will always appear if the front runs out far enough from the source. The viscous forces acting on the fluid at the wall will act to reduce the momentum of the flow and when the flow is long enough this force must have an effect on the motion of the front. The layer thickness at the source will grow so that the additional gravitational head at the source will be able to overcome the shear at the wall.

To make a simple estimate of the scaling laws for this transition, we examine the magnitude of the ratio of the boundary layer displacement thickness to the depth of the gravity current. When this ratio is very small, the influence of the the boundary layer is presumably negligible and when it reaches some limiting value, viscous effects will become important.

When the boundary layer between the current and the wall is laminar, we can make an estimate for the transition position by examining the ratio of viscous shear forces on the wall to the momentum flux in the layer at the source,

$$(0.5\,\rho_c\, v^2\, X\, Cf)/(\rho_c\, uv)$$

or the ratio of the displacement thickness δ to the original layer thickness, (δ/h),

$$\delta/h \propto (X/h)/\sqrt{(Xv/\nu)}$$

These ratios grow as the distance to the front, X, increases and when either reaches some small limiting value, we expect that the influence of viscous forces will become important.

Thus if we assume that the transition occurs when this ratio takes on some limiting value, we find by using either ratio that the transition length scales as:

$$X_t \propto vh^2/\nu$$

or

$$Re)_t = X_t v/\nu \propto (u/\nu)^2 \qquad (16)$$

When U is so small that the velocity of the current is given by v)o, equation (13), the dependence on the height of the channel is unimportant and the criterion becomes:

$$X \propto \sqrt{g'h}\, h^2/\nu \qquad (17)$$

Estimates of the position at which this viscous effect becomes important have been made by Chen et al (1976) and Chen (1980). Their experimental results agree with the form of equation 17 and the value of the proportionality constant was found experimentally to be about 0.10.

(iii) Viscous Regime:

In this regime, dimensional analysis and some experimental results, presented for example in Chen (1980), Chen and List (1976) and later by Didden and Maxworthy (1982), suggest that the velocity of the head of the current depends on the distance from the source of the front, X, and can be expressed as:

$$vf/((g'u^3/X\nu)^{1/4}) = j = (0.54) \qquad (18)$$

when U is so small that the duct height does not affect the velocity.

In this regime, the velocity of the front decreases with increasing X as X to the minus one fourth power and thus the depth of the current at the source must rise so that the gravitational forces can support the wall shear. The value of the constant j which appears in equation 18 gives a reasonable fit for a range of experiments.

5. Application of results for the subcritical source:

In many fire situations of interest, the flow will be entirely within the inertial regime and as a result the analysis presented above can be used to describe the flow.

As an example, consider the situation shown in the sketch of Figure 1 and let fires of various sizes be started in the small room adjacent to the hallway. Hot gas will flow from the room through the open door into a 2.5m square hallway and produce the hydraulic jump and gravity current shown in the sketches. Calculations have been made to show the properties of the ceiling currents produced by several fires and the results are shown in Table 5.

TABLE 5. EXAMPLES OF GRAVITY CURRENTS in a 2.5 m SQUARE HALL

EXAMPLE NUMBER:	#1	#2	#3	#4	#5	#6
1. PARAMETER VALUES ASSUMED:						
Fire size, kw:	50	50	50	200	200	800
Mass flux to current, kg/s :	0.5	1.0	2.0	1.5	3.0	3.0
2. PARAMETER VALUES CALCULATED:						
Temperature in current, C	120	70	45	153	86	285
flow rate in current u, m /s	0.22	0.39	0.72	0.73	1.23	1.90
density difference ratio, D	0.29	0.16	0.082	0.38	0.20	0.62
dimensionless flow rate, U s, for steady regime; us, unsteady flow regime	0.034 s	0.079 s	0.204 us	0.095 s	0.220 us	0.195 us
dimen. current height, H	0.09	0.17	0.37	0.20	0.40	0.35
dimen. velocity of head, Ff	0.38	0.47	0.50	0.49	0.50	0.50
dimen. velocity of bore, Fb	-	-	0.34	-	0.39	0.37
height of current h, m	0.22	0.42	0.93	0.49	1.00	0.87
height of head m	-	-	1.25	-	1.25	1.25
velocity of front vf, m/s	1.01	0.92	0.71	1.49	1.12	1.95
velocity of current v, m/s	1.01	0.92	0.95	1.49	1.23	2.79

Based on fire plume entrainment work, e.g., see Cetegen et al (1983), values were picked for the mass flux in the fire plume and then in the gravity currents which form downstream of the hydraulic jump. Then given the mass flux and enthalpy flux in the ceiling current, which is equated to the fire size, the rest of the parameters can be easily found, with the use of Table 1, for the case that the velocity far upstream of the front is zero.

In all examples in this table, the Reynolds number of each flow based on current velocity and depth is greater than ten thousand and the transition length is greater than 1000 meters. Hence, the Reynolds number and transition position are large enough to ensure that the flow will be in the inertial regime, and the influence of viscosity on the geometry and the propagation speed of the front should be negligible.

Examples 1 to 3, and 4 and 5 show the effects on the parameters of changing the mass flow in the current while holding constant the enthalpy flux, called here the fire size. For both the 50 and 200 kw examples, the depth of the layer increase almost linearly with the mass flux and the velocity decreases slightly. The reduction in the velocity of the front is due in part to the offsetting effects of the decrease in the density difference ratio D and the increase in the layer depth h.

The head of the current in these examples would traverse a 50 m long hall in from 25 to 70 seconds. Because the return wave would take a similar period, the total period required for the returning wave to reach the jump will be from one to two minutes.

For the first example, the gravity current occupies about 9% of the height of the hall. The depth behind the reflected wave will be larger by about a factor of about 1.5 and hence, the depth of hot gas in the hall will be about 15% of the height of the hall when the reflected wave submerges the hydraulic jump and suppresses further entrainment into the current. Thus, a considerable fraction of the hall will be filled with hot gas before the special conditions requiring modelling of the gravity current can be relaxed. In the other five examples, this depth is much larger. Hence, for many fire situations, the process by which the hall is filled with hot gas will be dominated by the gravity current flow described here.

In all of these examples, the current depth is greater than 0.22 m or about 9 inches and it is possible that the current would set off sprinklers located within this distance below the ceiling. Two of the examples produce gravity currents in the Unsteady Flow Regime and have a depth near the head of the current equal to one half of the hall height. Most of these flows would be threatening to a five foot high person (1.5 m or 60% of the hall height) standing or running within the hall although the velocity of the front, 0.7 to 1.5 m/s, would not be hard for an alert, healthy person to outrun.

The weakness of the discussion given here is that we have assumed values for the mass flow rate in the currents described in Table 5. In a later report we will describe the flow in the hydraulic jump at the entrance of the hall and a technique for matching the flow in the jump with that in the current. For the situations in which this jump is important, we will then be able to give a more complete picture for the flow.

C. CURRENT SALT WATER MODELING WORK

In our investigation, the salt-water modeling work will be used to obtain both a qualitative and where possible a quantitative picture of the flow for a number of fluid dynamic problem areas and will act as a guide for the gas phase experiments. Because of the ease in making flow visualization experiments, this technique is particularly useful in making a survey of new problem areas.

The standard problem to be investigated is that of a gravity current flowing steadily into a long hallway in which the ambient fluid is initially at rest. The source will be subcritical, as illustrated in Figure 1, and the Reynolds numbers will be high enough to keep the flow within the Inertial Regime. Both ends of the hall will be closed and the ambient fluid will be withdrawn from the end of the hall at which the current is introduced.

A number of important variations on the basic flow will also be investigated. An important experimental condition for these studies is the origin for the ceiling current. We plan to start the studies listed below with a subcritical source which leads to a current as shown in Figure 1c and 1d, and later will investigate some of the flows arising from the two other types of sources discussed above: one, which simulate a buoyant plume above a fire, Figure 3c, and a second which will be the supercritical source which has considerable momentum at the inlet and which will lead to conditions indicated in Figure 3a or 3b.

A second condition concerns the flow rate of the buoyant fluid. In a fire situation we expect that the flow rate of this fluid can change substantially even over the brief period during which the gravity current will be flowing down a long hall. The influence of this nonsteady supply will be investigated.

A third condition concerns the motion of the ambient, high density gas within the space. In most of the above discussion this fluid was at rest or was moving in response to the motion of the gravity current. In some fire situations, the high density fluid will be in motion due to a variety of causes. If the flow is against the direction of flow of the gravity current, the current can be stopped completely and the mixing between the current and ambient fluid will be different from that which exists when the ambient fluid is stationary. Thus, the point at which the ambient fluid is withdrawn from the hall and the presence of flow in the ambient gas produced by an imposed pressure field must also be investigated.

1. Problem Areas

Problem Areas to be studied with the salt-water/water modeling method include:

(i) For the standard subcritical-inlet problem, the determination of the dependence of the velocity of the front and the current depth, relative to hallway height, on the parameters of the system such as

volumetric flow rate, density difference ratio, the Reynolds number of the flow, and point of withdrawal of ambient fluid. We hope to check previous work here, rather than to break new ground, and to verify that our technique is correct.

(ii) The determination of the rates of mixing between gravity current and ambient fluid which occurs near the front of the current. Previous work suggests that in the high Reynolds number regime about 16% of the injected material is mixed with ambient fluid at the head of the flow. Again we want to check this result and to make sure that it is applicable to our problem. A quantitative measure of the concentration in the mixed layer will be made.

(iii) The interaction of the gravity current with (a) a closed end on the hall, (b) with a partially open end, and (c) with a right angle turn in the hall. As a part of this work we will determine the velocity of propagation of the reflected wave which is formed, at the interface between the current and ambient fluid, by these impingement processes.

(iv) The determination of the effect of rapidly changing the flow rate of hot gas which is supplied to the ceiling layer on the development of the layer and the mixing between the layer and ambient fluid.

(v) The effect on the flow of (a) roughness elements placed on the ceiling of the hall, with a range of roughness element heights ranging from a few percent to 10% of the hallway height, and (b) systematic variations in the width of the hall, such as result from inset doorways located in hotel corridors, with a variation in width of 10 to 20% of the hallway width.

(vi) The effect on the flow produced by the gravity current of the presence of a stratified layer of hot gas in the hallway before the introduction of the gravity current.

(vii) The effect on the flow and in particular on the mixing between the gravity current and the ambient fluid of turbulent velocity fluctuations of appreciable amplitude in the source flow for the current.

(viii) The effect on the flow of the location of the point at which fresh water is withdrawn from the duct and of a flow in the ambient fluid either opposing or aiding the motion of the gravity current.

In addition to these subjects which deal with the motion of the front we are interested in two other problem areas:

(ix) The rate of entrainment of ambient fluid into the current which occurs in the initial hydraulic jump described in Figure 1.

(x) The motion of waves produced by the impact of the current on the wall of the hallway and other disturbances in the hall.

2. Preliminary Experimental Results:

Preliminary experiments have been made in which we have recorded on video tapes the motion of gravity currents formed when dyed salt water (density in the range 1.04 to 1.10) is introduced into a duct which is filled with fresh water (density 1.00). The duct is 15cm square and 240 cm long, and thus has a length to height ratio of about 16. Some of the results obtained in these preliminary experiments are summarized below. In these tests, fresh water is withdrawn from the hallway at the end of the duct where the salt-water flow enters.

Preliminary observations are presented in the following paragraphs.

(i) The velocity of the front as measured in our experiment is less than the values we expected from a review of previous work presented above. The differences, between our data and the values predicted from inviscid theory, range from 50% at low flow rates, and hence small Reynolds numbers, to 20% at high flow rates, and hence higher Reynolds numbers. The difference may be due to the mixing process and to the development of the boundary layer, formed between the wall and the current, and the mixing layer, formed between the current and the ambient flow, which are ignored in the theory.

We are investigating the cause for this difference and are also reviewing data from a number of different authors whose normalized velocity data appear to lie between our results and the theoretical values. Of course, the effects of boundary layer growth will be more important in these small scale experiments than in the full scale case.

(ii) Visual inspection of the flow indicates that mixing between the gravity current and ambient fluid occurs only at the head of the current and nowhere else in the flow. The mixing appears to involve a small amount of the fluid from the current and a much larger amount from the ambient flow.

(iii) The velocity of the front decreases slightly when the head reaches a point several hall heights in front of the end wall of the duct. On impact, the front rides "down" the wall (see Figure 7a and 7b) and additional mixing does occur but, for the Reynolds number range we have investigated, it is very small and is restricted to the impact event.

(iv) After the current reaches the wall at the end of the hall, it is reflected as a series of waves which propagate from the closed end toward the source end of the duct, Figure 7c and 7d. The reflected waves have wave lengths of several hall heights; they do not "break" or cause any mixing; and they propagate at a roughly constant velocity toward the source of the current with a velocity which can be larger than that of the head of the current. The thickness of the layer behind the wave train is about 1.5 to 2 times that of the current in front of it.

(v) If a gravity current is introduced into a hallway which contains a thin stratified layer of fluid with density close to that in the gravity current, the head of the gravity current becomes a wave superimposed on the existing stratified layer. Depending on the depth

of the layer in the hall and the density difference ratio, the wave at the head of the gravity current may or may not break and its velocity may be reduced as compared to a similar current moving in a hall without the stratified layer. When the wave does not break, no mixing occurs at the head of the wave. Wood and Simpson (1984) have studied this phenomena.

Similarly, increasing the flow supplied to a gravity current which has started to move down a hall need not produce a second breaking front but can cause a non-breaking wave to propagate through the gravity current toward the front.

(vi) The interaction of the current with an obstacle placed on the ceiling, a square "beam" occupying about 12.5% of the height of the duct has been observed visually. The complete flow field produced by the interaction of the front with the obstacle is complex, and produces a flow which follows the description given in Figure 1 when the beam replaces the door soffit. The supercritical region and the hydraulic jump were observed to form just downstream of the beam and the jump was swamped by the reflected waves, as suggested in the Figure 1.

3. Implications for Modeling

These preliminary results suggest that:

(i) The scaling laws for transition and velocity described above are at least roughly applicable to our problem and the velocity of the front except for very thin layers will be in the range 0.5 to 2 m/s. Thus the time required for the front to flow down a hallway will be in the range of tens of seconds.

(ii) Mass lost by entrainment from the current and into the ambient gas occurs at the head of the current and is probably less than 15% of the injected flow. Thus, to a first approximation, we may be able to ignore it entirely in a simple room-fire model.

However, entrainment of ambient fluid into the current at a hydraulic jump, for example that produced by flow over a door soffit as shown in Figure 1, can be large compared to the flow in the current supplied to the room and hence must be modeled carefully.

Thus, details of the flow which lead to the production of the current, such as the entry of the current into the room shown in Figure 1, appear to be very important.

(iii) Once the current has reached the end of the hall, the motion at the interface between hot and cold fluid is that of a stratified layer disturbed by interfacial waves which do not produce additional mixing.

After the reflected wave has returned to submerge the hydraulic jump, see the example described in Figure 1, further mixing due to the gravity current can be ignored and the two-layer fire model used as usual.

(iv) Salt-water/water experiments will give us valuable insights into the flow processes without necessarily giving us quantitative results. A major problem here is to get Reynolds numbers high enough to ensure that the process is independent of viscous effects.

These results suggest that to a first approximation we were correct in ignoring entirely the lateral motion of gas in large rooms in the context of the two layer fire models.

However, for long hallways the time required for the current to traverse the space, and the effects of entrainment into the current and certainly of heat transfer will not be so easily dismissed and must be included in room-fire models.

In addition, the results described above were obtained with flows for which the Reynolds numbers, based on speed of the front and layer thickness, were in the range from 200 to 1000. Real flows of interest to us have Reynolds numbers about ten times larger than these values and these preliminary experiments suggest that the mixing may increase markedly with Reynolds number in this range. Hence, the optimistic conclusion that we may be able to ignore the lateral motion of the gas may not be realistic for high Reynolds number flows. However, this attractive idea will be pursued in our work.

Given the importance of the Reynolds number here, one of our important experimental objectives is to greatly increase the range of Reynolds numbers we can investigate in the salt-water modeling apparatus.

D. EXPERIMENTAL PROGRAM FOR GAS MODELING WORK

The experimental study of gravity currents in gasses will be used primarily to determine the influence of heat transfer on gravity currents. However, the duct has been designed to have about the same range of Reynolds numbers as the salt-water/water modeling apparatus and the other flow parameters can also be duplicated in the two experiments. Many of the problems mentioned above can be studied in both and, where ever possible, we will attempt to use the gas apparatus to verify novel findings discovered in salt-water/water modeling work.

The heat transfer studies will be carried out in an apparatus which is a model for a hallway. The dimensions of the duct are 50 cm square, 735 cm long, and a length to height ratio of about 14.5. This duct has glass side walls to allow flow visualization and reduce lateral heat transfer, a wooden floor to facilitate the insertion of instrumentation, and an aluminum top wall which is 1.27 cm (0.5 inches) thick. The height to width ratio for the duct can be easily changed so that the influence of aspect ratio can be studied.

Aluminum was selected for the top wall for the initial tests because it has sufficient thermal capacity and a large enough thermal conductivity to keep the surface temperature within a few tenths of a degree of the initial value during the transient test. This constant temperature boundary condition will greatly facilitate data reduction and the development of a good model for the flow. The apparatus is designed so that walls with other thermal properties can be studied easily.

Heat transfer gauges are located at 50 cm intervals on the centerline of the ceiling and at 150 cm intervals several can be placed across the width of the ceiling. A shadowgraph system is being developed as our principal flow visualization technique. Velocity and temperature distributions in the gravity current will be measured at one or two locations in each experiment with 5 to 10 hot wire probes mounted on a single support.

Both velocity and temperature will be measured from the same wire. The chief challenge which arises in the design of this probe is to make accurate measurements of either temperature or velocity at the very low gas speeds we anticipate will be present in the gravity currents.

The support for the velocity and temperature probe is designed so that the probe can to be moved easily throughout the duct between experiments; however, to cover a given flow throughout the whole duct will require that a number of separate but identical experiments be carried out.

Hot gas at temperatures up to 250 C will be supplied at a closed end of the duct at a known volumetric flow rate, and the motion of the front, the velocity and temperature distribution behind the front and the heat transfer to the ceiling will be measured. The initial tests will investigate the transient flow produced with an open end on the hall; later work will include the study of the reflected wave from a closed or partially closed end. The parameters to be investigated include: current

temperature and volume flow rate, end condition on the hall (i.e., open, closed and etc.) thermal properties of the ceiling, width to height ratio of the hall, and the presence of roughness on ceiling and side walls.

The duct has been constructed and the heat transfer instrumentation, installed for the initial experiments. At present, the heater for the hot gas supply is being tested. The hot wire probe apparatus is still under construction.

REFERENCES

Benjamin, T. Brooke, "Gravity currents and related phenomena" J. Fluid Mechanics 1968, vol. 31, part 2, pp. 209-248.

Cetegen, B., Kubota, T. and Zukoski, E. E., "Entrainment in fire plumes." to be published in Combustion Science and Technology.

Chen, J-C., and List, E. J., "Spreading of buoyant discharges." Proc. 1st CHMIT Seminar on Turbulent Buoyant Convection, Dubrovnik, 1976, pp. 171-182.

Chen, J-C., "Studies of Gravity Spreading Currents." Report No. KH-R-40, Keck Laboratory of Hydraulics and Water Resources, California Institute of Technology, Pasadena, Calif (1980).

Didden, N., and Maxworthy, T., "The viscous spreading of plane and axisymmetric gravity currents" J. Fluid Mechanics 1982, vol. 121, pp. 27-42.

Lee, J. H., Jirka, G. H., and Harleman D. R. F., "Stability and mixing of a vertical round buoyant jet in shallow water" Energy Laboratory Report No. MIT-EL 74-014, Massachusetts Institute of Technology, Nov. 1974.

Simpson, J. E., "Gravity Currents in the Laboratory, Atmosphere, and Ocean", Annual Reviews of Fluid Mechanics, Volume 14, 1982.

Simpson, J. E., and Britter, R. E., "The dynamics of the head of a gravity current advancing over a horizontal surface.", J. Fluid Mechanics 1979, part 3, pp.477-495.

Wilkinson, D. L., and Wood, I. R.,"A rapidly varying flow phenomena in a two-layer flow."J. Fluid Mechanics 1971, vol 47, part2, pp. 241-256.

Wilkinson, D. L., "Motion of air cavities in long horizontal tubes." J. Fluid Mechanics 1982, vol. 118, pp. 109-122.

Wood, I. R., and Simpson, J. E, "Jumps in layered miscible fluids." J. Fluid Mechanics 1984, vol 140, pp.329-342.

Zukoski, E. E., "Influence of viscosity, surface tension, and inclination angle on motion of long bubbles in closed tubes." J. Fluid Mechanics 1966, vol 25, pp. 821.

LIST OF SYMBOLS

The meanings for many of the symbols are illustrated in the sketches of Figures 2 and 4.

a,c,j, constants in equations

b, the hall width

D, the density difference ratio, $(\rho_a - \rho_c)/(\rho_a)$

Cf, skin friction coefficient

g, the gravitational acceleration, 9.8 m/s

g′, the reduced gravitational constant, $g' = Dg$

F, the current flow rate parameter, $v/\sqrt{g'ho}$

Fi, flow rate parameter, $vi/\sqrt{g'ho}$, note that various values for i are defined below

ho, the duct height

h, the current height near the source see Figures 2 and 4

h2, the depth of ambient fluid beneath the source, i.e., ho-h2; see Figure 2 and 4

hh, the height of the head above the current, see Figure 2

H2, the dimensionless depth of ambient fluid beneath the source, h2/ho

u, the volumetric flow rate per unit width of the hall supplied by the source, i.e., $u = V/b$, with units, m^2/s

U, the dimensionless value for the volumetric flow rate per unit width of the hall supplied by the source, i.e., $U = V/b\sqrt{g'ho^3}$

V, the normalized current speed based on the current depth, $v/\sqrt{g'h}$, rather than on the depth of the duct, ho

$\dot{V}$, the volumetric flow rate supplied by the source

v, the velocity of the flow in the current in the constant height region behind the bore, coordinates fixed in the wall, see Figure 4

vb, the velocity of bore or hydraulic jump, coordinates fixed in wall.

vf, the velocity of front or head, coordinates fixed in wall

vw, the velocity of the wave reflected from wall of hall

vo, the velocity of the flow far upstream of the head of the current, coordinates fixed in the wall

X, distance front has moved downstream of source

X_{ν}, distance at which transition to viscous regime occurs

δ^*, displacement thickness of the boundary layer

ρ_c, the density of the fluid in the current

ρ_a, the density of the ambient fluid in the hallway

ν, the viscosity of the fluids (taken as being equal for both)

Subscripts:

f, front

b, bore

2, flow in ambient fluid below source

Superscripts

( )′, prime denotes parameter values in a coordinate system with arbitrary velocity, v2′, in the flow beneath the source See section IV.3.B.v.

TABLE I: PARAMETERS FOR GRAVITY CURRENT IN A HALLWAY

H2	F	Ff	Fb	U	H	V
h2/ho	$v/\sqrt{g'ho}$	$vf/\sqrt{g'ho}$	$vb/\sqrt{g'ho}$	$u/\sqrt{g'ho^3}$	h/ho	$v/\sqrt{g'h}$
0.50	0.500	0.500	0.207	0.2500	0.50	0.707
0.51	0.506	0.500	0.218	0.2478	0.49	0.723
0.52	0.511	0.500	0.228	0.2454	0.48	0.738
0.53	0.517	0.500	0.239	0.2428	0.47	0.754
0.54	0.522	0.500	0.249	0.2400	0.46	0.769
0.55	0.527	0.500	0.260	0.2370	0.45	0.785
0.56	0.531	0.500	0.270	0.2338	0.44	0.801
0.57	0.536	0.500	0.281	0.2303	0.43	0.817
0.58	0.540	0.500	0.291	0.2267	0.42	0.833
0.59	0.543	0.500	0.302	0.2228	0.41	0.849
0.60	0.547	0.500	0.312	0.2188	0.40	0.865
0.61	0.550	0.500	0.323	0.2145	0.39	0.881
0.62	0.553	0.500	0.333	0.2100	0.38	0.897
0.63	0.555	0.500	0.344	0.2053	0.37	0.912
0.64	0.557	0.500	0.354	0.2004	0.36	0.928
0.65	0.558	0.500	0.365	0.1953	0.35	0.943
0.66	0.559	0.500	0.375	0.1900	0.34	0.958
0.67	0.559	0.500	0.385	0.1845	0.33	0.973
0.68	0.559	0.500	0.396	0.1788	0.32	0.988
0.69	0.558	0.500	0.406	0.1728	0.31	1.001
0.70	0.556	0.500	0.417	0.1667	0.30	1.014
0.71	0.553	0.500	0.427	0.1604	0.29	1.027
0.72	0.549	0.500	0.437	0.1538	0.28	1.038
0.73	0.545	0.500	0.448	0.1471	0.27	1.048
0.74	0.539	0.500	0.458	0.1401	0.26	1.057
0.75	0.532	0.500	0.468	0.1329	0.25	1.064
0.76	0.523	0.500	0.479	0.1256	0.24	1.068
0.77	0.513	0.500	0.489	0.1180	0.23	1.070
0.78	0.501	0.500	0.499	0.1102	0.22	1.068
0.79	0.495	0.495	0.495	0.1040	0.21	1.081
0.80	0.490	0.490	0.490	0.0980	0.20	1.095
0.81	0.484	0.484	0.484	0.0919	0.19	1.110
0.82	0.477	0.477	0.477	0.0859	0.18	1.125
0.83	0.470	0.470	0.470	0.0799	0.17	1.139
0.84	0.462	0.462	0.462	0.0739	0.16	1.154
0.85	0.453	0.453	0.453	0.0679	0.15	1.169
0.86	0.443	0.443	0.443	0.0621	0.14	1.185
0.87	0.433	0.433	0.433	0.0562	0.13	1.200
0.88	0.421	0.421	0.421	0.0505	0.12	1.215
0.89	0.408	0.408	0.408	0.0449	0.11	1.231
0.90	0.394	0.394	0.394	0.0394	0.10	1.247
0.91	0.379	0.379	0.379	0.0341	0.09	1.263
0.92	0.362	0.362	0.362	0.0289	0.08	1.279
0.93	0.343	0.343	0.343	0.0240	0.07	1.295
0.94	0.321	0.321	0.321	0.0193	0.06	1.312
0.95	0.297	0.297	0.297	0.0149	0.05	1.328
0.96	0.269	0.269	0.269	0.0108	0.04	1.345
0.97	0.236	0.236	0.236	0.0071	0.03	1.362
0.98	0.195	0.195	0.195	0.0039	0.02	1.379
0.99	0.140	0.140	0.140	0.0014	0.01	1.397
1.00	0.000	0.000	0.000	0.0000	0.00	1.414

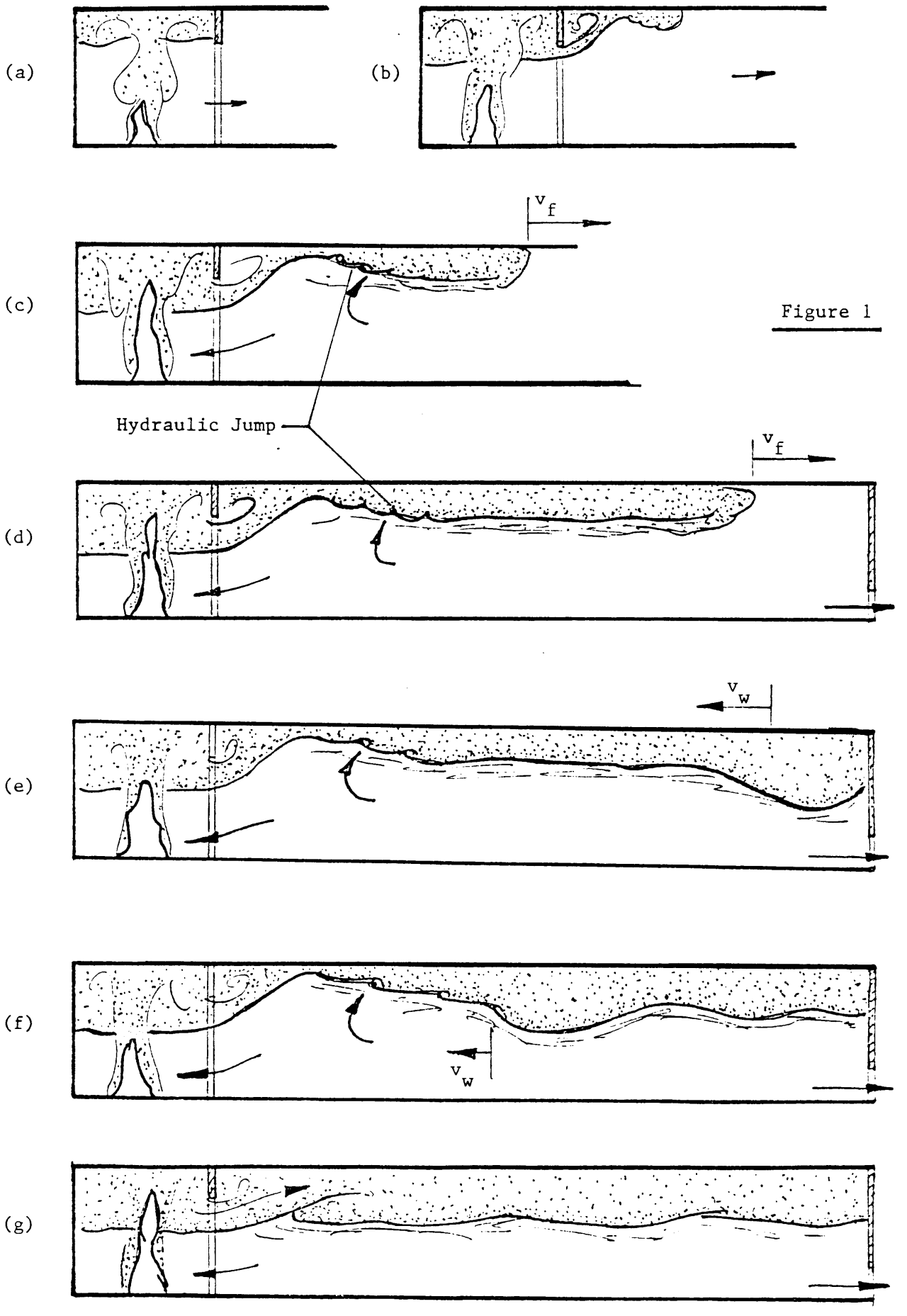

Figure 1

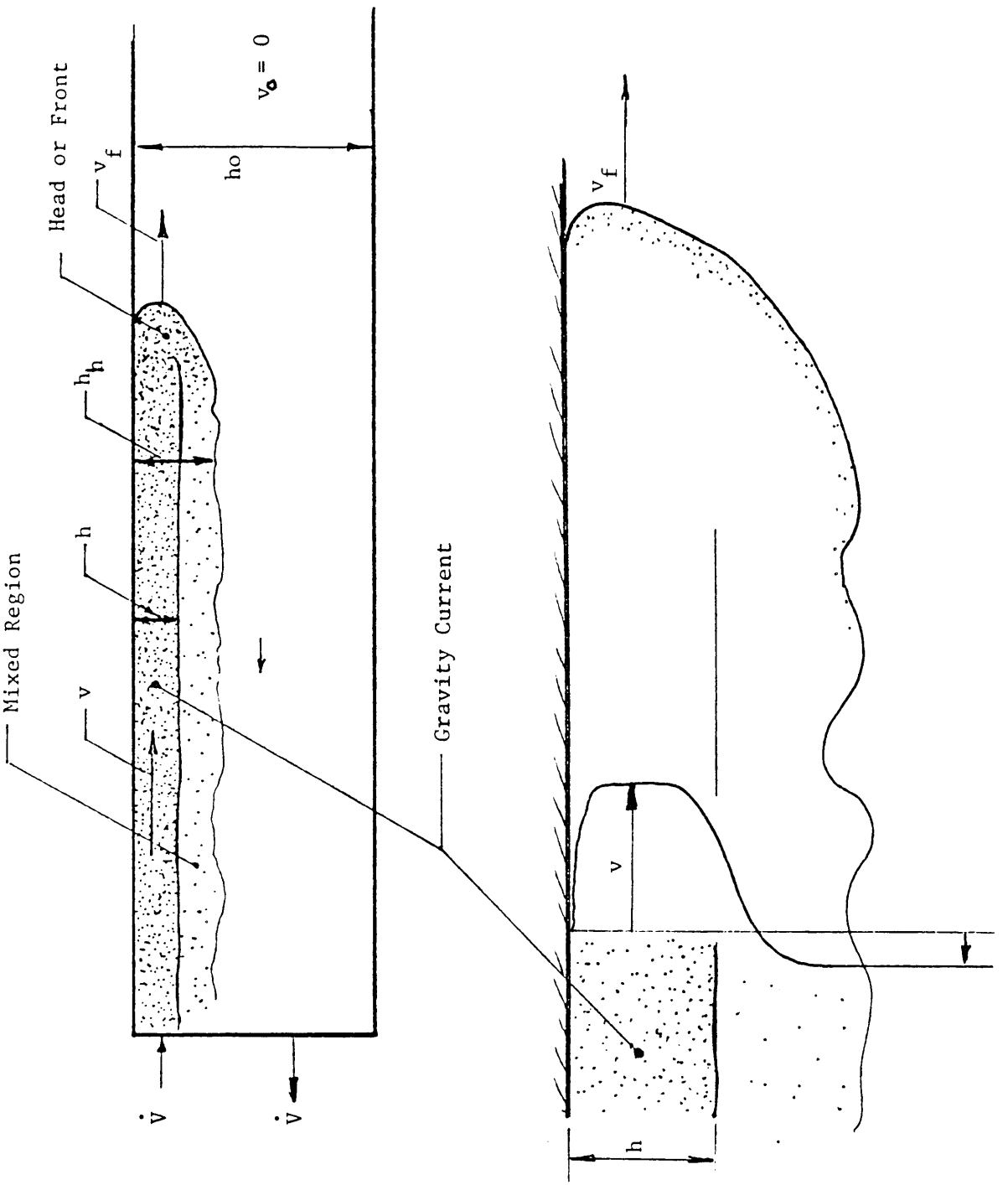

Figure 2. Subcritical Source

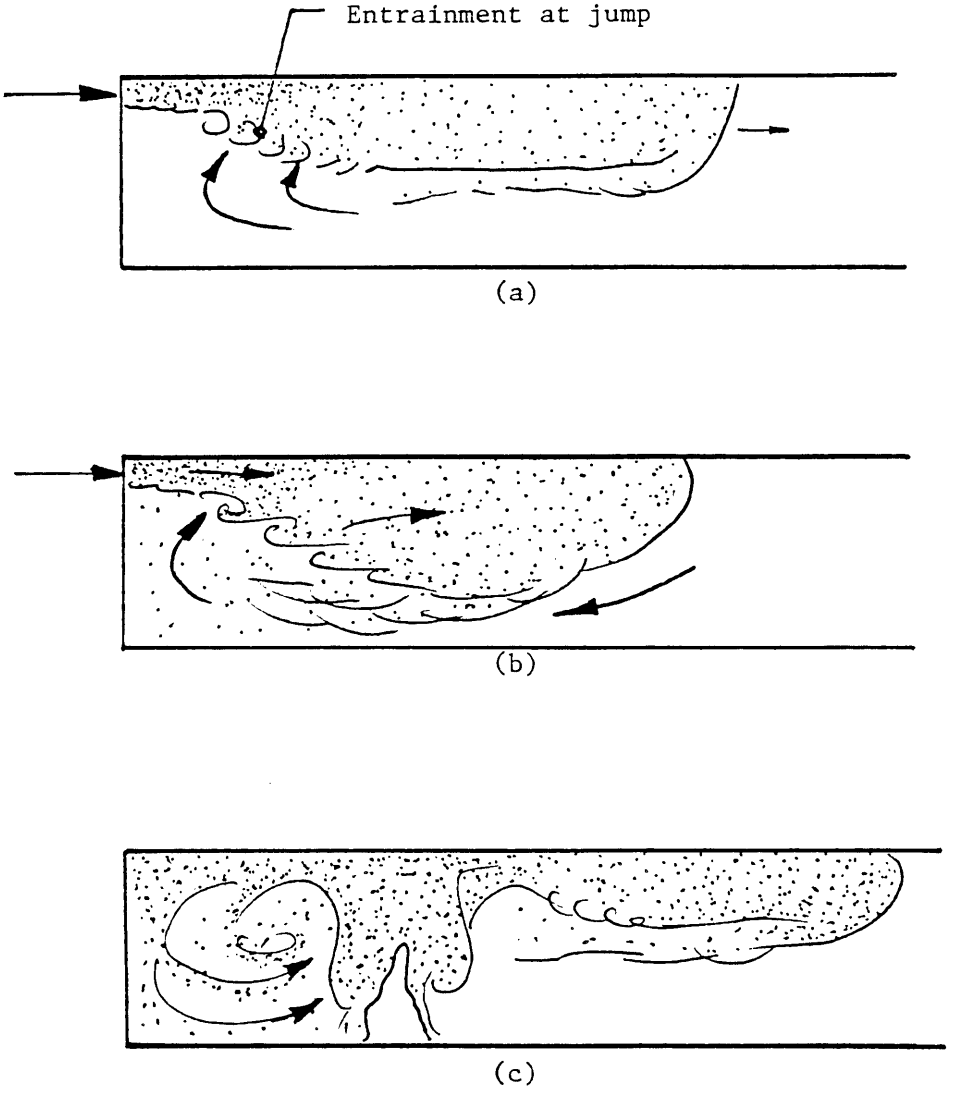

Figure 3. Alternate Sources

a. Supercritical Source
b. Supercritical Source with Secondary Mixing
c. Plume Source

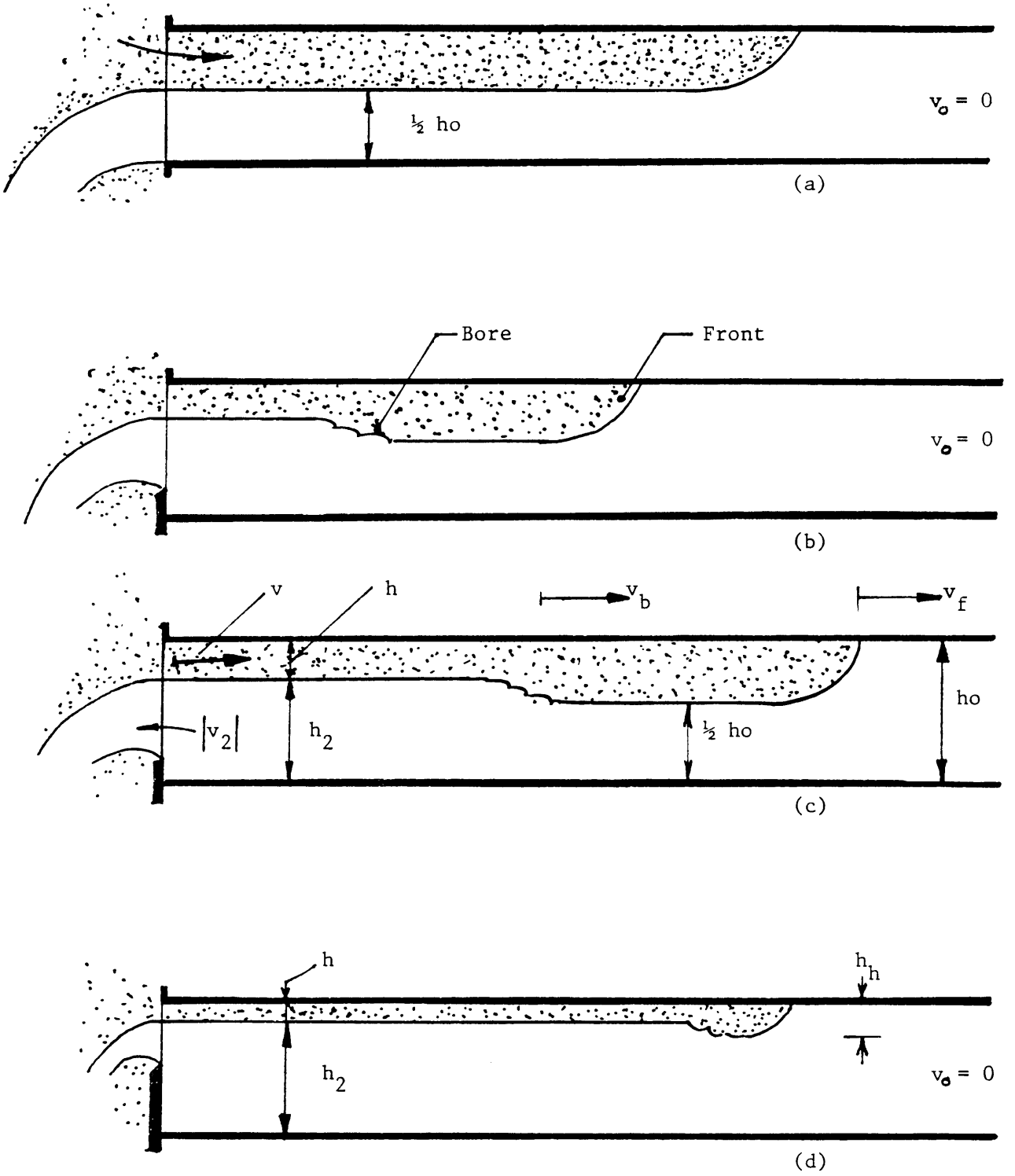

Figure 4. Flow Regimes: (a) Constant Energy; (b) + (c) Unsteady and (d) Steady Flow Regime

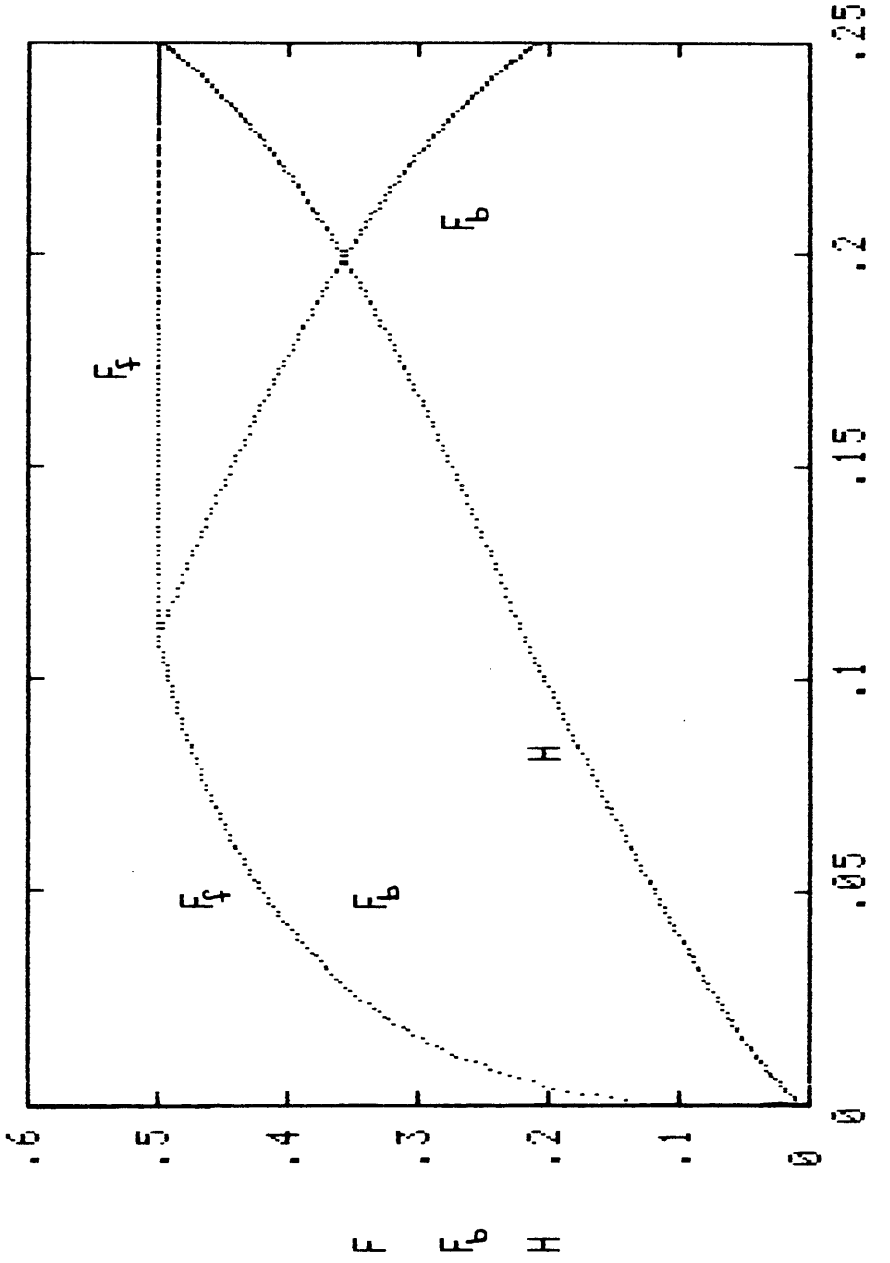

Figure 5. Inviscid Flow Parameters

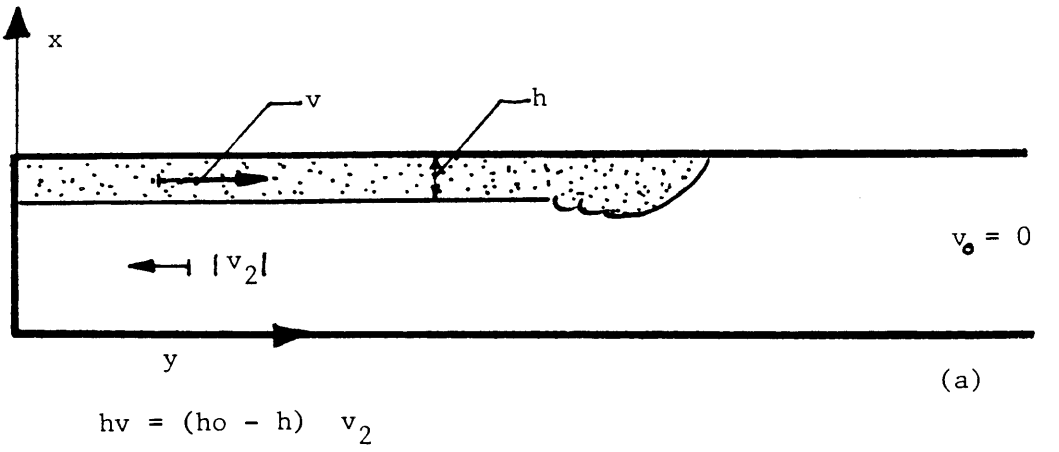

$$hv = (ho - h) \quad v_2$$

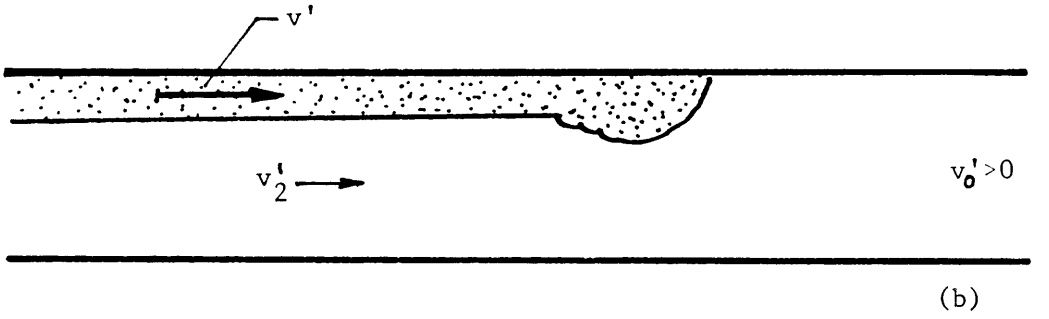

$$vo'ho = v'h + v_2' \ (ho - h)$$

Figure 6. Galilean Transformation

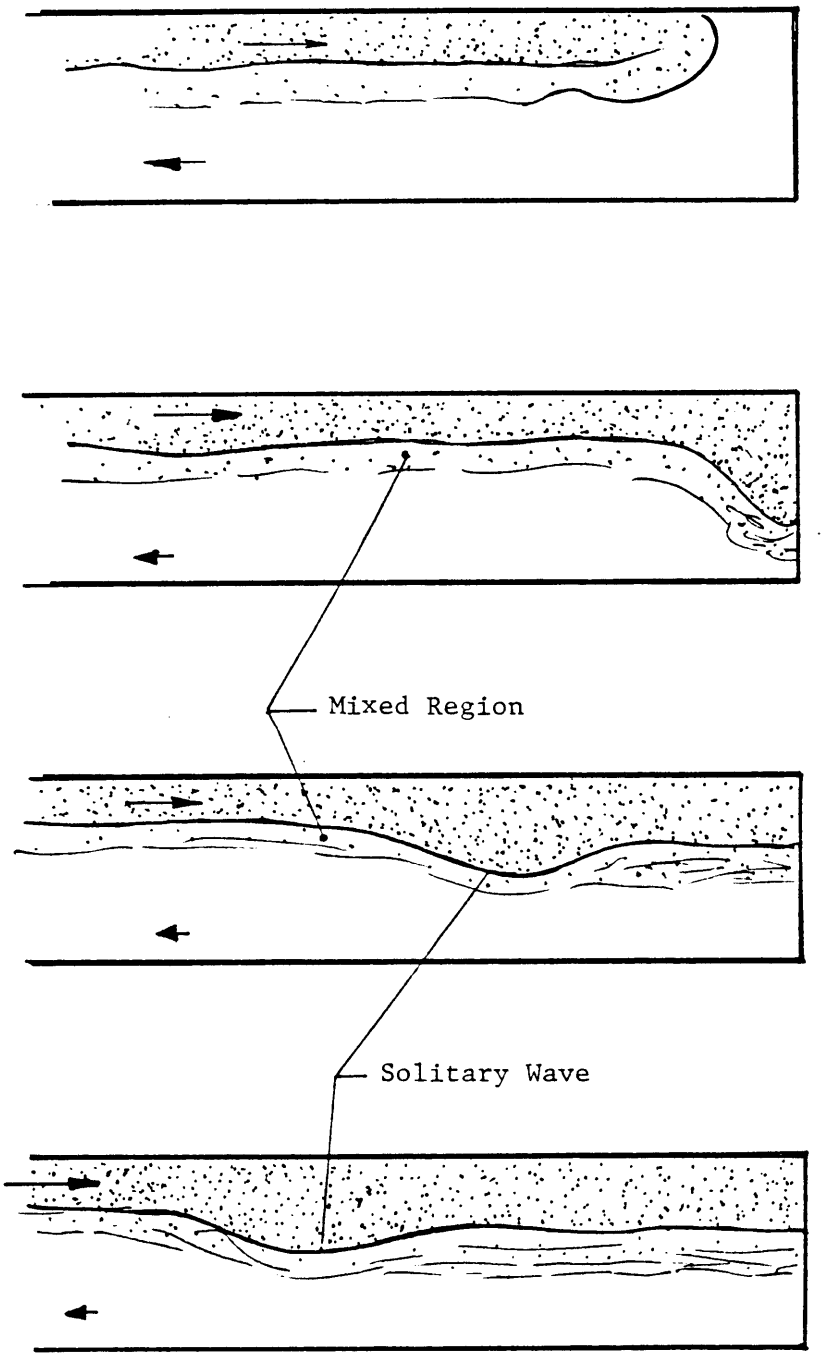

Figure 7. Impact on End Wall

CALIFORNIA INSTITUTE OF TECHNOLOGY

Daniel and Florence Guggenheim Jet Propulsion Center

MIXING IN DOORWAY FLOWS

and

ENTRAINMENT IN FIRE PLUMES

by

C. S. Lim, E. E. Zukoski and T. Kubota

June 1984

Supported Through Grant Number NB82NADA3033
U. S. Department of Commerce
National Bureau of Standards
Center for Fire Research

ACKNOWLEDGEMENTS

This report covers the work done during the period 1982 - 1984 by C. S. Lim, E. E. Zukoski and T. Kubota under grant NB82NADA3033 from The Center for Fire Research of the National Bureau of Standards, U. S. Department of Commerce. It constitutes the Aeronautical Engineer thesis of C. S. Lim, "I. Mixing in Doorway Flows, II. Entrainment in Fire Plumes," submitted to the California Institute of Technology on 30 April 1984. Authors are thankful to J. P. Huot, Hamid Johari and Brian Kravitz for their assistance in the experimental work. The support and encouragement of Drs. James Quintiere and Walter Jones of the National Bureau of Standards is also very much appreciated.

ABSTRACT

The motion of hot combustion products through a burning structure plays a dominant role in fixing the spread of the fire and the spread of toxic gases. The first part of this report is concerned with the effect of door geometry on the rate of turbulent mixing between the hot and cold layers near a doorway. The second part of the report deals with the entrainment rates in the near field of a buoyant diffusion methane flame.

In the study of the motion of the hot combustion products near a doorway, the gas in the burning room is assumed to be divided into two homogeneous layers--the ceiling layer which contains the hot combustion products and the floor layer which contains the denser fresh air. Temperature and carbon dioxide measurements are taken from a half-scale room which uses a pump and furnace to simulate the entrainment and heating of the fresh air by the fire plume. The mass transfer rates are calculated from these measurements and are found to be a function of a Richardson number that uses the interface height measured from the floor as the characteristic length and the average inflow velocity of fresh air as the characteristic velocity. This form for Ri_o is derived from an analysis based on Taylor's entrainment hypothesis. For a given fire size, i.e., for a given mass flow of fresh air into the room, the effect of reducing the door area is to reduce the value of Ri_o and hence increase the mixing rate in the room. The door height is found to be a much stronger influence on the mixing rate and interface height than the door width.

The entrainment rates of fresh air in the near field of a buoyant diffusion methane flame whose flames extend well above the interface between the hot gas layer and the fresh air layer are measured for several interface heights. In

a large steel hood over an axisymmetric burner. The hood may be raised or lowered to change the interface height. The entrainment measurements are obtained from a chemical analysis of a dried sample of combustion products taken from the ceiling layer. The measured species concentrations are compared with the theoretical equilibrium composition of the ceiling layer gas. For a given interface height, the ceiling layer gas temperature is found to be a linear function of the fuel-air ratio up to the stoichiometric fuel-air ratio. Increasing the fuel-air ratio above the stoichiometric value did not change the gas temperature significantly. This maximum temperature is observed to decrease with interface height. The air entrainment rates are found to be a weak function of the fuel-air ratio at very low elevations of the interface.

TABLE OF CONTENTS

LIST OF FIGURES

LIST OF TABLES

LIST OF SYMBOLS

A. MIXING IN DOORWAY FLOWS

b	Door width.
$E(x)$	Local entrainment coefficient (Eq. 3.5).
F	Froude number defined by Eq. 3.16c
H	Room height (= 48 in.)
K	CO_2 concentration expressed as $\%CO_2$ by volume.
$\dot{m}(x)$	Total mass flowrate of the cold layer jet; $= \dot{m}_d(x) + \dot{m}_{1c}$.
$\dot{m}_{1c}$	Total mass flowrate of inflowing fresh air.
$\dot{m}_{1h}$	Total mass flowrate of outflowing hot gas.
$\dot{m}_2$	Floor suction rate.
$\dot{m}_3$	Mass flowrate of gas leaving the furnace.
$\dot{m}_d(x)$	Mass entrainment rate of hot gas into the cold layer from x = 0 (doorway) to x.
$\dot{m}_d$	Total mass entrainment rate of hot gas into the cold layer; $\equiv \dot{m}_d(x_{cr})$.
$\dot{m}_u$	Mass entrainment rate of fresh air into the hot layer.
$\dot{Q}_f$	Fuel heat release rate. $\equiv 47.5\ MJ/kg \times \dot{m}_f$.
Ri_o	Overall Richardson number (Eq. 3.1).
$Ri_x(x)$	Local Richardson number (Eq. 2.6).
t_{res}	Residence time of the hot gas in the ceiling layer.
T	Gas temperature.
$U^*(x)$	Velocity scale based on jet momentum (Eq. 3.6).
$U_{max}(x)$	Local maximum velocity in the cold layer.
U_{1c}	Average velocity of the inflowing fresh air (Eq. 3.3).

W	Room width (= 48 in.)
x	Axis normal to the plane of the door.
y	Probe height measured from the floor.
Y_i	Interface height measured from the floor.
$\delta(x)$	Mixing layer thickness at station x (Fig. 2.3).
δ_C	Mixing layer thickness measured at the center of the room.
ρ	Density.

Subscripts

c	Property of the floor (or "cold") layer gas.
cr	Critical point where mixing is suppressed.
f	Property of the fuel.
h	Property of the ceiling (or "hot") layer gas.
3	Property of the hot gas leaving the furnace.
∞	Property of the ambient (or "fresh") air.

B. ENTRAINMENT IN FIRE PLUMES

C_f	Mass fraction of fuel in the ceiling layer.
C_o	Mass fraction of oxygen in the ceiling layer.
C_∞	Mass fraction of oxygen in the ambient air (=0.23).
D	Burner diameter (= 0.19 m.).
f_s	Stoichiometric fuel-air ratio (= 0.056 for methane).
$\dot{m}_E$	Mass entrainment rate of air into the plume.
$\dot{m}_f$	Mass flowrate of fuel.
$\dot{m}_{f_{added}}$	Mass flowrate of fuel injected directly into the ceiling layer.
$\dot{m}_{p_{in}}$	Plume mass flux into the small hood.
$\dot{m}_{p_{fl}}$	Plume mass flux at the flame top.
n_i	Number of moles of species i per mole fuel.

N_{hood}	Total number of moles in the hood per mole fuel.
N_{sample}	Total number of moles in the dried sample per mole fuel.
φ	Equivalence ratio.
$\dot{Q}_f$	Fire size; = 47.5 $MJ/kg \times \dot{m}_f$.
t_{res}	Residence time of the hot gas in the hood.
T_h	Average ceiling layer gas temperature.
T_∞	Ambient air temperature.
Y_i	Mole fraction of species i in the dried sample.
$\overline{Y}_i$	Mole fraction of species i in the ceiling layer.
Z_i	Interface height.
α	Fraction of added fuel consumed in the plume.

Chapter 1

INTRODUCTION

The motion of hot combustion products through a burning structure plays a dominant role in fixing the spread of the fire and the spread of toxic gases. The first part of this report is concerned with the effect of door geometry on the rate of turbulent mixing between the hot and cold layers near a doorway. The second part of the report deals with the entrainment rates in the near field of a buoyant diffusion flame.

1.1. Mixing in Doorway Flows

The motion of gases in a burning room is strongly influenced by the fire size, room geometry, and the presence of windows, doorways, and other openings. Fresh air in the floor region is entrained and heated by a buoyant plume produced by the fire. The hot gases then rise to the top of the room to form a distinct ceiling layer of hot combustion products. This ceiling layer of hot gases gradually becomes thicker, then flows out to the adjacent rooms through open doorways. Fresh air enters the room through the lower part of the door to replace the air entrained into the plume. Near the doorway, the motion of the hot gas and fresh air are in opposite directions, and a shear layer is formed between the two layers. The amount of mixing between the hot gas and fresh air in the shear layer is controlled largely by inertial and buoyancy forces. As the temperature in the room increases, the unignited objects in the room begin to pyrolize and contribute fuel to the ceiling layer. Since the room is evenly heated, the unburned fuel and objects in the room ignite at about the same time. This results in the phenomenon known as flashover: a sudden increase in temperature, a rapid increase in gas production, and an explosive and

spectacular fire growth that consumes the entire room.

During the period prior to flashover, the hot gas layer is usually so sharply stratified that the room may be approximated by dividing it into two homogeneous regions: the ceiling layer which contains the hot gases, and the floor layer which contains the cooler gas. Mass and energy conservation equations may then be applied to each layer to calculate the amount of mixing between the ceiling and floor layers, and the entrainment of outside air into the room.

The two-layer model for smoke movement was first used by Kawagoe (1958) who studied the movement of gases through an opening connecting two regions (i.e., the ambient air region and the room region which was considered to be a well-mixed, homogeneous region). A few years later, P. H. Thomas, et al (1963) studied flows in rooms with well-defined stratified hot and cold layers. Other works which use the model are discussed in papers by Zukoski, et al (1975, 1978, 1979, 1980).

The present investigation is concerned with the measurement of the amount of hot gas entrained by the fresh air entering through the door. In particular, the purpose of the experiments is to determine the effect of door geometry and fire size on the mixing rate. In the experiments, we used a pump and a furnace to simulate the entrainment and heating of the fresh air by the fire plume. Chapter 2 describes the model and the techniques used in calculating the mass flowrates. Chapter 3 discusses the results obtained for four different door geometries. The equations used in the calculations are derived in Appendix A and the data gathered from the experiments are tabulated in Appendix C.

1.2. Entrainment in Fire Plumes

While the turbulent mixing between the hot and cold layers generated by presence of doorways accounts for some of the entrainment of lower region air into the upper layer, the fire plume transports a much larger mass flowrate of gas into the ceiling layer. The entrainment rate of air into the plume is strongly dependent on the fire size, fire geometry, and the interface height. Experiments indicate that the fire plume may be divided into three regions: a region close to the burner surface where plume entrainment rates are independent of fire size; a far field region well above the top of the flames where a simple point source model may be used; and a not so well-defined intermediate region where turbulent flame approximations apply.

In the initial region near the base of the fire, Cetegen (1982) observed that the entrainment rates are independent of the fuel flowrate and scale with height above the burner raised to a power of approximately 3/4.

In this report, we describe the plume mass flux measurements in the near field of axisymmetric diffusion flames. The measurements were made by chemical analysis of the species in the ceiling layer. Chapter 4 describes in detail the technique and the apparatus used in the experiments. Chapter 5 discusses the experimental results and compares the results with the theoretical values obtained from a chemical equilibrium analysis. The equations used in the experiments are derived in Appendix B, and the experimental data are tabulated in Appendix D.

Chapter 2

ROOM EXPERIMENTAL SETUP

2.1. Experimental Technique and Apparatus

The motion of gases in a burning room is strongly influenced by the fire size, room geometry, and the presence of windows, doorways, and other openings. We have investigated the effects of fire size and door geometry on the turbulent mixing between the hot and cold layers in a half-scale model room, and the entrainment of outside air into the room. The room model used in our experiments is shown schematically in Figure 2.1. To simulate the fire entrainment rate, $\dot{m}_2$, a pump was used to draw room air through the floor and into a furnace where the air was heated to about 160 degrees Celsius. The furnace used city gas (methane) as fuel. Screens were placed in the furnace to ensure that the gas was heated uniformly. The walls of the room were well insulated to minimize heat loss to the surrounding air.

Gas samples from the room were obtained from six probes on an arm that extended across the width of the room. The probe arm could be swung 180 degrees in the horizontal plane, as well as moved in the vertical direction to reach most parts of the room. Additional probes were also placed in the furnace and in the ambient air.

A Beckman Model 864 Nondispersive Infrared Analyzer was used to measure the volume concentration of carbon dioxide. The analyzer was calibrated three times during each run with the use of certified calibration gases obtained from the Matheson Company. Iron-Constantan thermocouples were used to measure the gas temperatures.

In the experiments, the interface height was varied by increasing or decreasing the flowrate through the pump ($\dot{m}_2$), and appropriately adjusting the fuel flowrate to achieve the desired furnace temperature.

2.2. Mass Transfer Model

To model the mass transfer process, we assume that the room can be separated into four distinct regions with uniform thermodynamic properties: the hot layer, the cold layer, the furnace, and the ambient or outside air regions (Figures 2.2a,b). Then by applying mass balance equations to each region, the following mass flow relations can be obtained (see Appendix A):

$$\dot{m}_{1h} = \frac{(K_\infty - K_c)\dot{m}_2 + (K_3 - K_\infty)\dot{m}_3}{K_h - K_\infty} \tag{2.1}$$

$$\dot{m}_{1c} = \dot{m}_2 - \dot{m}_3 + \dot{m}_{1h} \tag{2.2}$$

$$\dot{m}_u = \frac{\dot{m}_3(K_h - K_3)}{K_c - K_h} \tag{2.3}$$

$$\dot{m}_d = \dot{m}_u + \dot{m}_2 - \dot{m}_{1c} \tag{2.4}$$

where $\dot{m}_{1h}$ is the mass flow of hot layer gas leaving the room through the door; $\dot{m}_{1c}$ the mass flow of ambient outside air entering the room through the door; $\dot{m}_u$ the mass flow of cold layer gas entrained into the hot layer; and $\dot{m}_d$ the mass flow of hot layer gas entrained into the cold layer. Here $\dot{m}_2$ is the floor suction rate, and $\dot{m}_3$ is the mass flowrate of gas leaving the furnace. K_h is the mole fraction of CO_2 in the hot layer; K_c the mole fraction in the cold layer; K_3 the mole fraction of the hot gas leaving the furnace; and K_∞ is the mole fraction of CO_2 in the ambient air.

The following quantities were measured in the experiments: $\dot{m}_g$, $\dot{m}_f$, K_h, K_c, K_3, and K_∞. These data and the above equations were then used to estimate the values of $\dot{m}_{1h}$, $\dot{m}_{1c}$, $\dot{m}_w$, and $\dot{m}_g$. The derivations of the above equations are presented in Appendix A.

2.3. Determination of Interface Height

Since the shear layer that separates the ceiling and floor layers has a finite thickness, the interface height is not clearly defined. In the experiments, we chose to base the interface height on both the temperature and carbon dioxide concentration profiles in the room. The interface height, Y_i, is defined to be the height where

$$\frac{T(y) - T_\infty}{T_3 - T_\infty} \text{ and } \frac{K(y) - K_\infty}{K_3 - K_\infty} \text{ equals } \frac{1}{2}.$$

$T(y)$ and $K(y)$ are the temperature and mole fraction of CO_2 measured y inches from the floor; T_∞ the temperature of the ambient air outside the room; and T_3 the furnace temperature. For cases where the two heights did not coincide, the average value was used. This arbitrarily defined interface height, Y_i, was used to calculate the average velocity, U_{1c}, of the ambient air entering through the door. Both terms appear in the definition of the overall Richardson number.

2.4. The Richardson Number

The Richardson number is a measure of the stability of flows with density variations. It is a dimensionless number and is equal to the ratio of the buoyancy force and the momentum flux, i.e.,

$$Ri_o = \frac{\Delta\rho g L}{\rho U^2} \tag{2.5}$$

where L is a characteristic length; ρ the density; g the gravitational constant; and U a characteristic velocity. The mixing process is suppressed by the gravitational forces when the momentum of the gases is small enough, i.e, at large Ri_o values. On the other hand, at low values of Ri_o, considerable mixing between the two layers occurs. Since Eq. 2.5 describes the entire flow, Ri_o is called the "overall" Richardson number.

A "local" Richardson number, which represents the stability of the layers at a given cross section in the room, is defined by

$$Ri_x(x) = \left[\frac{-\frac{1}{\rho}\frac{\partial\rho}{\partial y} g}{\left[\frac{\partial u}{\partial y}\right]^2} \right]_{y = Y_i} \tag{2.6}$$

where $\partial\rho/\partial y$ and $\partial u/\partial y$ are the local density and velocity gradients respectively.

From the experimental results, we have found that the mass transfer rates in the room correlate very well when plotted against an overall Richardson number that uses the interface height as the characteristic length and the average inflow velocity of fresh air into the room as the characteristic velocity. This form for Ri_o was derived from an assumption that the fresh air entered the room like a wall jet with a mixing layer separating the hot and cold layers (Figure 2.3). The mixing layer will grow with x and reach a stable thickness at a critical local Richardson number, $(Ri_x)_{cr}$. Beyond this point there is no mixing between the hot and cold layers (see Section 3.2).

2.5. Room Flow Patterns

The flow field within the room is sketched in Figure 2.3 where the flow is shown in two views. In the first, the viewing plane is the vertical plane perpendicular to the floor and including the centerline of the room and the door. The mixing (or shear) layer, which forms between the cool incoming flow and the hot ceiling gas, grows due to turbulent mixing up to a critical point, x_{cr}. Beyond this point, the effects of buoyancy are strong enough to suppress the mixing and entrainment processes, and the mass flux into the mixing layer stops. However, the layer does continue to move toward the back wall of the room and will eventually reach that wall and form a stagnation point flow in that impingement region. Thus, more mixing can occur there. Finally, the velocity profile in the cold jet will be affected by friction at the floor.

The second view in Figure 2.3 describes the flow in a plane parallel to the floor and slightly elevated above it. Mixing layers form between the cool jet of fresh air entering the through the door and the recirculating flows in the corners. Clearly, there will be a strong exchange between the cool gas in the door jet and the gas in the recirculation region. This exchange occurs as a result of entrainment along the shear layer, shown in this second view, and from the recirculation of shear layer gas required to supply material lost from the recirculation zone due to the entrainment process. In addition, hot gas from the ceiling layer will be entrained into this region across a horizontal surface which lies between the recirculation zone and the ceiling layer.

In the above picture, we assumed that the fluid velocities in the hot upper layer were negligible. In flow visualization experiments conducted in a salt water room model, Tangren, et. al. (1978) observed the existence of several counterflowing sublayers present in the ceiling layer. The flow in the upper layer is therefore very complicated and not well understood at the present time.

Because of the complex nature of the ceiling layer, we are forced to ignore the influence of currents present in that layer.

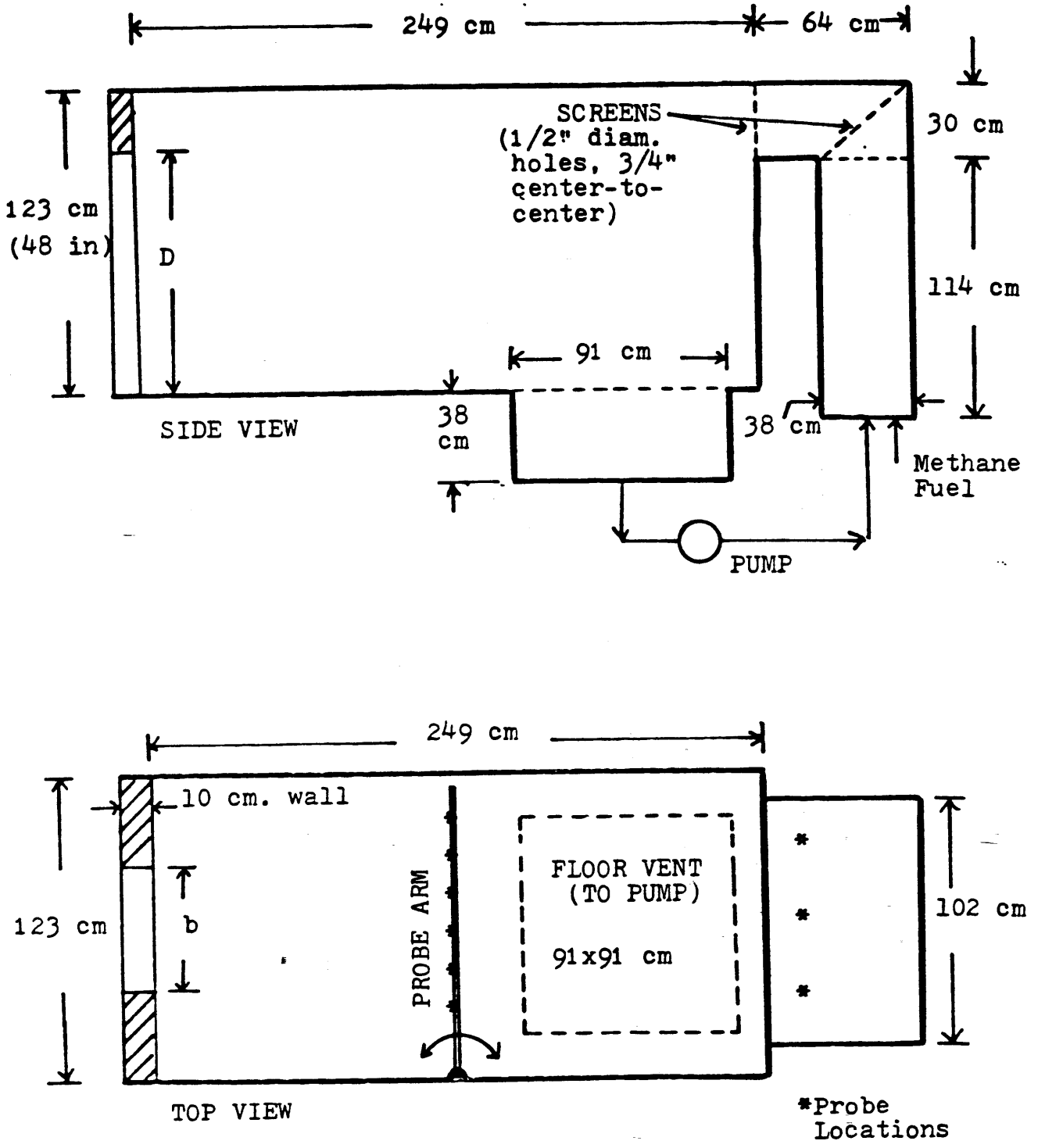
249 cm
64 cm
SCREENS
(1/2" diam. holes, 3/4" center-to-center)
30 cm
123 cm
(48 in)
D
114 cm
91 cm
SIDE VIEW
38 cm
38 cm
Methane Fuel
PUMP
249 cm
10 cm. wall
123 cm
b
PROBE ARM
FLOOR VENT
(TO PUMP)
91x91 cm
102 cm
TOP VIEW
*Probe Locations

Figure 2.1

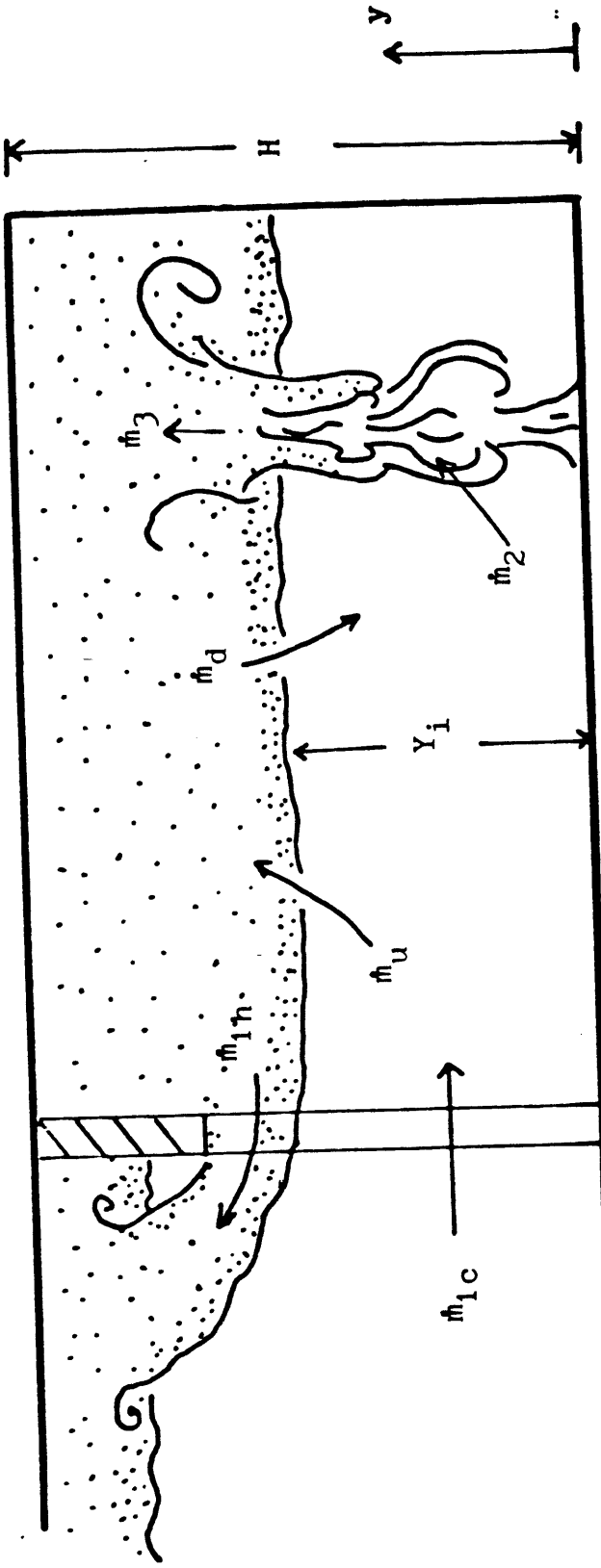

Figure 2.2 (a)

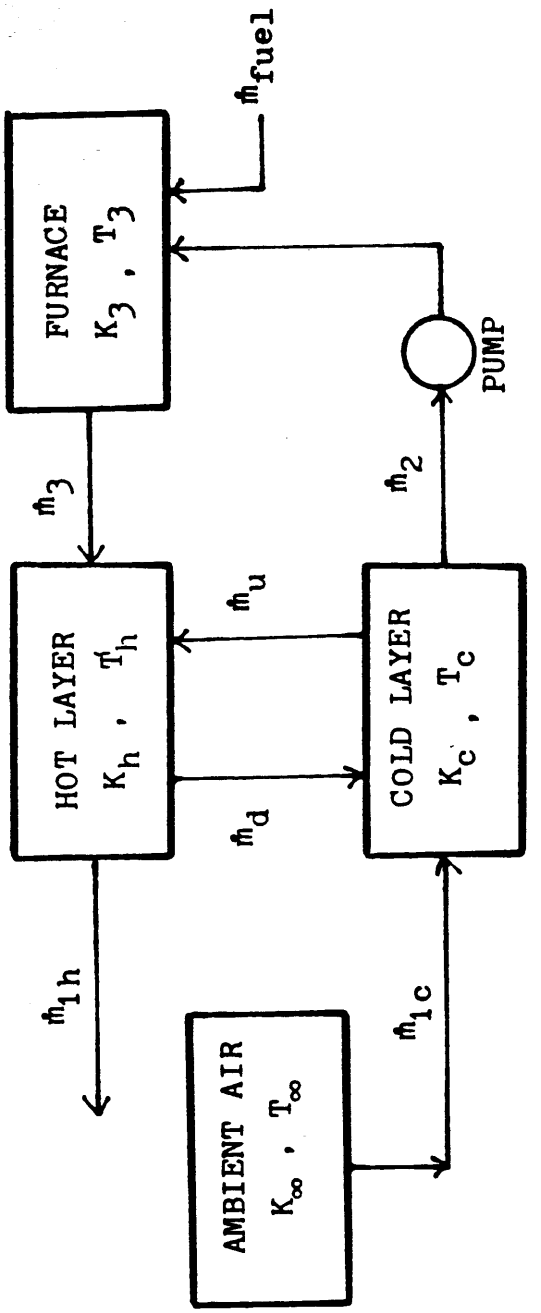
FURNACE
K_3 , T_3
$\dot{m}_{fuel}$
PUMP
$\dot{m}_3$
$\dot{m}_2$
HOT LAYER
K_h , T_h
$\dot{m}_u$
COLD LAYER
K_c , T_c
$\dot{m}_d$
$\dot{m}_{1h}$
$\dot{m}_{1c}$
AMBIENT AIR
K_∞ , T_∞

Figure 2.2(b)

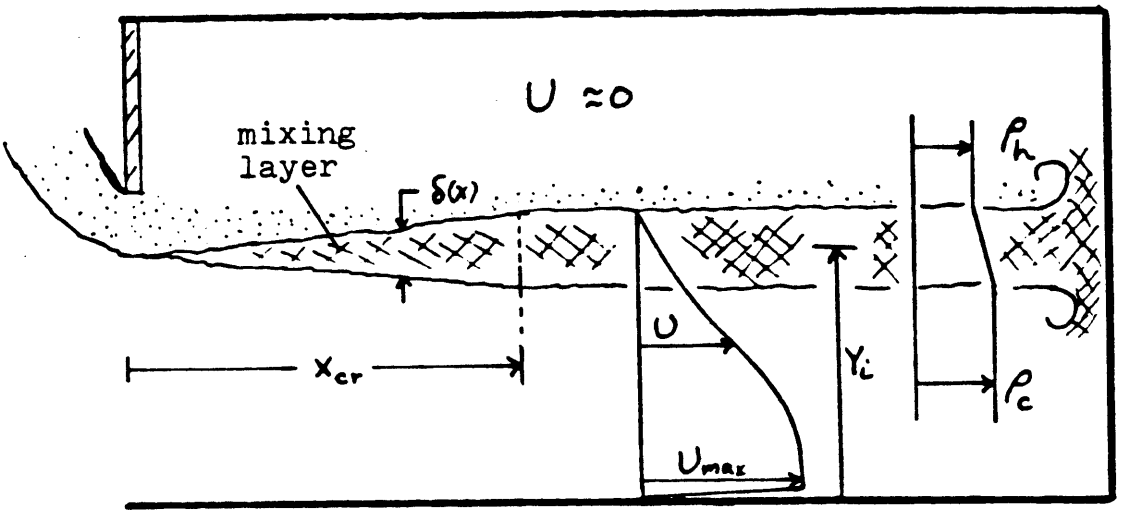
U ≈0
mixing
layer
δ(x)
x_{cr}
U
U_{max}
Y_i
ρ_h
ρ_c

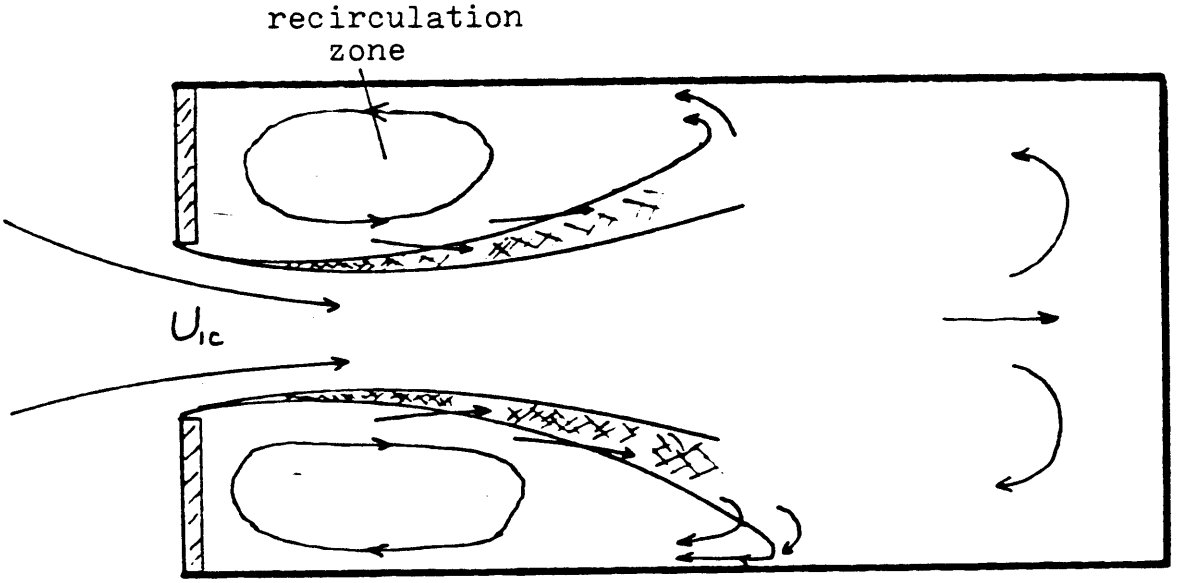
recirculation
zone
U_{ic}

Figure 2.3

Chapter 3

ROOM EXPERIMENTAL RESULTS

To determine the accuracy of the two-layer approximation, temperature measurements were made at various locations in the room (Figure 3.1). The measurements show that the vertical temperature profiles do not vary significantly in the room. Comparing the temperature profiles at corners A and E, it is observed that the temperature at the corner near the door (A) is about 10 to 20 degrees higher than in the corner near the furnace exit (E). Along the centerline (locations C,D,E), the temperature variation is less than 10 degrees Celsius. It may then be concluded that the room may be accurately approximated by the two-layer model. In the following experiments, we placed the probe in the center of the room and assumed that the vertical temperature and carbon dioxide profiles measured in the center of the room represent the average properties of the room gas.

Temperature and carbon dioxide concentration profiles in the center of the room were obtained for the following door geometries: 12"x39", 18"x39", 18"x24", and 12"x26" (width x height) doors. The temperature profile was used to estimate the density gradients, and the CO_2 profile was used to calculate the mass transfer rates.

3.1. Effect of Floor Suction Rate

We have studied the case where the furnace temperature was set at approximately 160 °C while the floor suction rate was varied from 0.03 kg/s to 0.20 kg/s. Typical temperature and carbon dioxide concentration profiles for low and high values of $\dot{m}_2$ are shown in Figure 3.2. For low values of $\dot{m}_2$, the interface is well above the floor and the carbon dioxide concentrations in the hot and

cold layers are sharply separated by a thin shear layer. For large values of $\dot{m}_2$, the interface is drawn very close to the floor and the boundary between shear layer and the cold layer becomes indistinguishable. It is also observed that for high interface heights, the temperature and the carbon dioxide profiles differ in shape in the hot layer but have a similar shape in the cold layer. On the other hand, when the interface is very close to the floor, both profiles have very similar shapes. Figure 3.3 is a dimensionless plot of Figure 3.2(a) where the ambient and furnace properties are used to normalize the temperature and carbon dioxide concentrations in the room. Figure 3.3 also demonstrates how we defined the interface height, Y_i.

3.1.1. *Temperature Profiles.* A comparison of Figures 3.2(a) and 3.2(b) shows that the slopes of the temperature profiles in the the shear layer do not change with interface height. Figure 3.4(a) shows the result when the dimensionless temperature profiles for the 12'x39" door are plotted as a function of distance from the interface for various values of $\dot{m}_2$. As expected, the dimensionless temperature profiles agree very well within the shear layer, but it is surprising that the profiles are also similar outside the shear layer. Figure 3.5(a) shows the temperature profiles when the door is widened. Again the profiles agree very well within and outside the shear layer.

Figure 3.6(a) shows the temperature profiles for the 12'x26" door which has the same aspect ratio as the 18'x39" door. Again the profile shapes are similar but the shape is substantially different from the profiles in Figures 3.4(a) and 3.5(a).

Figure 3.7(a) shows the profiles for the 18'x24" door. For low values of $\dot{m}_2$, the profiles are similar to those of the 12'x26" door. But when the floor suction rate is increased, the profiles become more similar to that of the 18'x39" and 12'x39" doors; i.e., the temperature distribution in the hot layer becomes more

uniform as $\dot{m}_2$ is increased.

3.1.2. *Carbon Dioxide Concentration Profiles.* Although the temperature profiles show good correlation when plotted against distance from the interface, the carbon dioxide concentration profiles are not similar to each other as is shown in Figure 3.4(b). This is because the slopes of the profiles are an indication of the amount of mixing between the hot and cold layers and, hence, we do not expect the slopes to be independent of $\dot{m}_2$. Figure 3.4(c) gives a clearer view of the effect of changing $\dot{m}_2$. As $\dot{m}_2$ is increased, the interface is drawn closer to the floor and the shear layer becomes thicker. Figures 3.5(b), 3.6(b), and 3.7(b) show the profiles for the other door geometries. Unlike the temperature profiles, the carbon dioxide concentration in the hot layer is constant regardless of door geometry. The difference between the shapes of the temperature and CO_2 profiles may be attributed to the fact that the mass transfer and heat transfer processes are not similar; the heat transfer from the hot gas occurs along the walls of the room as well as through the shear layer, while the mass transfer process between the hot gas and fresh air is essentially confined to the thin shear layer.

3.1.3. *Mixing between the Hot and Cold Layers.* For a given floor suction rate, the effect of decreasing the door area (lowering and/or narrowing the door) is to lower the interface and increase the velocity of the inflowing fresh air. This translates into a higher mixing rate in the room (see Table 3.1 on the following page). It is observed from Table 3.1 that the door height has a much stronger influence on the mixing rate and interface height than the door width.

The mixing process is dependent upon the Richardson number which was discussed in section 2.4. (In our experiments, the Reynolds number of the inflowing fresh air ranged from 5000 to 20,000; the flow is therefore turbulent and Reynolds number effects may be neglected.) From the experimental results,

Table 3.1. Effect of Door Geometry on the Mixing Rate

$\dot{m}_2$	Door Geometry	Y_i	$\dot{m}_d/\dot{m}_2$
0.146 kg/s	18" x 39"	19.7 in.	0.113
	12" x 39"	13.7 in.	0.180
	18" x 24"	6.5 in.	0.373
0.067 kg/s	18" x 39"	27.0 in.	0.015
	12" x 39"	25.4 in.	0.017
	18" x 24"	13.2 in.	0.104

we have found that the mixing rates correlated well when plotted against an overall Richardson number that has the interface height as the characteristic length and the inflow velocity of fresh air as the characteristic velocity. We propose that the appropriate form for the Richardson number is

$$Ri_o = \frac{\Delta\rho g Y_i}{\rho_\infty U_{1c}^2} \tag{3.1}$$

where Y_i is the interface height (see section 2.3), $\Delta\rho$ is $\rho_c - \rho_h$, the difference in density of the cold and hot layers, and U_{1c} is the average inflow velocity of fresh air through the door. If the pressure and molecular weight of the gas in the room are assumed to be nearly equal to the ambient pressure and molecular weight, the densities ρ_c, and ρ_h can be calculated by measuring the appropriate temperatures, i.e.,

$$\frac{\Delta\rho}{\rho_\infty} \equiv \frac{\rho_c - \rho_h}{\rho_\infty} \approx \frac{T_\infty}{T_c} - \frac{T_\infty}{T_h}. \tag{3.2}$$

The inflow velocity U_{1c} is estimated with the use of the the inflow mass flowrate, $\dot{m}_{1c}$; the interface height, Y_i; and the door width, b.

$$U_{1c} = \frac{\dot{m}_{1c}}{\rho_\infty b Y_i} \tag{3.3}$$

Experimental values of the ratio of the cold layer entrainment rate, $\dot{m}_d$, to the floor suction rate, $\dot{m}_2$, are shown in Figure 3.8 as a function of $Ri_0^{-1/2}$ for the four different door geometries used in the experiments. The experimental curve from a salt water model used by Tangren, et. al. (1978) is also shown in Figure 3.8 as a comparison with our gas model. The salt water technique is based on the use of water to model the unheated fluid medium and a flow of salt brine to represent the heat source. The salt water experiments were conducted in a 38 cm. x 38 cm. x 38 cm. room with a 4.6 cm. wide x 10 cm. high door. The fresh water to salt water density ratio was about 0.9. From Figure 3.8, we see that the mixing between the two layers is five times greater in the gas model than in the salt water model for a given value of Ri_0. It must be noted that the salt water technique ignores the effects of heat transfer and is accurate only for extremely weak fires. The salt water model simulates the mass transfer rates in an isothermal room, while in our experiments the mass transfer process is inherently connected with the temperature distribution in the room. For example, when the hot gas cools along the walls, the resulting denser gas flows down the wall into the mixing layer; this form of mass transfer is not present in the isothermal salt water experiment.

Two questions may arise concerning Figure 3.8: First, in the definition of the Richardson number, why did we use the interface height and the inflow velocity as the characteristic properties of the entire flow? Several different forms for the Richardson number were tried, and it was found (by trial and error) that Eq. 3.1 gave the best correlation for the data; we really have not presented any evidence that Eq. 3.1 is indeed the appropriate form for Ri_o. Second, because the door and room geometries are certainly important parameters, we question how do these parameters affect the mixing rates? In Figure 3.8, we note that that the spread of the data points may be reduced by multiplying $1/\sqrt{Ri_o}$ by b/W, where b is the door width and W is the room width (= 48 in. for our experiments). In fact, since (b/W) is about 0.3 for our gas experiments and about 0.12 for the salt water experiments, multiplying $1/\sqrt{Ri_o}$ by the parameter b/W would reduce significantly the large difference between the salt water and gas experimental data in Figure 3.8. In the next section, we will present a simple entrainment model in which we will make an attempt to find the exact relationship between the mixing rates and the parameters Ri_o, b, and W.

3.2. Entrainment Model

As was pointed out in Sec. 2.5, the flow under study is clearly a very complex one, even when we ignore the currents which are present in the ceiling layer. The analysis which follows is more in the nature of a complex dimensional analysis than an attempt to derive flow properties from first principles. Our aim is to develop the scaling parameters in a rational manner. The analysis ignores the influence of the counterflowing jets at the door and the mixing in the impingement region near the back wall opposite the door.

The relationship between the mixing rates and Ri_o may be derived from an assumption that the fresh air enters the room like a turbulent wall jet with a mixing layer separating the hot and cold layers (Figure 2.3). This mixing layer

will grow with x (the distance normal to the door) and reach a stable thickness at a critical local Richardson number, $(Ri_x)_{cr} \approx 0.25$ (Scotti & Corcos 1972). (The term "local Richardson number" refers to the gradient Richardson number at the interface; see section 2.4.) Beyond this point there is no mixing between the hot and cold layers.

The jet may then be divided into two distinct regions: the "supercritical" region where the flow is independent of the downstream conditions and has entrainment characteristics similar to a neutral wall jet; and the "subcritical" region where gravitational forces suppress the mixing between the hot and cold layers. The supercritical and subcritical regions are separated by a not well-defined "hydraulic (or density) jump" region which is characterized by the breaking of internal waves and reverse flow (Chu & Vanvari 1976).

Behind the door, there is a recirculation region which actively exchanges material with both the hot layer and the door jet (Fig. 2.3). Since the flow is steady, the amount of hot layer gas entrained into the recirculation region is equal to the amount of material lost to the door jet. In other words, the door jet is entraining hot layer gas indirectly through the recirculation region. As far as the entrainment process is concerned, it follows then that we may approximate the actual three-dimensional jet whose width varies with x by an "equivalent" two-dimensional jet with a width equal to that of the room. Instead of an initial jet velocity of U_{1c}, the equivalent two-dimensional jet will have an initial velocity of $U_{1c}b/W$. This is equivalent to saying that the jet expands suddenly and instantaneously from an initial width of b (the door width) to a final width of W (the room width). It must be noted that this assumption is a rather drastic simplification of the actual flow.

The basic assumption of the following analysis is that the entrainment characteristics of the inflowing fresh air is similar to that of a two-dimensional

wall jet flowing under a semi-infinite layer of lighter gas; i.e., wall effects and the velocity of the hot layer gas are taken to be negligible. Taylor's entrainment hypothesis (Morton, et. al. 1956) states that the local entrainment rate into a jet is proportional to the local maximum velocity and the local entrainment coefficient, i.e.,

$$\frac{d\dot{m}_d(x)}{dx} = \rho_h E(Ri_x) U_{max}(x) W \tag{3.4}$$

where $\dot{m}_d(x)$ is the mass flowrate of hot layer gas entrained into the mixing layer from the door ($x = 0$) to station x (the x-axis is the axis normal to the plane of the door); $E(Ri_x)$ is the local entrainment coefficient; and $U_{max}(x)$ is the local maximum velocity of the two-dimensional wall jet.

The entrainment coefficient, E, is a function of the local Richardson number and a function of x since $Ri_x = Ri_x(x)$ (Ellison & Turner 1959). As a first approximation, we will use a simple power law relation between E and x:

$$E(x) = E_0\left[1 - \frac{x}{x_{cr}}\right]^n \tag{3.5}$$

where x_{cr} is defined by $Ri_x(x_{cr}) \equiv (Ri_x)_{cr}$, and E_0 and n are constants to be determined experimentally. For neutral (constant density) wall jets, $E(x) = E_0$ = constant. From the experimental data of Chu & Vanvari (1976), we found that

$$E(Ri_x) \approx 0.036\left[1 - \frac{Ri_x}{(Ri_x)_{cr}}\right]^2 .$$

If we assume that $Ri_x(x) \propto x$ (Scotti & Corcos 1972), the constants E_0 and n in

Eq. 3.5 are 0.036 and 2 respectively.

Since we have not made any measurements of the velocity profiles in the room, we do not know the exact relation between U_{max} and x. To complicate the problem, the jet may be divided into three regions with a different relationship between U_{max} and x for each region (Abramovich 1963): (1) the near field (potential core) region where U_{max} = constant; (2) the far field (self-preserving) region where $U_{max} \propto x^{-n}$, $n > 0$; and (3) a transition region between the near field and far field, usually between 5 and 15 diameters downstream of the jet exit. With few exceptions, most of our entrainment data fall within the transition region. However, we are able to avoid the problems involved in using U_{max} by introducing an alternate velocity scale based on the momentum of the jet (see Appendix A.2):

$$\dot{m}(x)\, U^*(x) = \dot{m}_{1c}\, U_{1c}\, \frac{b}{W} \tag{3.6}$$

where $U^*(x)$ is the new velocity scale; $\dot{m}_{1c}\, U_{1c}$ is the initial jet momentum; $\dot{m}(x) = \dot{m}_{1c} + \dot{m}_d(x)$, the total mass flow at station x; b is the door width; and W is the room width. The term $(\dot{m}_{1c}\, U_{1c})(b/W)$ is the momentum of the jet after the loss due to the sudden expansion of the jet width (from b to W) has been taken into account. The basic assumption of Eq. 3.6 is that the total momentum of the jet does not vary significantly in the supercritical (momentum-dominated) region where the entrainment process takes place, i.e., we have assumed that the losses due to the presence of pressure gradients and wall friction are negligible compared to $(\dot{m}_{1c}\, U_{1c})(b/W)$. In the far field region, U_{max} may be shown to be related to U^* by (see Appendix A.3)

$$U_{max}(x) = A_1 U^*(x) = A_1 \frac{\dot{m}_{1c} U_{1c}}{\dot{m}_{1c} + \dot{m}_d(x)} \frac{b}{W} \tag{3.7}$$

where A_1 is a constant which must be determined experimentally. After substituting Eqs. 3.3, 3.5, 3.6 and 3.7 into Eq. 3.4, we have

$$\left[\frac{\dot{m}_d(x)}{\dot{m}_{1c}} + 1\right] \frac{d(\dot{m}_d(x)/\dot{m}_{1c})}{d(x/Y_1)} = A_1 E_0 \frac{\rho_h}{\rho_\infty} \left[1 - \frac{x}{x_{cr}}\right]^n . \tag{3.8}$$

This equation is valid for the self-preserving region of a turbulent, two-dimensional, constant momentum jet. Note that, since $U^* \to (b/W)U_{1c}$ as $x \to 0$, the solution to Eq. 3.8 may extend as far upstream as the near field (potential core) region. If we assume that buoyancy effects prevent mixing for $x > x_{cr}$, the total entrainment rate, $\dot{m}_d = \dot{m}_d(x_{cr})$, can be found by integrating Eq. 3.8 from $x = 0$ to $x = x_{cr}$:

$$\frac{1}{2}\left[\frac{\dot{m}_d}{\dot{m}_{1c}}\right]^2 + \frac{\dot{m}_d}{\dot{m}_{1c}} = A_1 \frac{E_0}{n+1} \frac{\rho_h}{\rho_\infty} \left[\frac{x_{cr}}{Y_1}\right] . \tag{3.9}$$

The critical length, x_{cr}, may be calculated from the definition of the critical local Richardson number, $(Ri_x)_{cr}$:

$$(Ri_x)_{cr} = Ri_x(x_{cr}) = \left[\frac{-\frac{1}{\rho}\frac{\partial \rho}{\partial y} g}{\left[\frac{\partial U}{\partial y}\right]^2}\right]_{x = x_{cr},\, y = Y_1} . \tag{3.10}$$

To evaluate the right hand side of Eq. 3.10, we will make the following approximations for the density gradient:

$$\left[-\frac{1}{\rho}\frac{\partial \rho}{\partial y}\right]_{y=Y_i} \approx \frac{1}{\delta(x)}\frac{\rho_c - \rho_h}{\rho_h} = \frac{1}{\delta(x)}\frac{\Delta\rho}{\rho_h} \tag{3.11}$$

where $\delta(x)$ is the thickness of the mixing layer at station x. For the velocity gradient, we assume that (cf. Chu & Vanvari 1976)

$$\left[\frac{\partial U}{\partial y}\right]_{y=Y_i} \approx \frac{U_{max}(x)}{\delta(x)}. \tag{3.12}$$

For the growth rate of the mixing layer, we will assume that (Abramovich 1963):

$$\delta(x) = A_2 x, \qquad (x < x_{cr}) \tag{3.13}$$

where A_2 is approximately 0.23 for two-layer stratified flows with a density ratio of about 1.4 (Abramovich 1963). After substituting Eqs. 3.11 to 3.13 into 3.10 and using Eq. 3.7 to evaluate U_{max}, we have

$$\begin{aligned}(Ri_x)_{cr} &= \frac{\Delta\rho\, g\, \delta(x_{cr})}{\rho_h\, U_{max}^2(x_{cr})} \\ &= \frac{\Delta\rho\, g\, A_2 x_{cr}}{\rho_h A_1^2 \left[\dfrac{\dot{m}_{1c} U_{1c}}{\dot{m}_{1c} + \dot{m}_d(x_{cr})}\dfrac{b}{W}\right]^2}.\end{aligned} \tag{3.14}$$

Eq. (3.14) may then be rearranged to find $\frac{x_{cr}}{Y_i}$:

$$\frac{x_{cr}}{Y_i} = \left[\frac{A_1^2}{A_2}(Ri_x)_{cr}\frac{\rho_h}{\rho_\infty}\left[\frac{b}{W}\right]^2\frac{1}{Ri_0}\right]\left[\frac{\dot{m}_{1c}}{\dot{m}_{1c} + \dot{m}_d(x_{cr})}\right]^2 \tag{3.15}$$

where Ri_o is the overall Richardson number defined in Eq. 3.1. The equation for the entrainment rate into the cold layer is finally obtained by substituting Eq. 3.15 into Eq. 3.9:

$$\left[\frac{1}{2}\left[\frac{\dot{m}_d}{\dot{m}_{1c}}\right]^2 + \frac{\dot{m}_d}{\dot{m}_{1c}}\right]\left[1 + \frac{\dot{m}_d}{\dot{m}_{1c}}\right]^2 = A F^2 \tag{3.16a}$$

where

$$A = \frac{A_1^3}{A_2}\frac{E_0}{n+1}(Ri_x)_{cr} \tag{3.16b}$$

$$F = \frac{\rho_h}{\rho_\infty}\frac{b}{W}\frac{1}{\sqrt{Ri_o}}. \tag{3.16c}$$

Using the relationship suggested by Eq. 3.16, the experimental data are replotted in Figure 3.9. From our data, we found the mean value of the empirical constant A to be 11.7 ± 5.3. When we use the mean value of A, Eq. 3.16a becomes

$$\left[\frac{1}{2}\left[\frac{\dot{m}_d}{\dot{m}_{1c}}\right]^2 + \frac{\dot{m}_d}{\dot{m}_{1c}}\right]\left[1 + \frac{\dot{m}_d}{\dot{m}_{1c}}\right]^2 = 11.7 F^2 \tag{3.17}$$

This is the equation of solid line shown in Figure 3.9. Despite the large deviation of the empirical constant, A, which is attributable to the numerous simplifying assumptions we had made, our simple analysis accurately predicts the shape of the curve. Our analysis did not take into account the following: (1) three-dimensional effects (see, for example, Sforza & Herbst 1970); this would mean that the maximum velocity decay, U_{max}, the entrainment coefficient, E, and the rate of growth of the mixing layer layer may be functions of the door geometry; (2) the presence of the wall normal to the flow has not been taken into account,

i.e., we have not considered the effect of the jet impinging on the wall; (3) the losses due to the presence of wall friction and pressure gradients in the room may be large in certain portions of the room; this is certainly true far downstream of the door where the influence of the wall boundary layer and wall heat transfer are no longer negligible; (4) effect of a counterflowing hot layer.

We can estimate the value of A_1 from our data with the aid of the following relationships obtained from the literature: (1) for the critical Richardson number: $(Ri_x)_{cr} \approx 0.25$ (Scotti & Corcos 1972); (2) for the entrainment coefficient: $E_0 \approx 0.036$ and $n \approx 2$ (Chu & Vanvari 1976); (3) for the growth rate of the mixing layer: $A_2 \approx 0.23$ (Abramovich 1963). With these relationships, we found the mean value of the empirical constant A_1 to be 9.46 ± 1.37 for our range of experiments. The value of A_1 is dependent on the shape of the velocity profile; as a comparison, A_1 is approximately 1.4 for a Gaussian velocity profile (see Appendix A.3).

3.3. Effect of Furnace Temperature

To determine the effect of the magnitude of the furnace temperature, we ran a series of experiments in which the floor suction rate, $\dot{m}_2$, was held constant while the furnace temperature was varied.

The temperature and carbon dioxide concentration profiles for the 12"x26" door are presented in Figure 3.10. As the furnace temperature is decreased the temperature gradient in the hot layer is reduced, and the temperature and carbon dioxide concentration profile shapes become more and more similar. It is interesting to note that, even though the maximum temperature in the hot layer was lowered from 150 °C to 65 °C, the temperatures in the cold layer did not change significantly. The carbon dioxide profiles show a similar behavior. This phenomenon can be explained by the fact that reducing the temperature of the hot gas will reduce the buoyant energy of the hot layer and hence increase

the rate of mixing between the hot and cold layers. Apparently, the increase in mixing rates is just enough to keep the temperature and carbon dioxide concentrations in the cold layer constant. The mixing rates versus Richardson number are plotted in Figures 3.8 and 3.9 as a comparison with the previous results where the furnace temperature was held constant. The data agree very well, and it is observed that the mixing rate increased by a factor of 2.3 when the furnace temperature was reduced by a factor of 1.3. Note that the correlation between the 12"x26" door data points in Figure 3.9 is much better than in Figure 3.8. This suggests that the density ratio, ρ_h/ρ_∞, is an important factor in Eq. 3.16. To summarize: the mixing rate between the hot and cold layers is strongly influenced by the ratios b/W and ρ_h/ρ_∞ in addition to the overall Richardson number defined by Eq. 3.1.

Figure 3.10(c) shows the dimensionless temperature as a function of distance from the interface. As in the case where we held the furnace temperature constant (Figure 3.6(a)), the profiles are similar in shape for furnace temperatures above 67 °C.

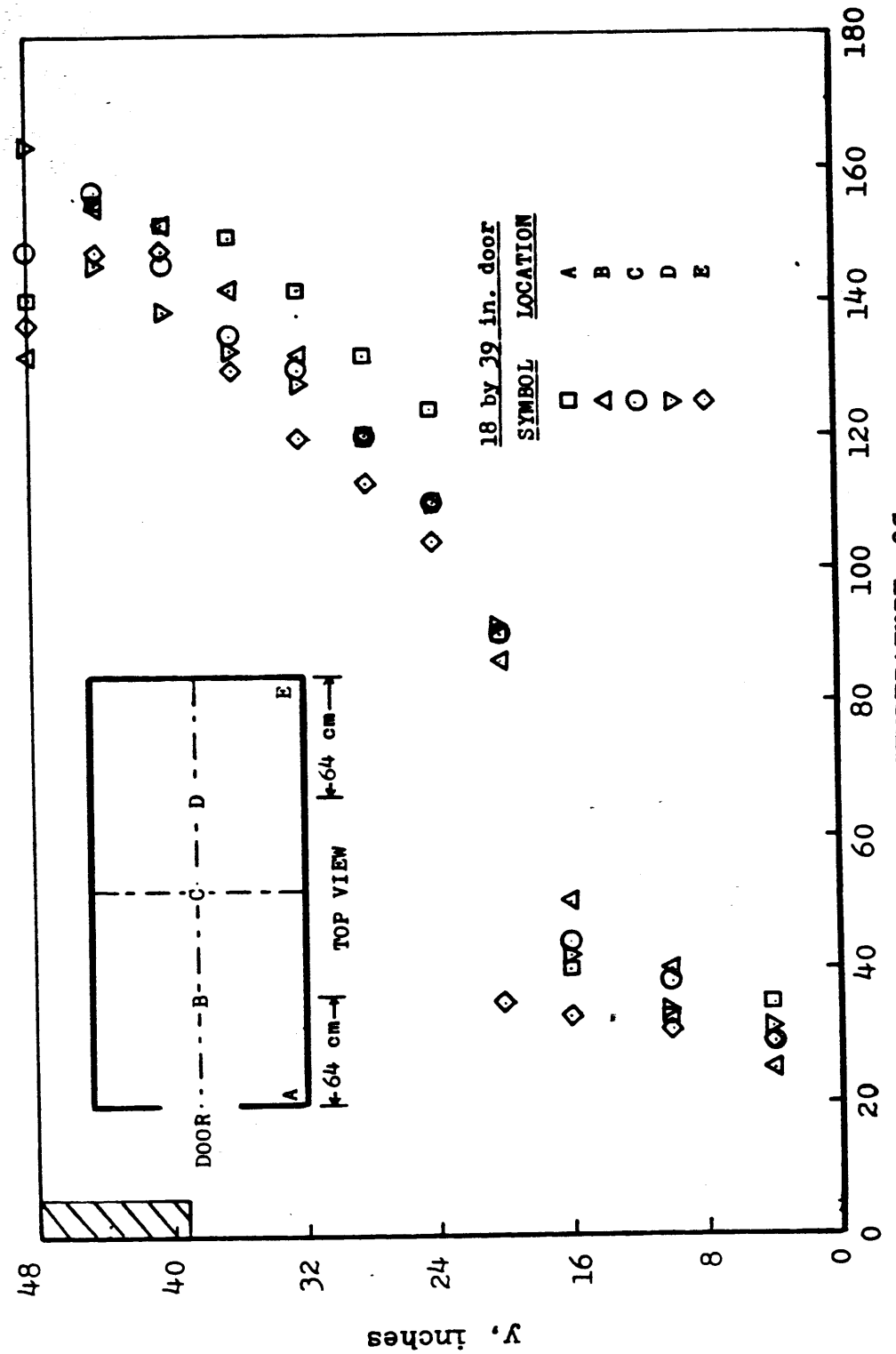
y, inches
TEMPERATURE, °C
18 by 39 in. door
SYMBOL LOCATION
A
B
C
D
E
TOP VIEW
64 cm
64 cm
DOOR
A
B
C
D
E
0
8
16
24
32
40
48
0
20
40
60
80
100
120
140
160
180

Figure 3.1

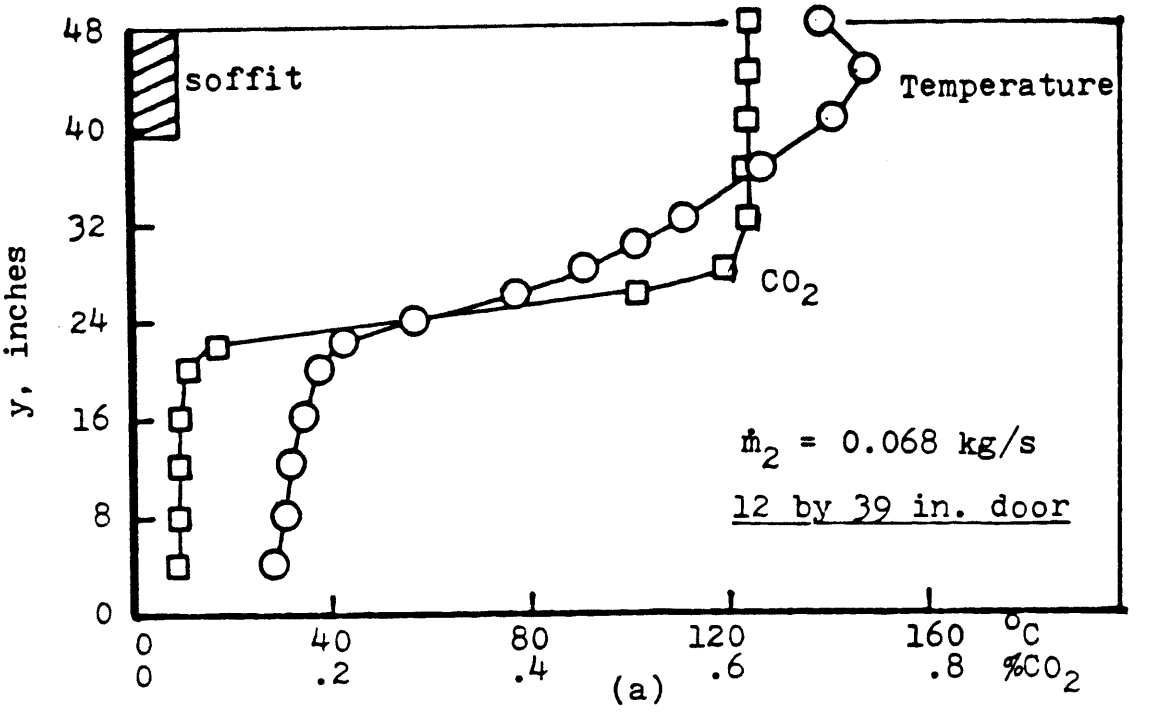
48
40
32
24
16
8
0
y, inches
soffit
Temperature
CO_2
$\dot{m}_2$ = 0.068 kg/s
12 by 39 in. door
0
0
40
.2
80
.4
120
.6
160
.8
°C
$\%CO_2$
(a)

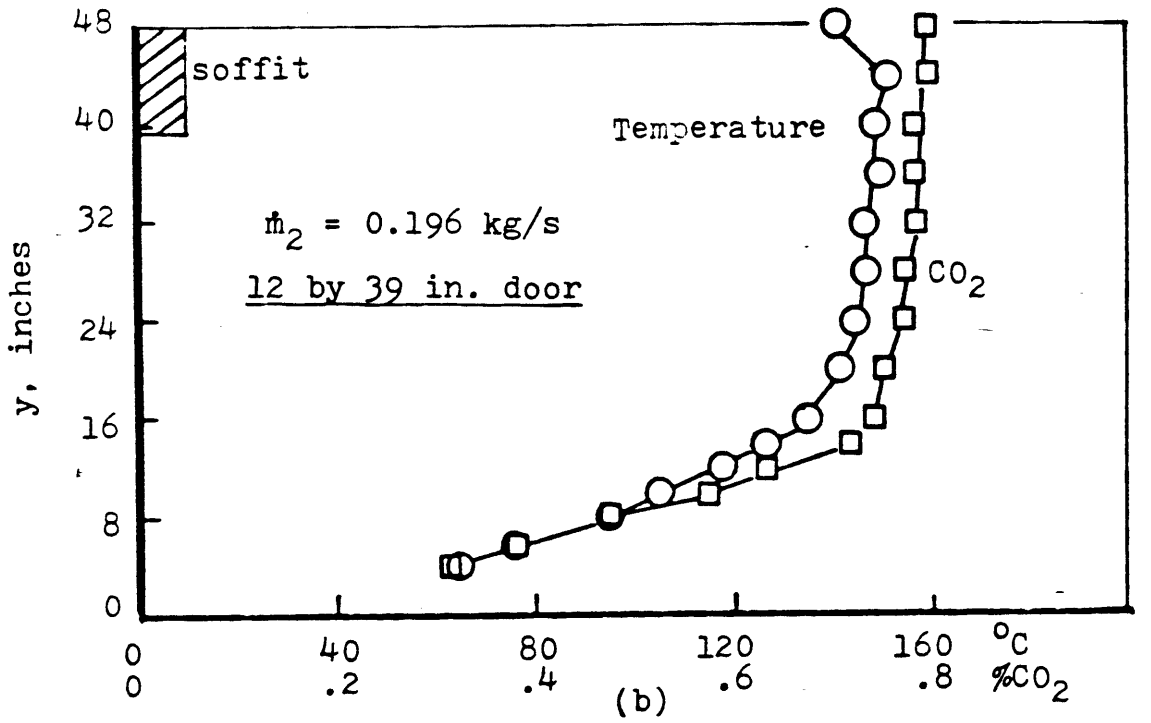
48
40
32
24
16
8
0
y, inches
soffit
Temperature
$\dot{m}_2$ = 0.196 kg/s
12 by 39 in. door
CO_2
0
0
40
.2
80
.4
120
.6
160
.8
°C
$\%CO_2$
(b)

Figure 3.2

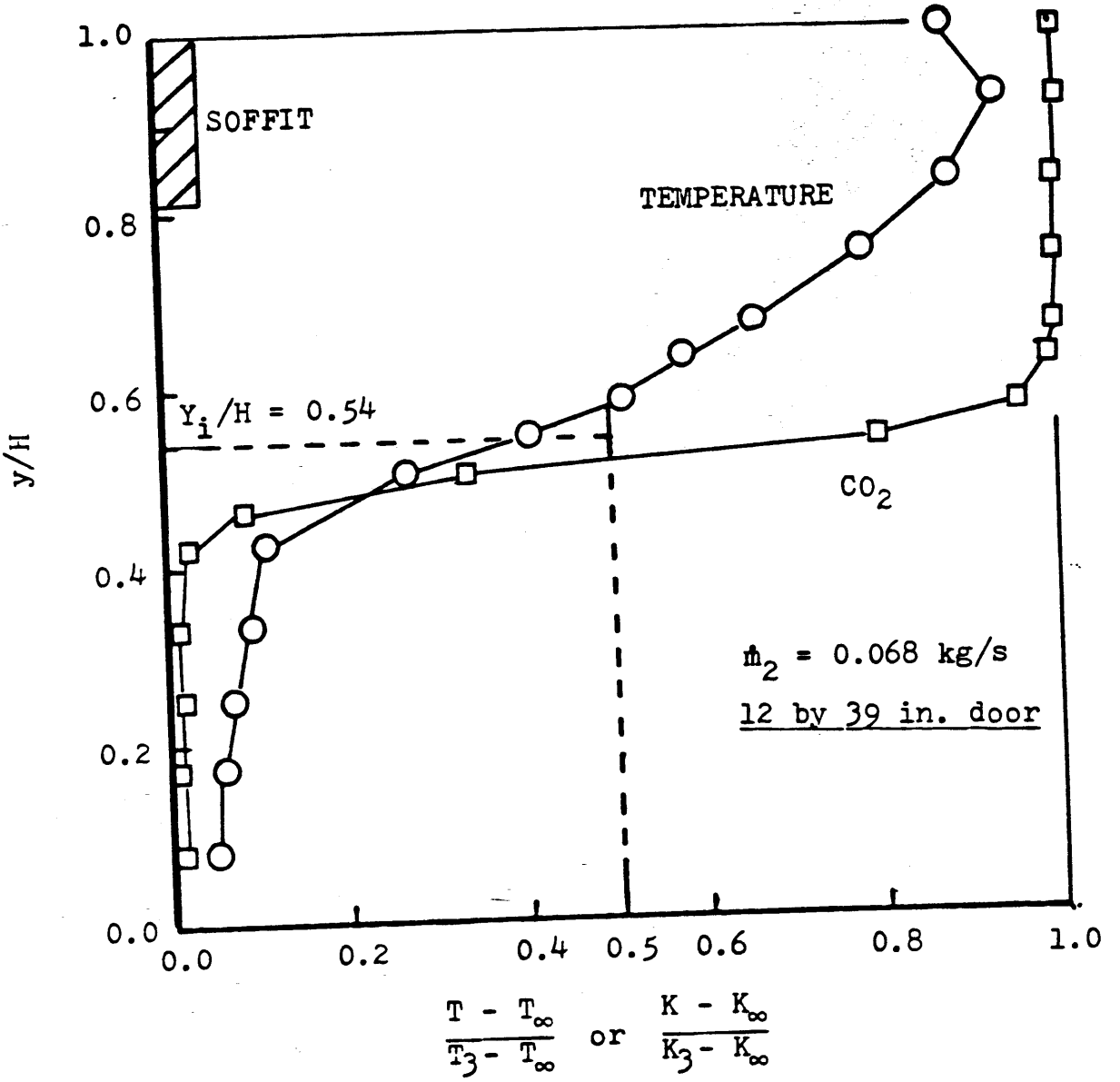
1.0
0.8
0.6
0.4
0.2
0.0
y/H
SOFFIT
TEMPERATURE
$Y_i/H = 0.54$
CO_2
$\dot{m}_2$ = 0.068 kg/s
12 by 39 in. door
0.0
0.2
0.4
0.5
0.6
0.8
1.0
$\frac{T - T_\infty}{T_3 - T_\infty}$ or $\frac{K - K_\infty}{K_3 - K_\infty}$

Figure 3.3

Legend for Figures 3.4 (a,b,c)

Symbol	$\dot{m}_2$, kg/s	Y_i, in.	Run
◇	0.196	7.0	41
△	0.147	13.7	39
+	0.112	17.8	42
▽	0.100	21.1	43
○	0.068	25.4	38
□	0.044	31.2	40

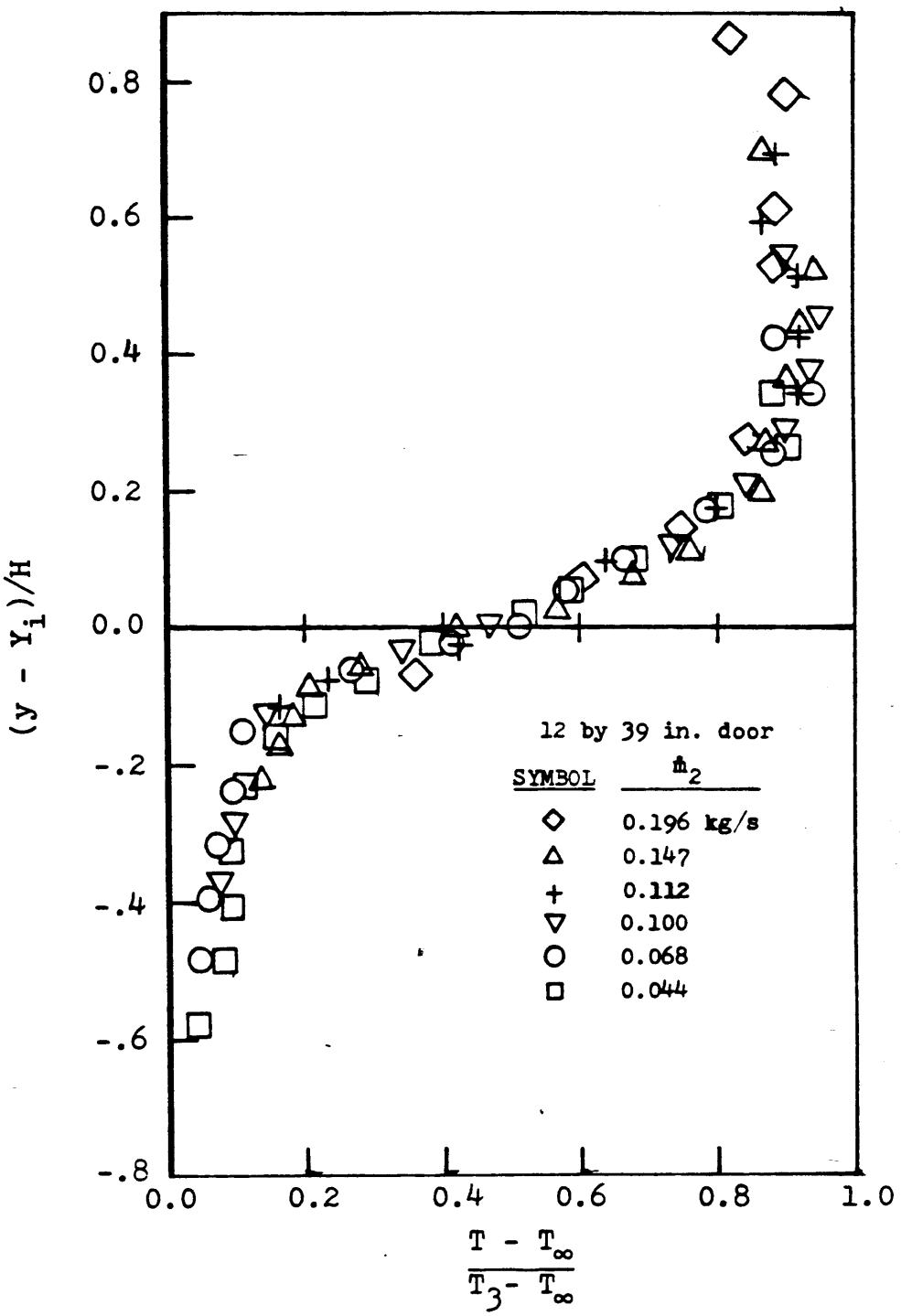
0.8
0.6
0.4
0.2
0.0
-.2
-.4
-.6
-.8
0.0
0.2
0.4
0.6
0.8
1.0
(y - Y_i)/H
(T - T∞)/(T3 - T∞)
12 by 39 in. door
SYMBOL
ṁ2
0.196 kg/s
0.147
0.112
0.100
0.068
0.044

Figure 3.4(a)

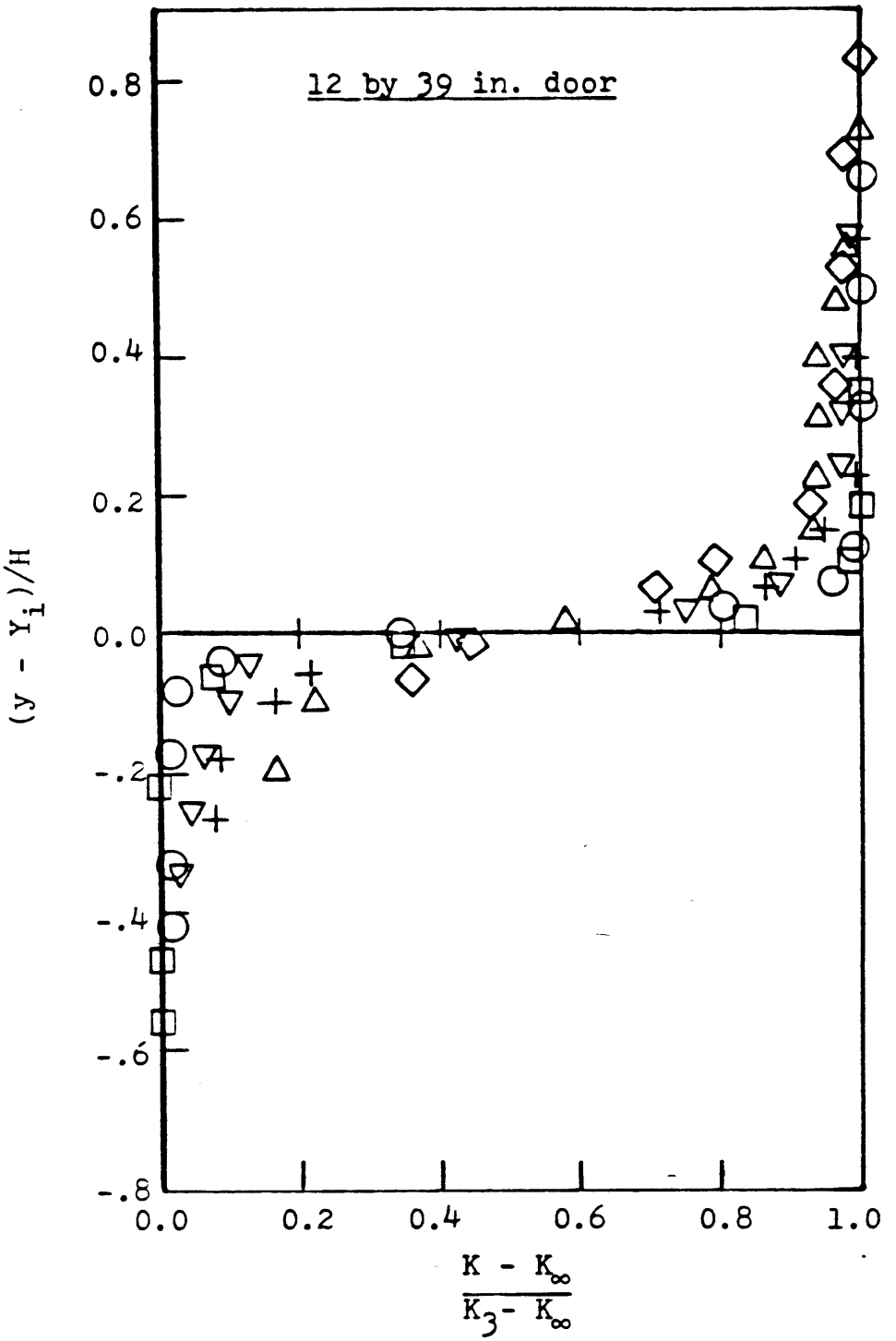

Figure 3.4(b)

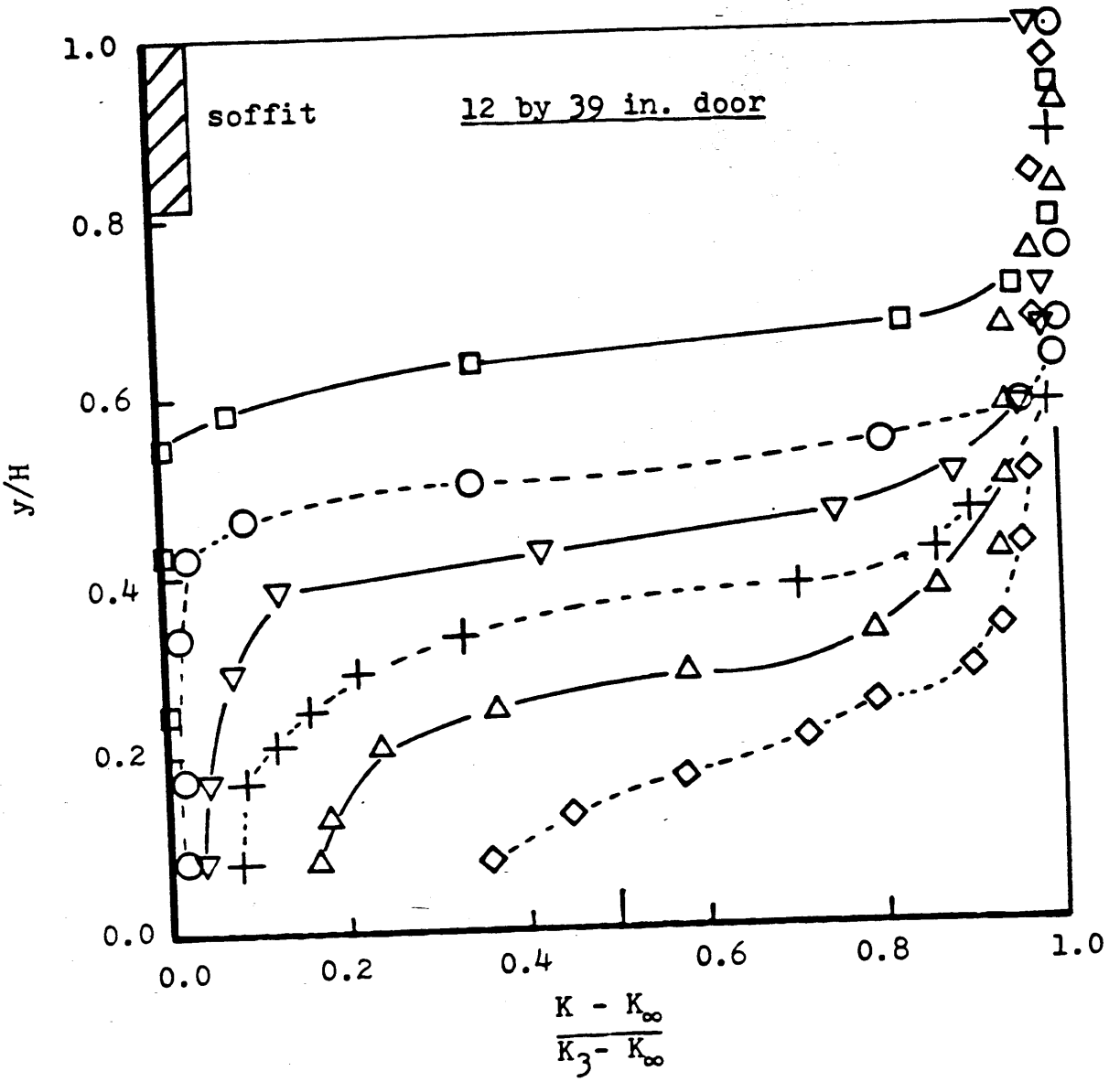

Figure 3.4(c)

Legend for Figures 3.5 (a,b)

Symbol	$\dot{m}_g$, kg/s	Y_i, in.	Run
⬡	0.200	11.5	31
◇	0.186	14.0	28
△	0.176	14.9	26
▽	0.165	17.3	30
□	0.146	19.7	25
○	0.076	27.6	24
+	0.037	34.3	29

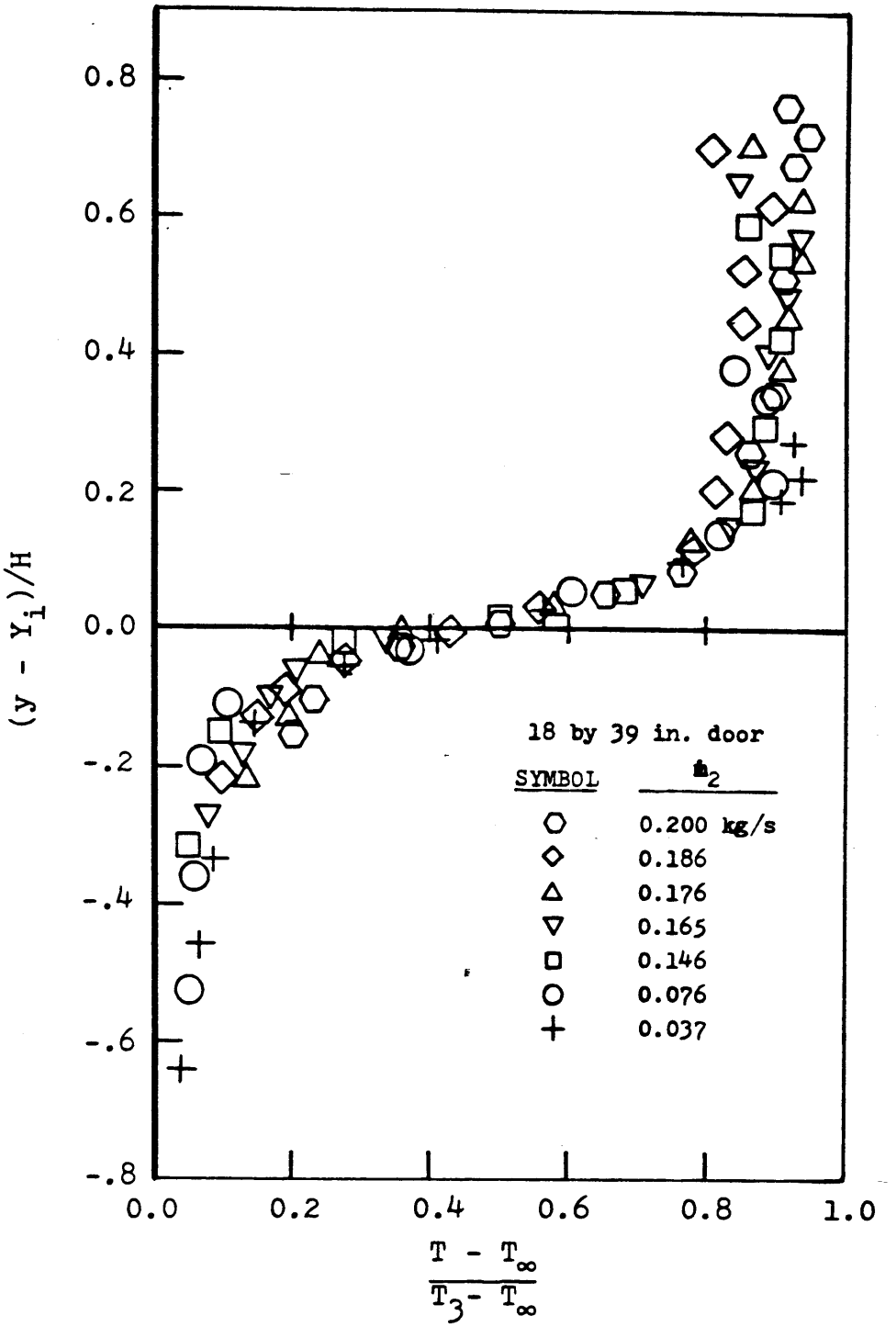
0.8
0.6
0.4
0.2
0.0
-.2
-.4
-.6
-.8
0.0
0.2
0.4
0.6
0.8
1.0
(y - Y_i)/H
(T - T∞)/(T3 - T∞)
18 by 39 in. door
SYMBOL
ṁ2
0.200 kg/s
0.186
0.176
0.165
0.146
0.076
0.037

Figure 3.5(a)

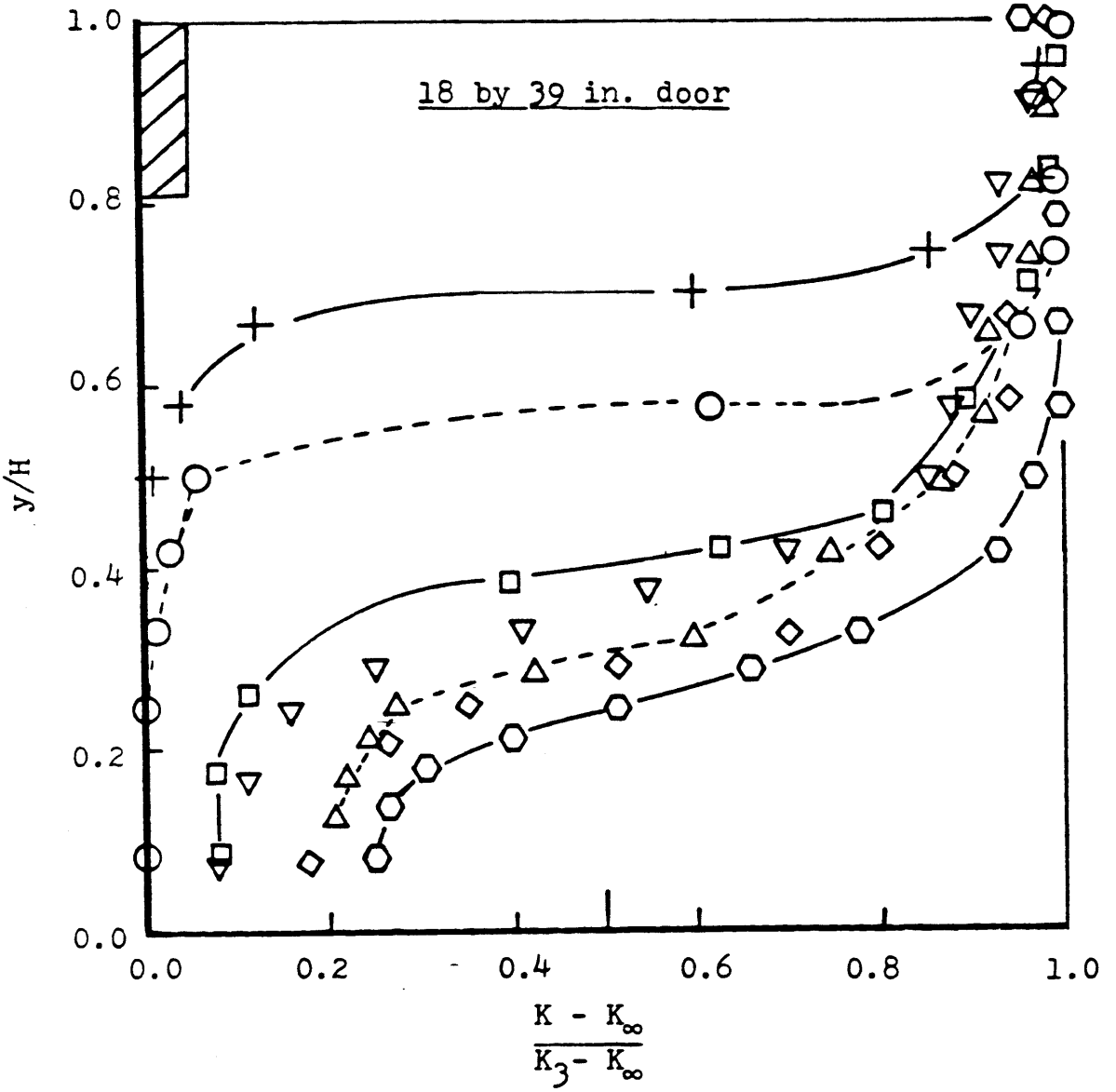

Figure 3.5(b)

Legend for Figures 3.6 (a,b)

Symbol	$\dot{m}_p$, kg/s	Y_i, in.	Run
⬡	0.094	7.2	49
◇	0.078	9.1	47
○	0.067	11.0	44
▽	0.057	13.4	48
□	0.044	15.4	45
△	0.033	18.7	46

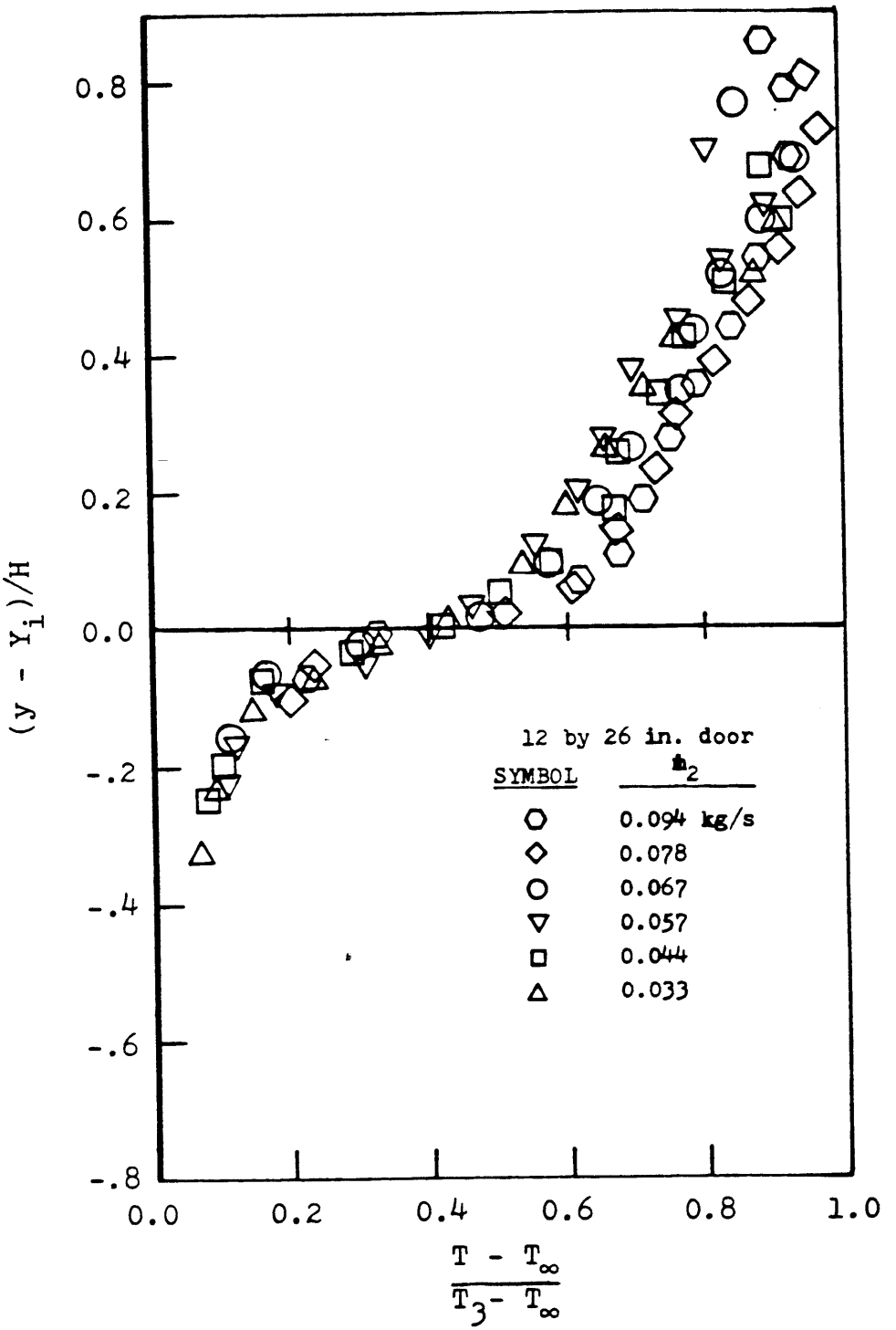
0.8
0.6
0.4
0.2
0.0
-.2
-.4
-.6
-.8
0.0
0.2
0.4
0.6
0.8
1.0
(y - Yi)/H
T - T∞ / T3 - T∞
12 by 26 in. door
SYMBOL
ṁ2
0.094 kg/s
0.078
0.067
0.057
0.044
0.033

Figure 3.6(a)

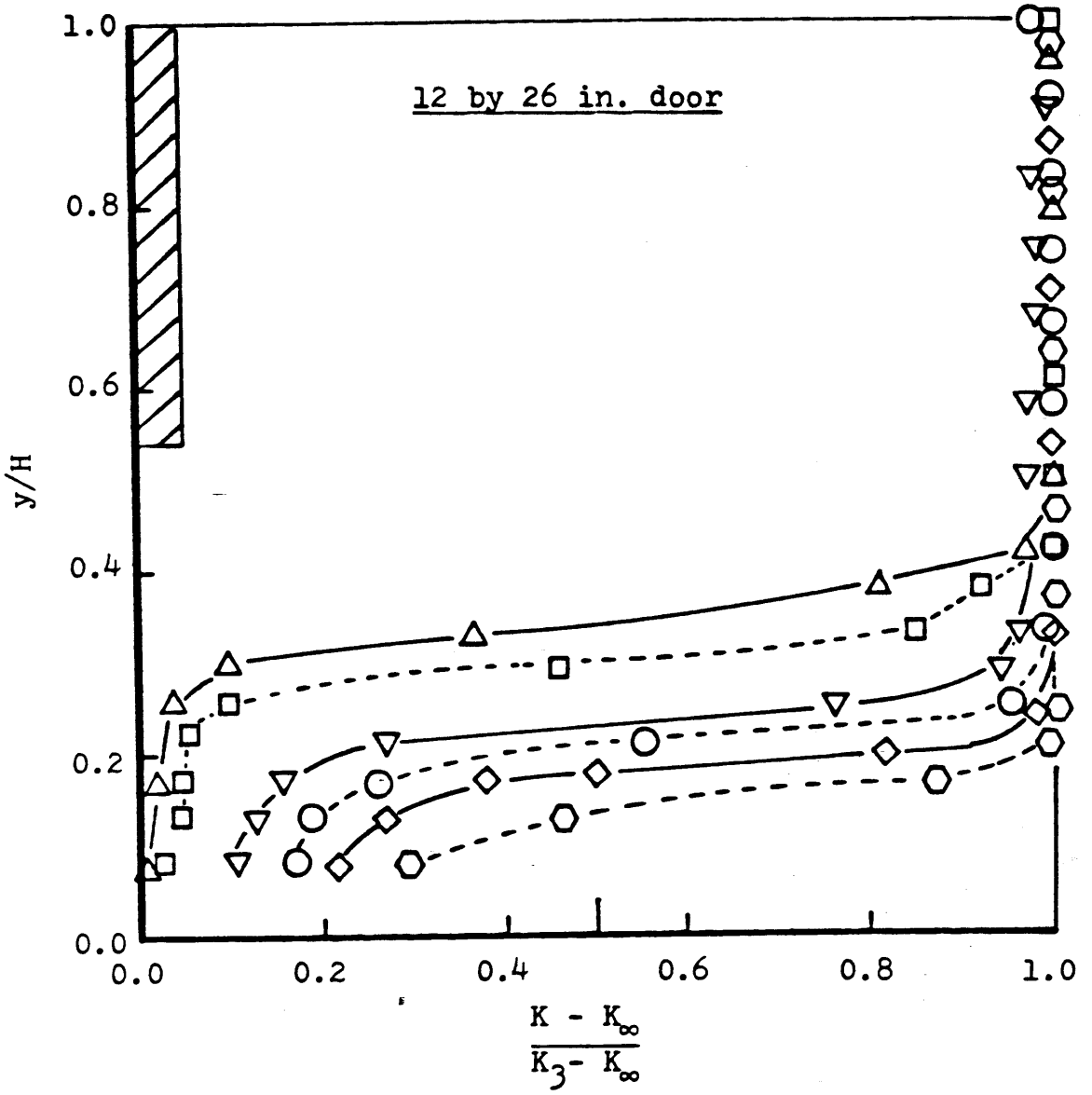

Figure 3.6(b)

Legend for Figures 3.7 (a,b)

Symbol	$\dot{m}_2$, kg/s	Y_1, in.	Run
△	0.208	4.3	34
▽	0.146	6.5	36
⊙	0.067	11.0	32
◇	0.067	13.2	35
⬡	0.050	15.8	37
□	0.030	18.2	33

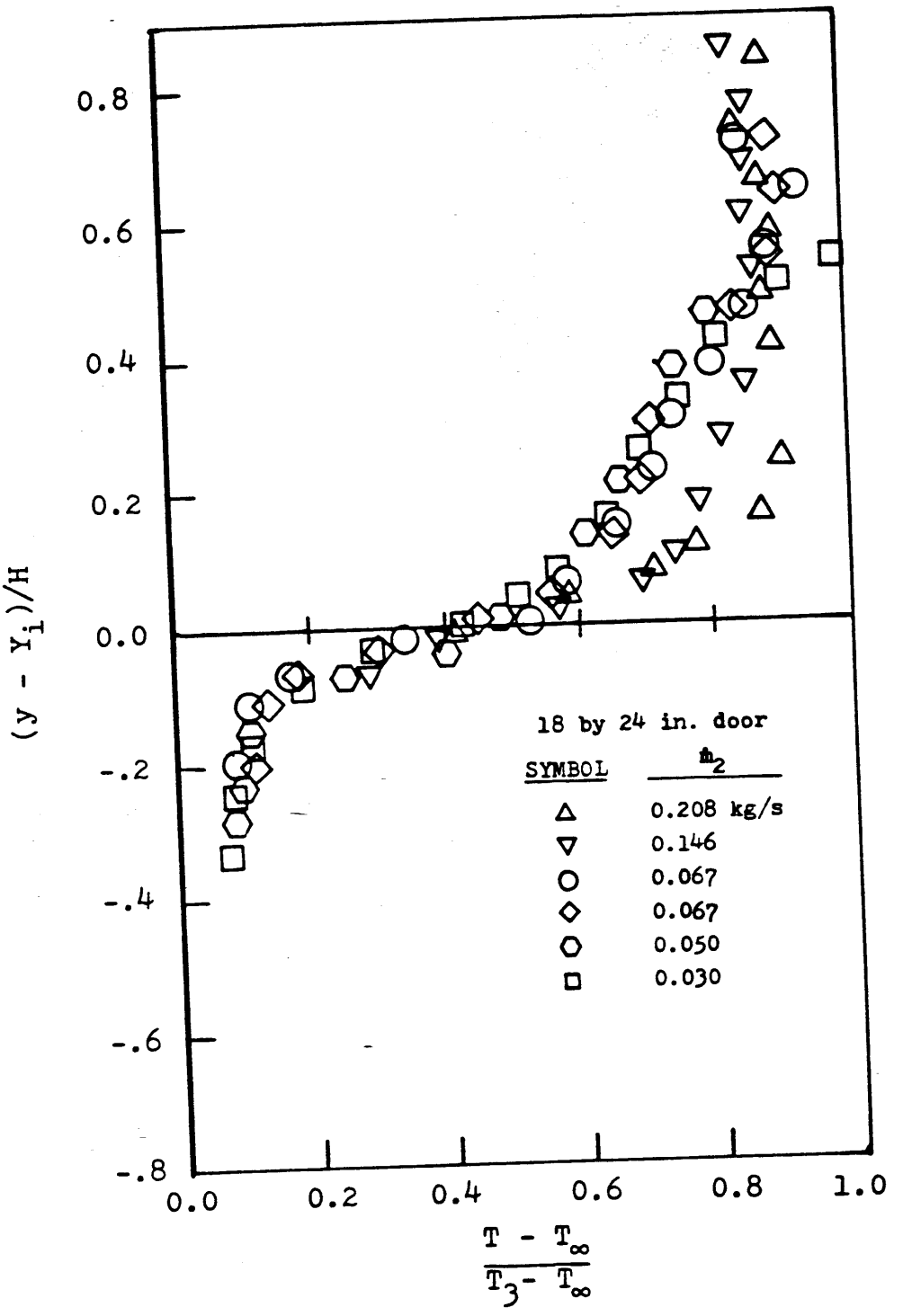
0.8
0.6
0.4
0.2
0.0
-.2
-.4
-.6
-.8
0.0
0.2
0.4
0.6
0.8
1.0
(y - Y_i)/H
(T - T∞)/(T3 - T∞)
18 by 24 in. door
SYMBOL
ṁ2
0.208 kg/s
0.146
0.067
0.067
0.050
0.030

Figure 3.7(a)

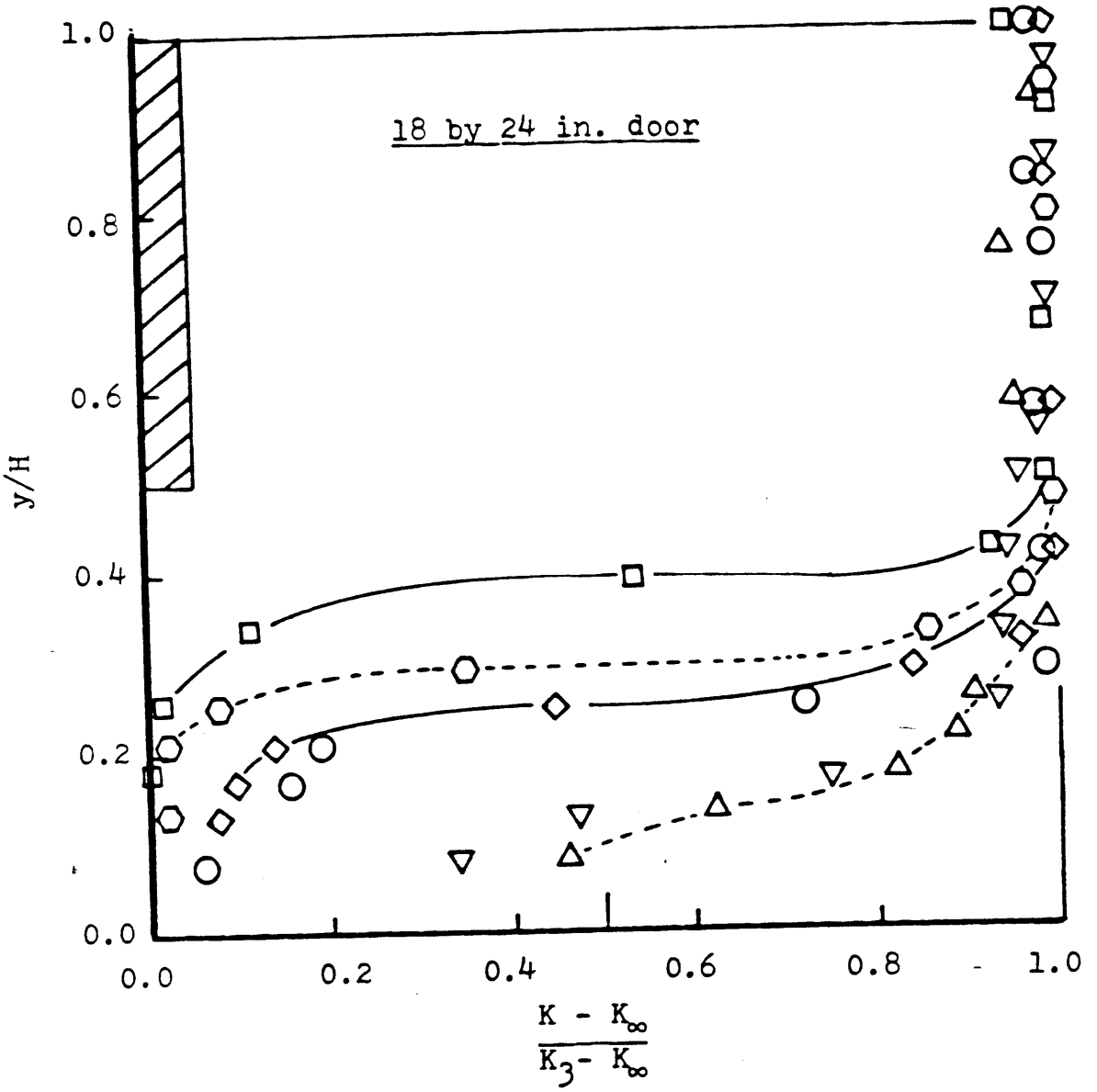

Figure 3.7(b)

Legend for Figures 3.8 and 3.9

Symbol	Door Geometry	
⊙	18"x39"	
◇	18"x24"	
⊡	12"x39"	
△	12"x26"	
◺	12"x26"	variable T_3

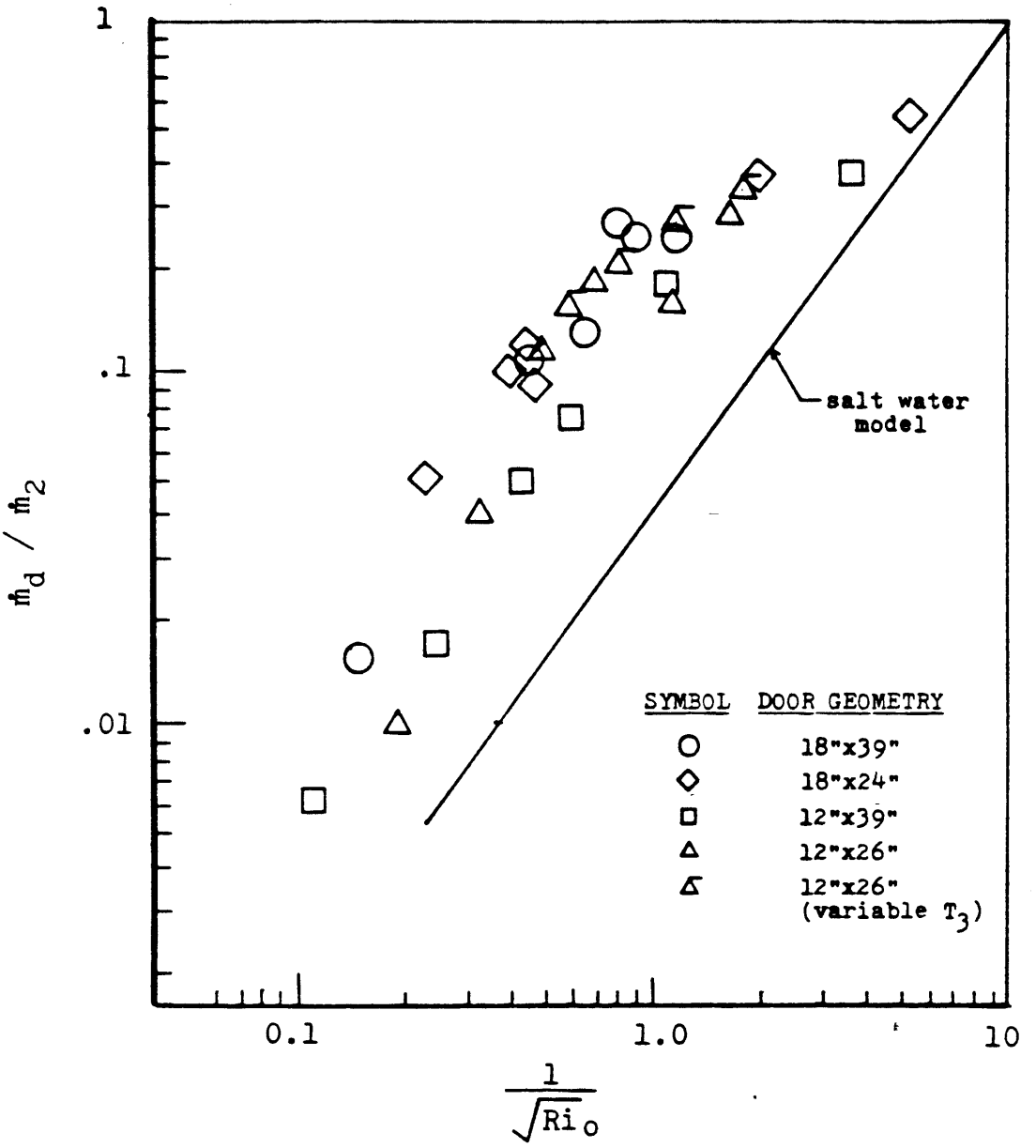
1
.1
.01
$\dot{m}_d / \dot{m}_2$
0.1
1.0
10
$\frac{1}{\sqrt{Ri_o}}$
salt water model
SYMBOL DOOR GEOMETRY
18"x39"
18"x24"
12"x39"
12"x26"
12"x26" (variable T_3)

Figure 3.8

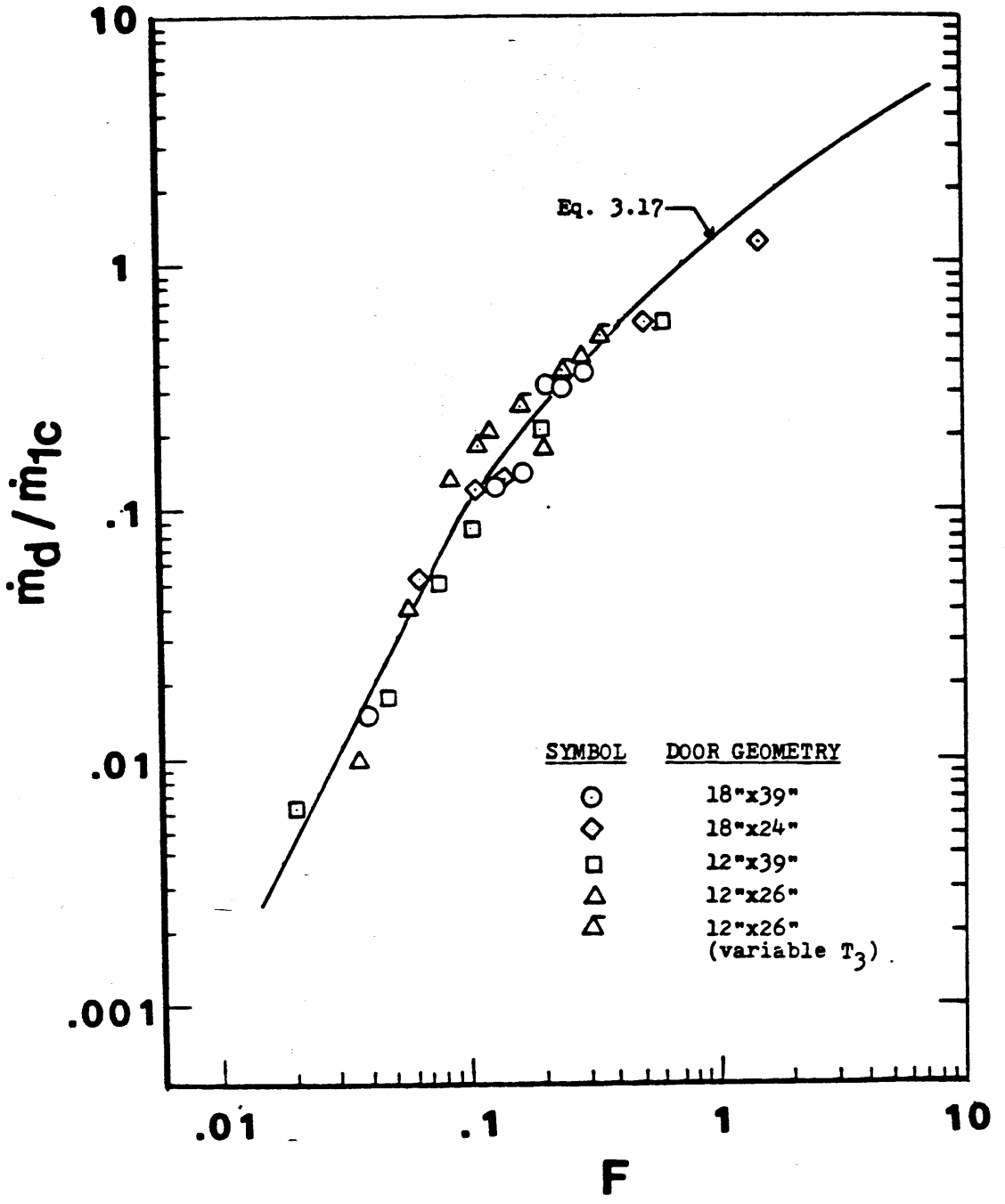
10
1
.1
.01
.001
$\dot{m}_d / \dot{m}_{1c}$
Eq. 3.17
SYMBOL
DOOR GEOMETRY
18"x39"
18"x24"
12"x39"
12"x26"
12"x26"
(variable T_3)
.01
.1
1
10
F

Figure 3.9

Legend for Figures 3.10 (a,b,c)

Symbol	T_s, °C	Y_i, in.	Run
○	166	13.4	48
⊡	131	12.0	50
△	98	10.3	52
⬡	67	9.0	53

$\dot{m}_2 = 0.057$ kg/s

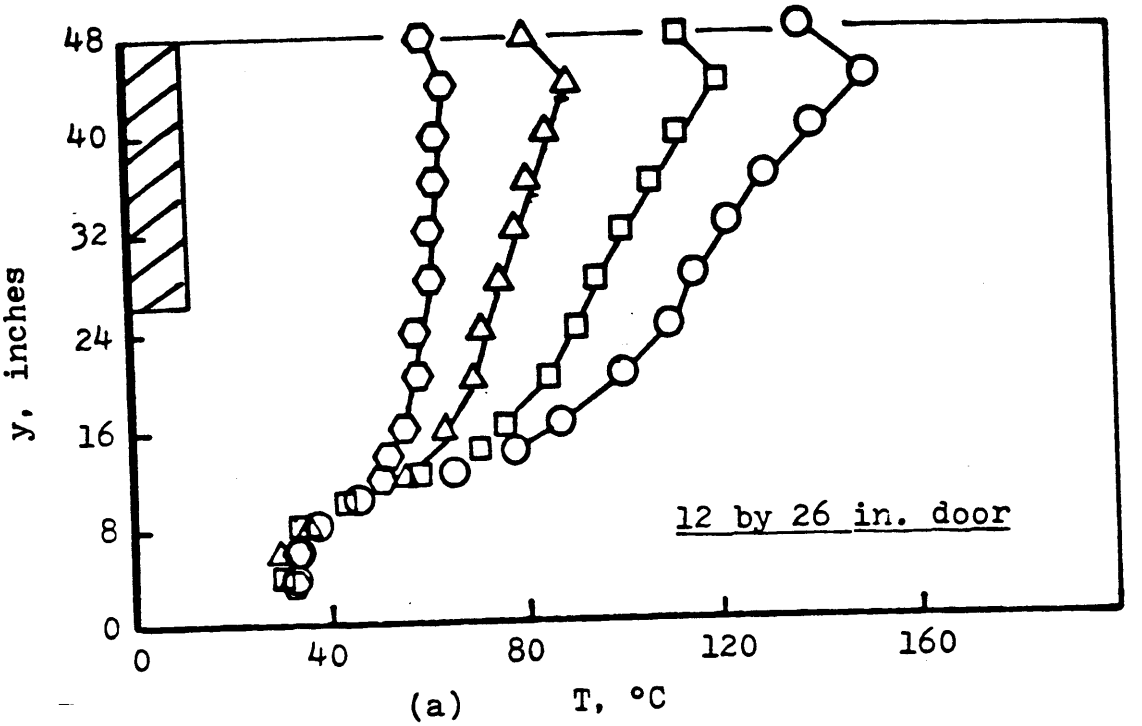
48
40
32
24
16
8
0
y, inches
0
40
80
120
160
12 by 26 in. door
(a) T, °C

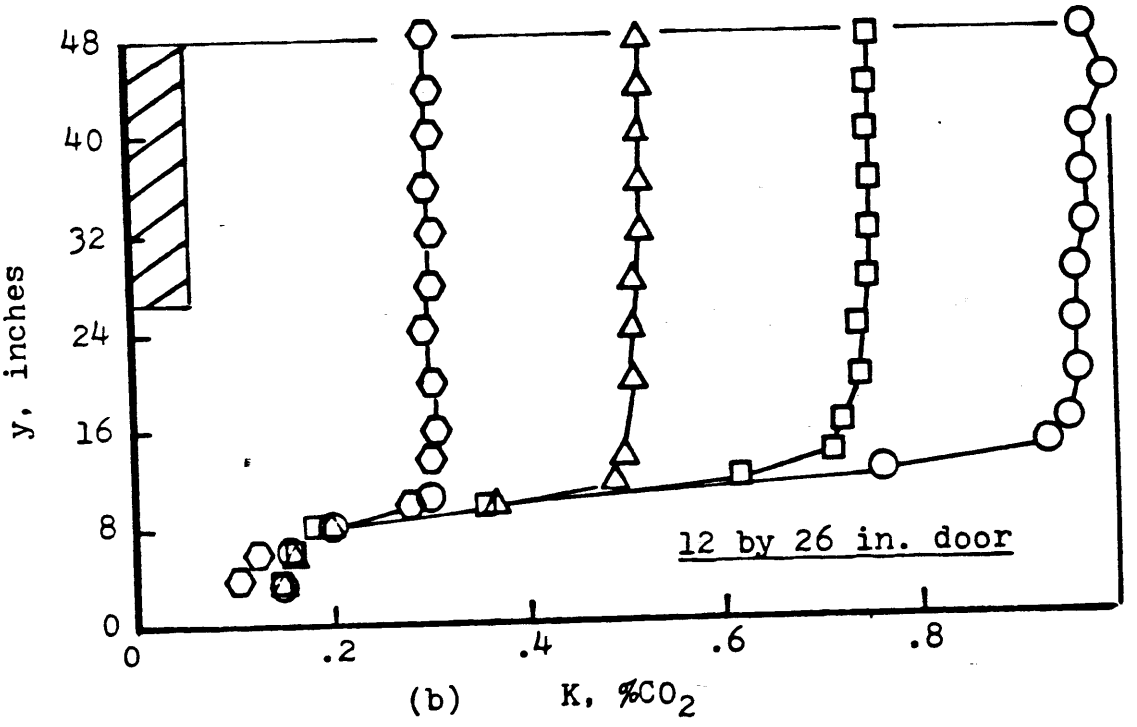
48
40
32
24
16
8
0
y, inches
0
.2
.4
.6
.8
12 by 26 in. door
(b) K, %CO2

Figure 3.10

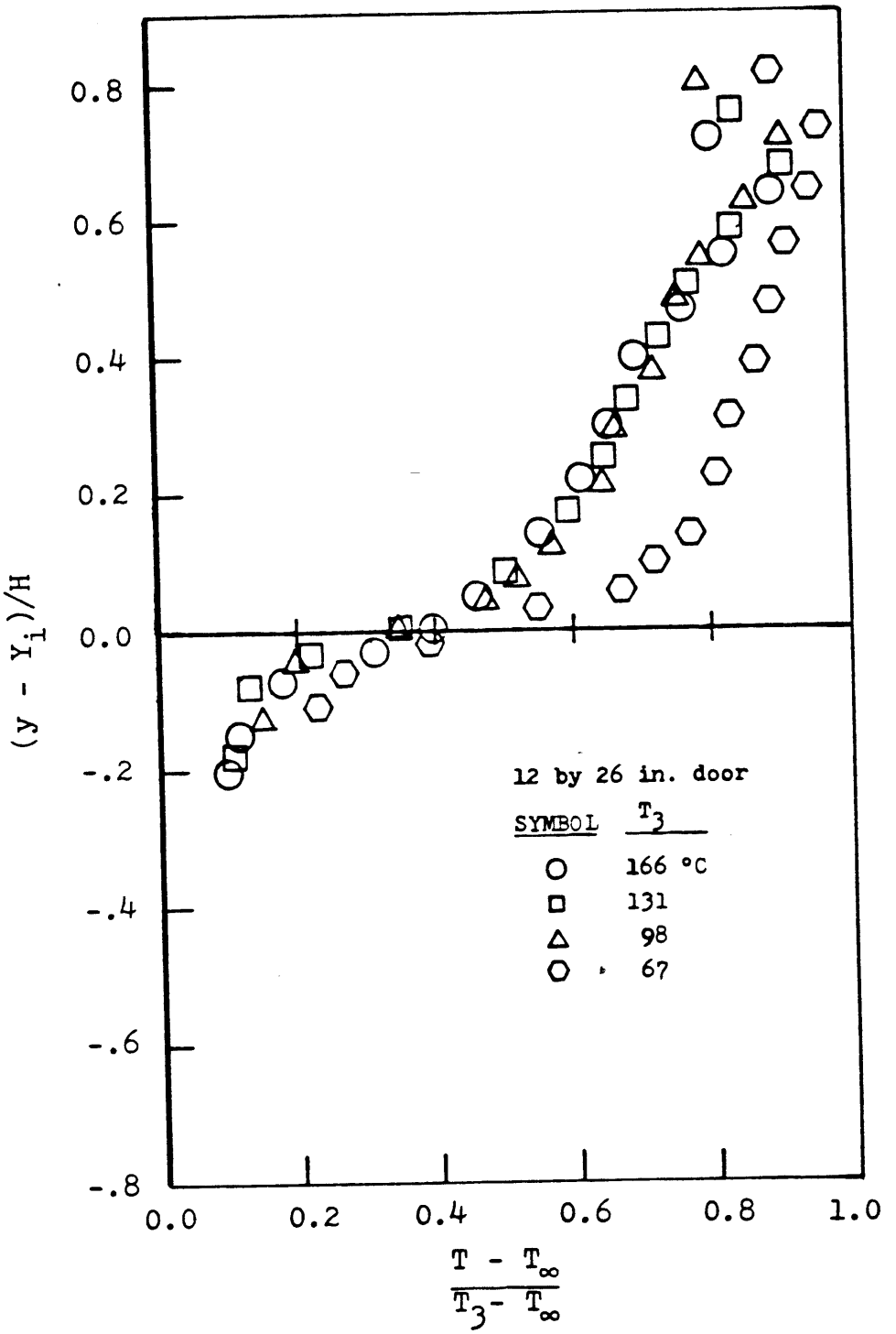
0.8
0.6
0.4
0.2
0.0
-.2
-.4
-.6
-.8
0.0
0.2
0.4
0.6
0.8
1.0
(y - Y_i)/H
(T - T∞)/(T3 - T∞)
12 by 26 in. door
SYMBOL T3
166 °C
131
98
67

Figure 3.10(c)

Chapter 4

ENTRAINMENT IN FIRE PLUMES

4.1. Experimental Technique and Apparatus

The primary purposes of the experiment are to measure the air entrainment rates, $\dot{m}_E$, in the near field of a buoyant diffusion flame where the interface height is below the top of the flames and to determine the chemical composition of the product gas in the hot layer above the interface. The entrainment rates and the gas composition are expressed as functions of the interface height, Z_i; heat release rate, $\dot{Q}_f$; and the initial fire geometry, D. A 0.19 m. diameter stainless steel burner was used in all the experiments. This experiment is an extension of the work done by Cetegen (1982).

The method used to measure the mass flow rates in the near field of the fire plume was based upon measuring the fuel flow rate and the mole fractions of combustion products taken from a small hood. The apparatus used in the experiments is shown in Figure 4.1. The burner is under a 1.2 meter cubical hood which is inside a much larger hood. The small hood is made out of steel and is lowered upon the fire by a pulley mechanism. The large hood dimensions are 2.4x2.4x1.56 m. deep; it is made out of steel and insulated with 10 cm. thick glasswool.

The hot gas was allowed to spill out under the edges of the bottom side of the small hood and up into the large hood where an exhaust fan was used to remove the gas from the laboratory. Two layers of 16x18 mesh screens made of 0.05 cm diameter wire were placed around the large hood so as to reduce the disturbances present in the laboratory air as this gas was sucked into the plume by

the entrainment process. The location of the hot-cold gas interface was determined by a shadowgraph system.

A sample of combustion products was withdrawn from inside the small hood at a rate of about 1.25 liters/minute through a 6.4 mm. diameter stainless-steel tube. An aspirated chromel-alumel thermocouple with a radiation shield was placed at the entrance of the probe to measure the incoming gas temperature. The sample was first sent through two cold (ice) baths to remove the moisture, then filtered to remove the particulates in the gas stream. The sample was then sent through a Beckman Model 864 Nondispersive Infrared CO_2 analyzer, a Beckman Model 400 Flame Ionization Hydrocarbon (CH_4) analyzer, a Beckman Model 755 O_2 analyzer, and an Anarad Model AR-600 Infrared CO analyzer. The analyzers would then give the mole fractions of CO_2, CO, O_2, and CH_4 in the dried sample.

By assuming that the sample was completely free of water vapor and solid carbon (soot), the measured mole fractions of CO_2, CO, O_2, and CH_4 were used (by mass balance) to calculate the actual mole fractions of CO_2, CO, O_2, CH_4, N_2, H_2, and H_2O. The equivalence ratio, φ, was then computed along with the entrainment rate, $\dot{m}_E$.

The fuel used in the experiments was city gas (methane) taken without processing from the Southern California Gas Company mains. The lower heating value of the methane fuel is about 47.5 MJ/kg and the density is about 0.72 kg/m^3 at 20 degrees Celsius and one atmosphere. A Meriam laminar flowmeter was used to measure the volume flow rate of the fuel.

The fuel was fed into the flame after passing through a porous bed of spherical glass beads, whose surface was made flat and flush with the metal edge of the burner. The burner used in the experiments had a diameter of 0.19 m. and

had a 5 cm. thick layer of 6.3 mm. diameter glass beads. The burner-hood set-up described above is identical to the one used by Cetegen (1982) in his experiments.

4.2. Calculation of Species Concentrations

The combustion of methane in the presence of x moles of excess air can be written as

$$\left[CH_4 + (2+x)(O_2 + 3.76N_2)\right] \rightarrow \left[n_{CO_2}CO_2 + n_{CO}CO + n_{CH_4}CH_4 + n_{O_2}O_2 + n_{H_2O}H_2O + n_{H_2}H_2 + n_{N_2}N_2 + n_C C\right] \quad (4.1)$$

where n_i represents the number of moles of species i per mole of CH_4 fuel input. The air entrainment rate can then be calculated if the composition of the products is known.

In our experiments, the concentrations of CH_4, CO_2, CO, and O_2 in a dried sample were measured, and the concentration of solid carbon (soot) was assumed to be negligible. To calculate the mole fractions of the other species, mass balance equations were written for each of the elements O, C, H, and N. Then by manipulating the equations, we were able to obtain the following equations for the concentrations of the other species in the dried sample (see Appendix B):

$$Y_{N_2} = \frac{1}{0.4681}\left[Y_{CH_4} - 3Y_{CO_2} - 2Y_{CO} - 3Y_{O_2} - \frac{2}{N_{sample}} + 1\right] \quad (4.2)$$

$$Y_{H_2O} = 2\left[\frac{1}{3.76}Y_{N_2} - Y_{CO_2} - Y_{O_2}\right] - Y_{CO} \quad (4.3)$$

$$Y_{H_2} = \frac{2}{N_{sample}} - 2Y_{CH_4} - Y_{H_2O} \tag{4.4}$$

where Y_i is the mole fraction of species i in the dried sample, and N_{sample} is the total number of moles in the dried sample per mole of CH_4 fuel input, i.e.,

$$N_{sample} = n_{CO_2} + n_{CO} + n_{CH_4} + n_{O_2} + n_{N_2} + n_{H_2}$$

and it may be shown that

$$N_{sample} = \frac{1}{Y_{CO_2} + Y_{CO} + Y_{CH_4}}. \tag{4.5}$$

It must be noted that since water vapor was not present in the analyzed sample, the term Y_{H_2O} does not represent the mole fraction of water vapor in the sample. The term Y_{H_2O} is simply defined to be the ratio of the number of moles of water in the initial sample, n_{H_2O}, to the total number of moles in the *dried* sample.

To obtain the actual mole fractions of the species in the ceiling layer, the sample mole fractions, Y_i, must be multiplied by the factor $\frac{1}{1 + Y_{H_2O}}$. Thus,

$$\bar{Y}_i = \frac{Y_i}{1 + Y_{H_2O}} \tag{4.6}$$

where $\bar{Y}_i$ is the actual mole fraction of species i in the ceiling layer.

Finally, the equivalence ratio, φ, of the reactants is given by

$$\varphi = \frac{2}{2+x} = \frac{7.52}{Y_{N_2} N_{sample}}. \qquad (4.7)$$

The equivalence ratio is defined to be the fuel-air ratio divided by the stoichiometric fuel-air ratio (= 0.056 for methane fuel).

The derivations of the above equations are presented in Appendix B.

4.3. Calculation of Air Entrainment Rates

The air entrainment rate into the plume is given by

$$\dot{m}_E = \left[\frac{17.16}{\varphi}\right] \dot{m}_f \qquad (4.8)$$

and the plume mass flowrate into the hood is

$$\dot{m}_{p_{in}} = \dot{m}_E + \dot{m}_f \qquad (4.9)$$

where $\dot{m}_f$ is the mass flowrate of fuel.

4.4. The CEC72 Program

The theoretical composition of products was obtained through the use of the "CEC72 (Chemical Equilibrium Calculation)" computer program developed at the NASA Lewis Research Center by S. Gordon and B.J. McBride (1976). Briefly, the program can be used to calculate equilibrium composition of a mixture for assigned thermodynamic states. The thermodynamic states were assigned by specifying two thermodynamic state functions: temperature and pressure.

The program uses the ideal gas law as the equation of state for the mixture. The analysis assumes that interactions between phases are negligible. In the

event that condensed species are present, it is assumed that the condensed species occupies a negligible volume and exerts a negligible pressure compared to the gaseous species.

A free-energy minimization technique is used by the program to determine the equilibrium composition. The program considers gaseous species, condensed species, and ions. With a few exceptions, the thermodynamic data (e.g., heats of formation) are taken from the JANAF Thermochemical Tables.

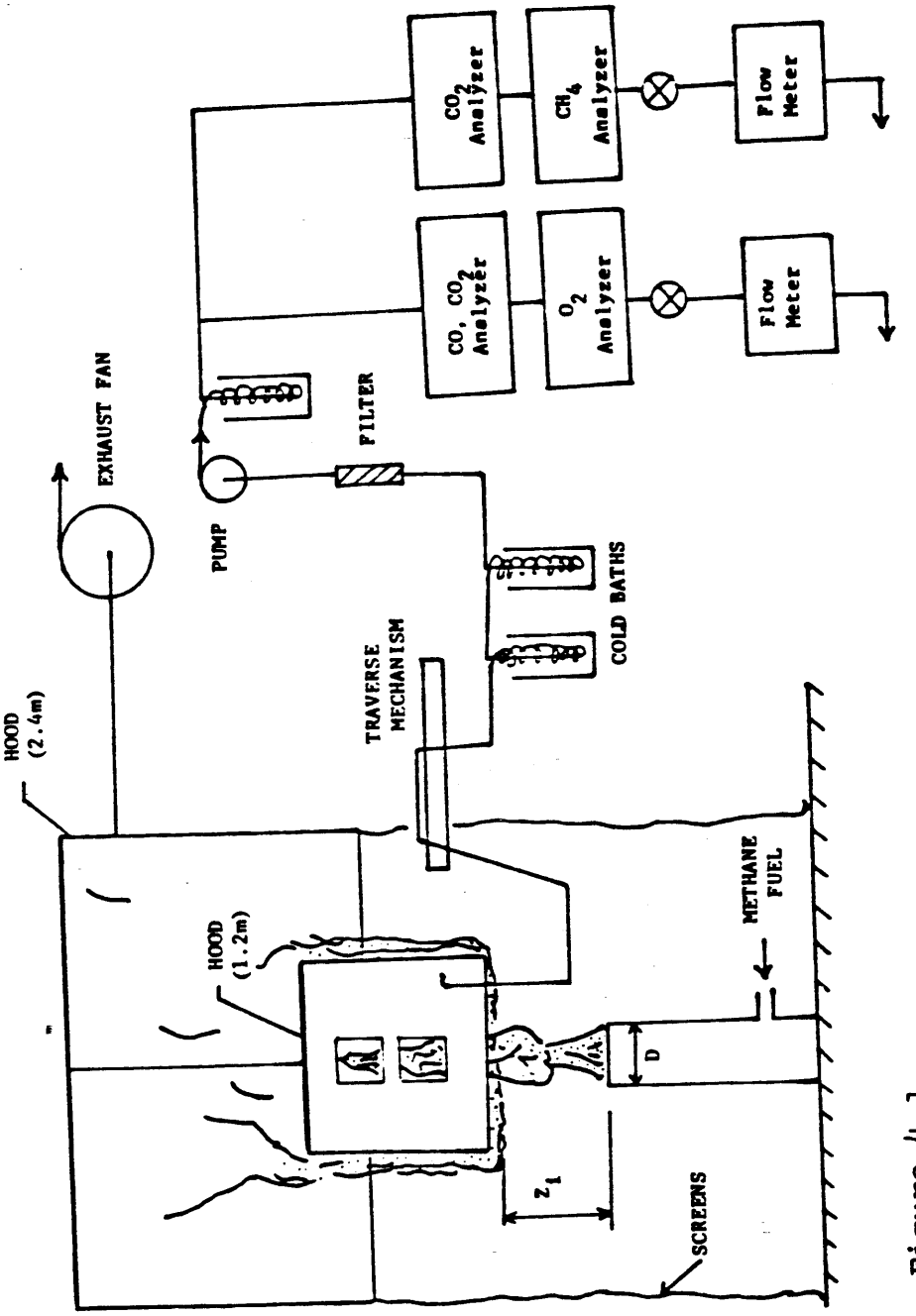
HOOD (2.4m)
EXHAUST FAN
PUMP
FILTER
COLD BATHS
TRAVERSE MECHANISM
HOOD (1.2m)
METHANE FUEL
D
z_1
SCREENS
CO_2 Analyzer
CH_4 Analyzer
Flow Meter
CO, CO_2 Analyzer
O_2 Analyzer
Flow Meter

Figure 4.1

Chapter 5

FIRE PLUME EXPERIMENTAL RESULTS

Measurements of the plume entrainment rates in the near field of a buoyant methane diffusion flame were made for interface heights of 0.01 m., 0.07 m., 0.10 m., and 0.23 m. above a 0.19 m. diameter burner. The entrainment measurements were made by analyzing the composition of the combustion products in the ceiling layer. In calculating the species concentrations, it was assumed that the solid carbon concentration was negligible in our experiments.

A problem that arose in the initial experiments was that the water vapor in the sample was not completely removed — water was observed to be condensing downstream of the pump. The problem was that the mole fraction of water vapor in the sample must be known in order to solve our system of equations. A non-zero value for the mole fraction of water vapor in the sample would make our estimates of the actual water vapor concentrations too high. The problem was eliminated in subsequent experiments by the addition of another cold bath downstream of the pump. Tests for leaks in the system were made by sending pure nitrogen into the sampling system and using the analyzers to detect any leak in the system by measuring the oxygen concentration of the gas at the detection station.

It was found that the temperature and species concentrations in the hood did not vary significantly with the vertical probe location as long as the probe was well away from the flame plume (see Table 5.1). Using this fact, the probe was placed in a corner half way between the top and lower edges of the hood. The temperature and species concentrations measured at this position were assumed to be representative of the properties of the combustion products.

Figure 5.1 shows the equivalence ratio, φ, as a function of the heat release rates, $\dot{Q}_f$, for four interface heights. For a given fuel flow rate, lowering the interface results in a higher equivalence ratio. This is because the air entrainment rate into the plume is proportional to the interface height, and lowering the interface will decrease the amount of oxygen available for combustion. The measured values of this air entrainment rate will be discussed in the section 5.3.

Figure 5.2 shows the average temperature of the ceiling layer gas, T_h, as a function of the equivalence ratio of the reactants. For $\varphi < 1$, the gas temperature increases linearly with equivalence ratio for a fixed interface height. But as the fuel-air ratio is increased above the stoichiometric value ($\varphi > 1$), the temperature reaches a maximum value. This implies that the air entrainment rate in the near field of a fire plume is independent of the fire size since the heat release is limited by the amount of oxygen available for combustion. Lowering the interface decreases the amount of oxygen available for combustion and therefore reduces the maximum temperature in the hood.

To summarize: For a fixed fuel flow rate, reducing the interface height results in a lower gas temperature and a higher equivalence ratio. This result can be explained by the fact that the amount of fuel consumed (and hence the heat released) is strongly dependent upon the mass flowrate of oxygen entrained into the plume. This fact is important since, theoretically, the equilibrium composition of a mixture is a strong function of the equilibrium temperature of the mixture. In the next section, we will compare the species concentrations measured in our experiments with the theoretical values obtained from the CEC72 computer program written by Gordon and McBride (1976).

5.1. Species Concentrations

Figures 5.3 to 5.9 show the estimated species concentrations in the hood as a function of the equivalence ratio. The plots also compare the experimental data with the theoretical equilibrium composition obtained from the CEC72 computer program. The results show that the measured CO_2, CO, O_2, and CH_4 concentrations are almost independent of the gas temperatures while the H_2O and H_2 data points show a great deal of scatter. When φ is less than 0.7, the estimated concentrations of the incomplete combustion products, CO and CH_4, are negligible but the concentration of H_2 is quite high. The differences between the experimental and theoretical values may be due to: (1) the accuracy of the instruments; (2) our assumption of negligible soot formation; (3) equilibrium not being established in the hood.

5.1.1. *Sensitivity of Calculations.* The accuracies of the instruments are: $Y_{CO_2} \pm 0.005$, $Y_{O_2} \pm 0.005$, $Y_{CH_4} \pm 0.001$, and $Y_{CO} \pm 0.0005$. To test the sensitivity of the calculations, the measured mole fractions of CO_2, O_2, and CH_4 were varied by ± 0.005. The error bars in Figures 5.3 to 5.9 show the range of values when this was done. The results show that the equivalence ratio and the mole fractions of CO_2, O_2, CO, and CH_4 are moderately sensitive to changes in the measured data. On the other hand, the calculated mole fractions of H_2 and H_2O have a very large range of values. The fact that the $\bar{Y}_{H_2}$ and $\bar{Y}_{H_2O}$ are very sensitive to the accuracy of the measurements could explain the large scatter in Figures 5.7 and 5.8

5.1.2. *The Concentration of Solid Carbon.* In making the calculations, we had assumed that the concentration of soot was negligible to the other species concentrations. Figure 5.10 is a plot of the theoretical solid carbon concentration obtained from the CEC72 computer program as a function of the equilibrium temperature. The plot shows that the equilibrium concentration of solid carbon

is a strong function of the equilibrium temperature and becomes negligible at very high temperatures. In our experiments, the temperature range was approximately from 500 to 900 degrees Kelvin, and the maximum equivalence ratio was approximately 2.5. From Figure 5.10, the highest solid carbon concentration in our experiments would be about 0.06. So the *maximum* error resulting from the assumption of negligible solid carbon is approximately 6% for our experiments. Since the calculated mole fractions of H_2 and H_2O are very sensitive to small changes in the measured data, this error is enough to create a considerable amount of scatter in the data.

5.1.3. *Effect of Equilibrium Temperature.* For $\varphi > 1$ the theoretical equilibrium species concentrations are strong functions of the equilibrium temperature. Figures 5.11 to 5.15 show the theoretical species concentrations as a function of equilibrium temperature. It is observed that a species may have the same concentration at two different temperatures. Care should therefore be used in comparing the experimental data with the theoretical curves in Figures 5.3 to 5.10 because the theoretical curves may cross or even overlap each other. Figure 5.13 shows that the theoretical concentration of methane vanishes at 300 degrees Kelvin even in fuel-rich mixtures. This error results from the assumption in the equilibrium analysis that the condensed species (water) occupies a negligible volume and exerts a negligible pressure compared to the gaseous species. This assumption greatly simplifies the theoretical analysis and allows the use of the ideal gas law as the equation of state. At 300 degrees Kelvin, the condensed water is no longer negligible and the calculations break down. Therefore the theoretical equibrium calculations are accurate for equilibrium temperatures which are well above the boiling point of water.

It was found that while the temperature of the gas differed by as much as 40 degrees Kelvin between the top and bottom of the hood, the measured species

concentrations hardly changed (see Table 5.1). The residence times of the hot gas in the hood (mass of gas in the hood divided by the plume mass flowrate) ranged from a low of 30 seconds for $Z_i = 0.23m$ to as long as 190 seconds for $Z_i = 0.01m$. It would seem then that the gas in the hood is well mixed and that chemical equilibrium would be established.

5.2. Mass Entrainment Rates

The mass entrainment of air into the fire plume is calculated by the chemical analysis of combustion products in the hood as was described in Chapter 4. The plume mass fluxes have been measured for interface heights of 0.23, 0.10, 0.07, and 0.01 m. above a 0.19 diameter burner. The heat input rates ranged from 10 to 120 kW. Figure 5.16 shows the mass entrainment rate of air into the plume as a function of the equivalence ratio for four interface heights. Our data correlated well with the results of Cetegen (1982). As was observed by Cetegen (1982), the entrainment rate is a weak function of the equivalence ratio and heat release rate of the fire at very low elevations of the interface, with the entrainment rate approximately proportional to the interface height above the burner raised to a power of about 3/4.

5.3. Fuel Rich Ceiling Layer

It was observed that there is a critical fire size for a given interface height in which flamelets start to form in the interface and spread until the entire interface is set on fire. Table 5.2 gives the critical fire size, gas temperatures, and equivalence ratios for four interface heights. At this point the interface gas is much hotter than the gas above it and this instability causes an inversion of the hot and cooler gases. This sudden turnover results in the generation of vortices and strong air currents that blow the fire plume to one side of the hood (see Figure 5.17(a)). After a while (a few seconds) the flamelets in the interface burned out and the fire plume returned to its normally upright position. It was

observed that the entire process described above occurred in regular cycles with the period being inversely proportional to the fire size. In fact, after a certain fire size was reached, the interface was observed to be continuously on fire.

Measurements of the period of the inversion cycle were made with the use of a thermocouple placed 4 in. above the lower edge of the hood, and 8 in. away from a corner. The thermocouple was well within the zone where the flamelets in the interface were observed. Table 5.3 shows the periods of the inversion cycle for $Z_i = 0.07\ m$ for several fire sizes.

The thermocouple was then connected to a strip chart recorder to obtain a continuous temperature reading. Figure 5.17(b,II) shows interface temperature as a function of time during the inversion cycle for $Z_i = 0.07\ m$ and $\dot{Q}_f = 91\ kW$. As a comparison, Figure 5.17(b,I) shows the temperature history in the top of the hood, and Figure 5.17(b,III) shows the carbon monoxide concentration in the interface as a function of time.

Between times A and B in Figure 5.17(b), the temperature in the interface is constant while the CO concentration rises until it reaches a maximum at time B. At time B, the unburnt fuel (methane, hydrogen, and carbon monoxide) in the interface begin to burn, and the temperatures increase sharply. At time C, the gas temperature reaches a maximum, and the gas starts to cool down. Finally, at time D, the flames in the interface die out and the cycle starts all over again.

5.4. Oxygen Rich Ceiling Layer

In situations where the interface is well below the top of the flames, the gas in the ceiling layer is entrained and heated to very high temperatures by the fire plume several times before it finally leaves the hood. If fuel is supplied directly into an oxygen rich ceiling layer, the resulting mixture may or may not react as it passes through the flames.

We have carried out some preliminary experiments in which methane fuel is injected directly into the ceiling layer to determine if the oxygen inside the hood reacts with the fuel. In the following paragraphs, we will describe the apparatus and techniques used to measure the fraction of the added fuel that reacts in an oxygen rich ceiling layer. Briefly, mass conservation equations for the fuel and oxygen are used to estimate: (1) the mass fraction of methane in the ceiling layer in which the fuel entrained into the flames is *entirely* consumed; (2) the mass fraction of methane in the ceiling layer in which the fuel entrained into the flames *does not react at all* with the oxygen; and (3) the mass fraction of oxygen in the ceiling layer, *given* the fraction of fuel that reacts in the flames. The *measured* mass fraction of methane is then compared with the values obtained from (1) and (2) to determine the fraction of added fuel that actually reacts in the flames. To check the accuracy of the models, the oxygen concentration in the hood is measured and then compared with the value obtained from (3).

5.4.1. *Apparatus.* The apparatus used in these experiments was essentially the same as the one used in the near field measurements. A 0.25 in. diameter copper pipe was used to inject methane fuel into the hood. The heat release rates of the added fuel ranged from 4.0 to 22.8 kW. The pipe and the probe were placed in opposite corners, 0.6 m. from the bottom lip of the hood. To obtain a ceiling layer with a high oxygen content (low φ) and a high gas temperature, we chose to use a fire size of 31.6 kW and an interface height of 0.23 m. (cf. Figure 5.2). The average flame height was about 0.78 m. from the top of the 0.19 m. diameter burner.

5.4.2. ***Fuel Mass Model.*** **For steady state conditions, a mass balance of the fuel entering and leaving the hood may be written as**

$$\dot{m}_{f_{added}} - \alpha C_f (\dot{m}_{p_{fl}} - \dot{m}_{p_{in}}) - C_f \dot{m}_{p_{in}} = 0 \qquad (5.1)$$

where $\dot{m}_{f_{added}}$ is the added amount of fuel; C_f the mass fraction of fuel in the ceiling layer; $\dot{m}_{p_{fl}}$ the total plume flux at the flame height; and $\dot{m}_{p_{in}}$ is the total mass flux entering the hood as was defined in section 4.3. The term $\dot{m}_{p_{fl}} - \dot{m}_{p_{in}}$ is the rate of entrainment of the ceiling layer gas into the fire plume. The parameter α represents the fraction of fuel that is consumed by the plume, i.e., if $\alpha = 1$ all the fuel that is entrained into the fire plume is consumed, and if $\alpha = 0$ all the fuel that is entrained into the flames leaves the fire plume unburned. The term $C_f \dot{m}_{p_{in}}$ is the mass flowrate of fuel leaving the hood. Equation (5.1) may be used predict the mass fraction of methane, C_f, if α is known:

$$C_f = \frac{\dot{m}_{f_{added}}}{\alpha (\dot{m}_{p_{fl}} - \dot{m}_{p_{in}}) + \dot{m}_{p_{in}}}. \qquad (5.2)$$

We were able to measure $\dot{m}_{f_{added}}$, C_f, and $\dot{m}_{p_{in}}$ by the same techniques described in Chapter 4. The value for $\dot{m}_{p_{fl}}$ was obtained from the entrainment recipe given by Cetegen (1982). The measured species concentrations and the calculated mass flowrates for the ceiling layer with no fuel added are listed in Table 5.4. Table 5.5 lists the data obtained for four flowrates of added fuel.

In Table 5.6, the measured mass fraction of methane is compared with the values obtained from Eq. 5.2 for the cases where: (1) the entrained fuel is not burned by the flames ($\alpha = 0$); and (2) the entrained fuel is completely consumed ($\alpha = 1$). The results show that a fraction of the fuel entrained into the fire

plume is burned, with the mass consumed being:

$$\frac{(\dot{m}_{f_{added}})_{burned}}{\dot{m}_{f_{added}}} = 1 - C_f \frac{\dot{m}_{p_{in}}}{\dot{m}_{f_{added}}} = 1 - \frac{C_f}{\left[C_f\right]_{a=0}}. \qquad (5.3)$$

5.4.3. *Oxygen Mass Model.* The steady state mass balance of oxygen in the hood may be written as

$$C_\infty (\dot{m}_{p_{in}} - \dot{m}_f) - \dot{m}_{p_{in}} C_o - C_\infty \frac{\dot{m}_f}{f_s} - C_o \frac{(\dot{m}_{f_{added}})_{burned}}{f_s} = 0 \qquad (5.4)$$

where C_∞ is the oxygen mass fraction in the ambient air (= 0.23); $\dot{m}_{p_{in}} - \dot{m}_f$ is the entrainment rate of ambient air into the plume; C_o is the mass fraction of oxygen in the ceiling layer; f_s is the stoichiometric fuel-air ratio (= 0.058 for methane fuel); and $(\dot{m}_{f_{added}})_{burned}$ is the amount of added fuel that was burned in the fire (as was defined in Eq. 5.3). The first term in Eq. 5.4 represents the amount of oxygen entering the hood; the second term is the amount leaving the hood; the third term is the amount of entrained O_2 that reacts with $\dot{m}_f$; and the last term is the amount of O_2 that reacts with $(\dot{m}_{f_{added}})_{burned}$. By neglecting $\dot{m}_f$ compared to $\dot{m}_{p_{in}}$ in the first term and using the relation $\varphi \approx (\dot{m}_f / \dot{m}_{p_{in}}) \times (1/f_s)$, Eq. 5.4 may be reduced to

$$C_o = \frac{C_\infty (1 - \varphi)}{1 + \dfrac{(\dot{m}_{f_{added}})_{burned}}{f_s \dot{m}_{p_{in}}}}. \qquad (5.5)$$

Using the data in Tables 5.4 to 5.6, Eq. 5.5 may be used to predict the mass fraction of oxygen in the ceiling layer. This predicted value may then be compared

with the measured mass fraction of oxygen to determine the accuracy of the fuel and oxygen mass models (Table 5.7). The term $(\dot{Q}_f)_{added\ Burned}$ in the second column of Table 5.7 was calculated using Eq. 5.3.

The results show that the difference between the predicted and measured concentration of oxygen in the ceiling layer increases as more fuel is injected. This is because we had assumed that $\dot{m}_{p_{in}}$ and $\dot{m}_{p_{fl}}$ were independent of the amount of fuel added into the ceiling layer. In reality, the fire size and plume entrainment rates increase as more of the added fuel is consumed. It must be noted that these are preliminary experiments, and more refined methods must be used to determine accurately the effect of adding fuel into an oxygen rich ceiling layer.

5.4.4. *Critical Oxygen Concentration.* In another experiment to determine if the fuel and oxygen will react in the ceiling layer, the pipe used to inject the fuel was lighted and then placed inside the hood. The heat release rate of the added fuel was set at 1 kW. The fire size of the plume was then varied to change the oxygen concentration in the ceiling layer. It was found that the critical oxygen concentration is about 13% by volume for the injected fuel to keep burning. This value is in close agreement with the critical oxygen index of 12% given by Lewis and Elbe (1951, p. 754). Just above the critical value, the flame on the pipe was observed to have a transparent blue color. The more familiar yellow flames (which are associated with soot formation) became more evident as the oxygen content of the ceiling layer was increased. At the critical value, the flame was very unstable and a small disturbance (such as moving the pipe slightly) was enough to kill the flame. The fire on the pipe immediately died out when the oxygen concentration fell below the critical value.

Table 5.1. Temperature and Species Concentrations vs. Probe Location

$\dot{Q}_f$ = 73.7 kW
Z_i = 0.100 m.

	Probe Location		
	Top of hood	Middle of hood	Bottom of hood
$T°K$	722	702	695
Y_{CO_2}	0.0960	0.0970	0.0960
Y_{O_2}	0.0010	0.0003	0.0020
Y_{CO}	0.0250	0.0250	0.0250
Y_{CH_4}	0.0860	0.0920	0.0890

$\dot{Q}_f$ = 52.6 kW
Z_i = 0.230 m.

	Probe Location		
	Top of hood	Middle of hood	Bottom of hood
$T°K$	847	833	810
Y_{CO_2}	0.0890	0.0890	0.0890
Y_{O_2}	0.0540	0.0580	0.0560
Y_{CO}	0.0031	0.0026	0.0032
Y_{CH_4}	0.0004	0.0004	0.0003

Table 5.2. Critical Fire Size for Four Interface Heights

Z_i	Critical Fire Size	φ	T_h
0.01 m	40 kW	2.4	560 °K
0.07 m	60 kW	2.2	650 °K
0.10 m	100 kW	2.5	730 °K
0.23 m	150 kW	1.9	840 °K

The critical fire size refers to the fire size below which flamelets in the interface did not appear.

Table 5.3. Periods of the Inversion Cycle for Three Fire Sizes

Z_i	$\dot{Q}_f$	Period	φ
0.07 m	68 kW	75 s	2.3
0.07 m	91 kW	62 s	3.5
0.07 m	128 kW	45 s	4.5

Table 5.4. Ceiling Layer Composition with No Added Fuel

$\dot{Q}_f$ = 31.6 kW
Z_ℓ = 0.23 m.
$\dot{m}_f$ = 0.000663 kg/s
$\dot{m}_{p_{in}}$ = 0.0307 kg/s

T_h = 618 °K

Avg. flame height = 0.78 m.
$\dot{m}_{p_{fl}}$ = 0.124 kg/s

Mole Fractions

$\bar{Y}_{O_2}$ = 0.1237
$\bar{Y}_{CO}$ = 0.0000
$\bar{Y}_{H_2}$ = 0.0000
$\bar{Y}_{N_2}$ = 0.7635

$\bar{Y}_{CH_4}$ = 0.0000
$\bar{Y}_{CO_2}$ = 0.0376
$\bar{Y}_{H_2O}$ = 0.0836

φ = 0.370
Molecular Weight = 28.4 kg/kmol.

Table 5.5. Ceiling Layer Composition with Added Fuel

$(\dot{Q}_f)_{added}$	$\bar{Y}_{O_2}$	$\bar{Y}_{CH_4}$	$\bar{Y}_{CO_2}$	$\bar{Y}_{CO}$	T_h
4.0 kW	0.1241	0.0024	0.0377	0.0000	623 °K
7.5 kW	0.1212	0.0036	0.0374	0.0000	628 °K
14.8 kW	0.1172	0.0072	0.0370	0.0000	640 °K
22.8 kW	0.1065	0.0091	0.0399	0.0004	668 °K

Table 5.6. Measured vs. Predicted Mass Fraction of Methane

$(\dot{Q}_f)_{added}$	C_f if unburned	C_f if completely burned	C_f measured	α
4.0 kW	0.0027	0.0007	0.0014	0.31
7.5 kW	0.0051	0.0013	0.0020	0.51
14.8 kW	0.0101	0.0025	0.0041	0.48
22.8 kW	0.0156	0.0039	0.0051	0.68

The predicted mass fractions of methane are based on the flame height, the plume mass fluxes, and the amount of added fuel. α is the fraction of entrained fuel that was consumed in the fire plume.

Table 5.7. Measured vs. Predicted Mass Fraction of Oxygen

$(\dot{Q}_f)_{added}$	$(\dot{Q}_f)_{added}$ Burned	C_o Predicted	C_o Measured
40 kW	2.0 kW	0.144	0.140
7.5 kW	4.6 kW	0.141	0.136
14.8 kW	8.8 kW	0.138	0.132
22.8 kW	15.3 kW	0.130	0.121

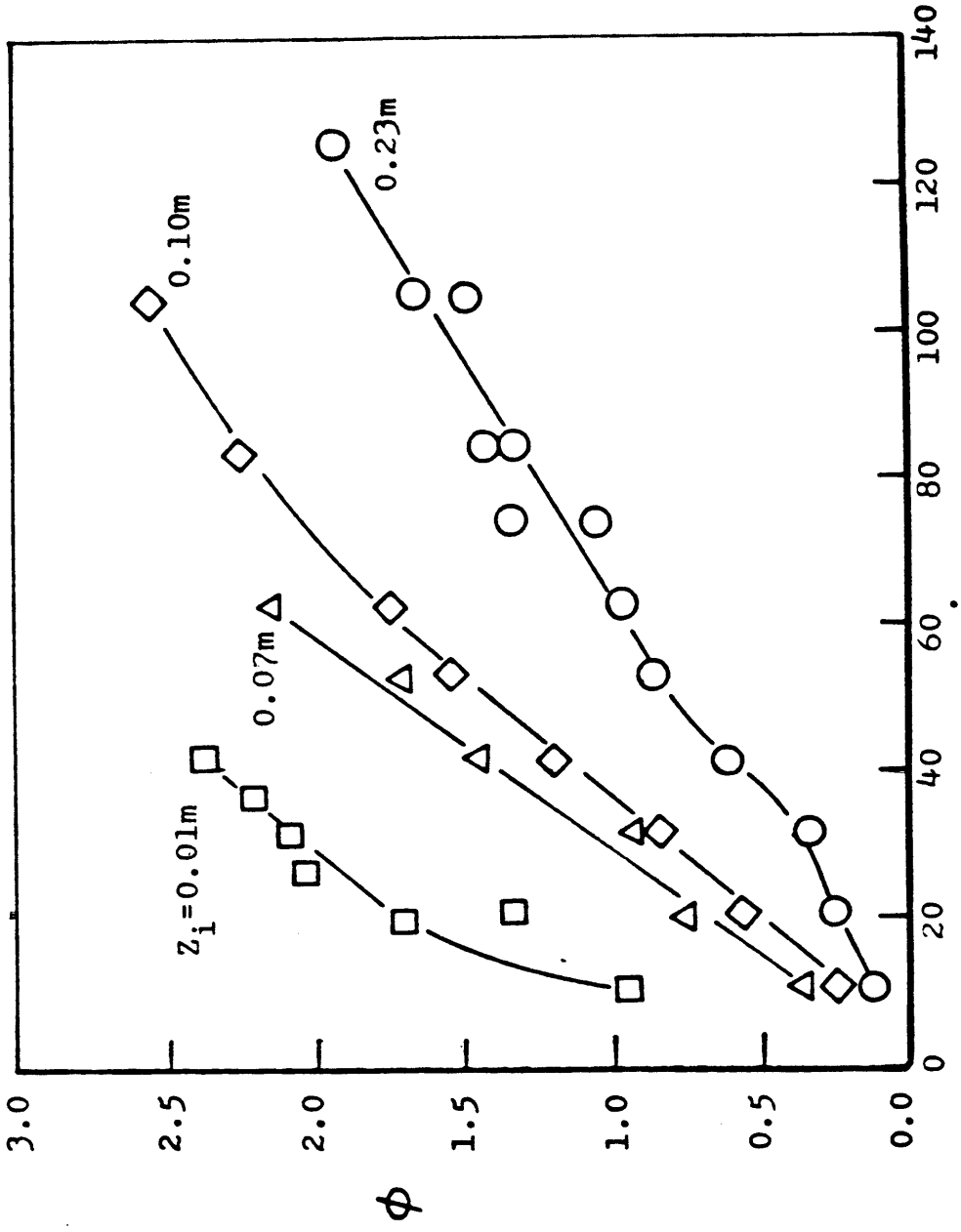
3.0
2.5
2.0
1.5
1.0
0.5
0.0
ϕ
0
20
40
60
80
100
120
140
$\dot{Q}_f$, kW
Z_i=0.01m
0.07m
0.10m
0.23m

Figure 5.1

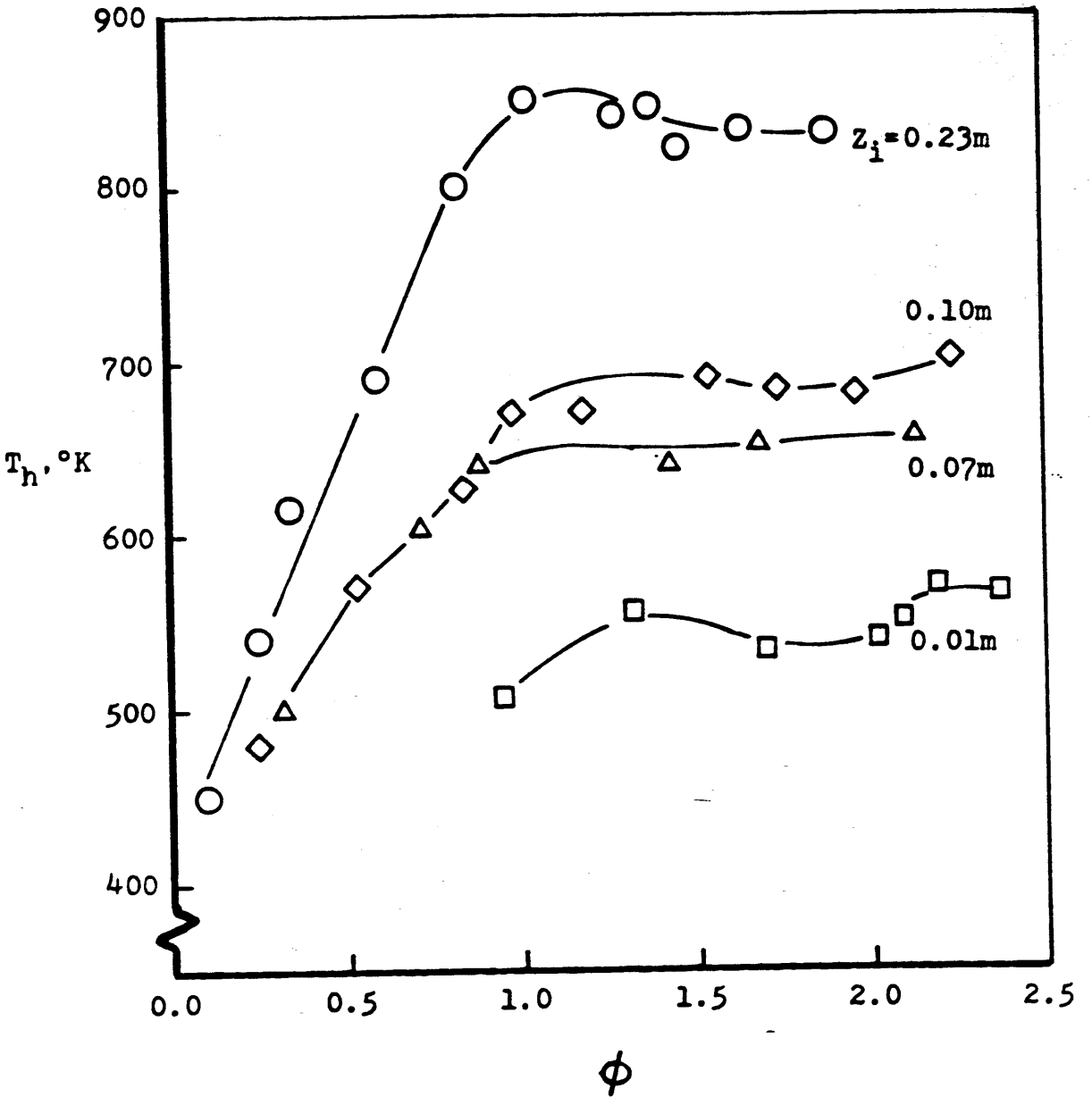
900
800
700
600
500
400
T_h, °K
z_i=0.23m
0.10m
0.07m
0.01m
0.0
0.5
1.0
1.5
2.0
2.5
ϕ

Figure 5.2

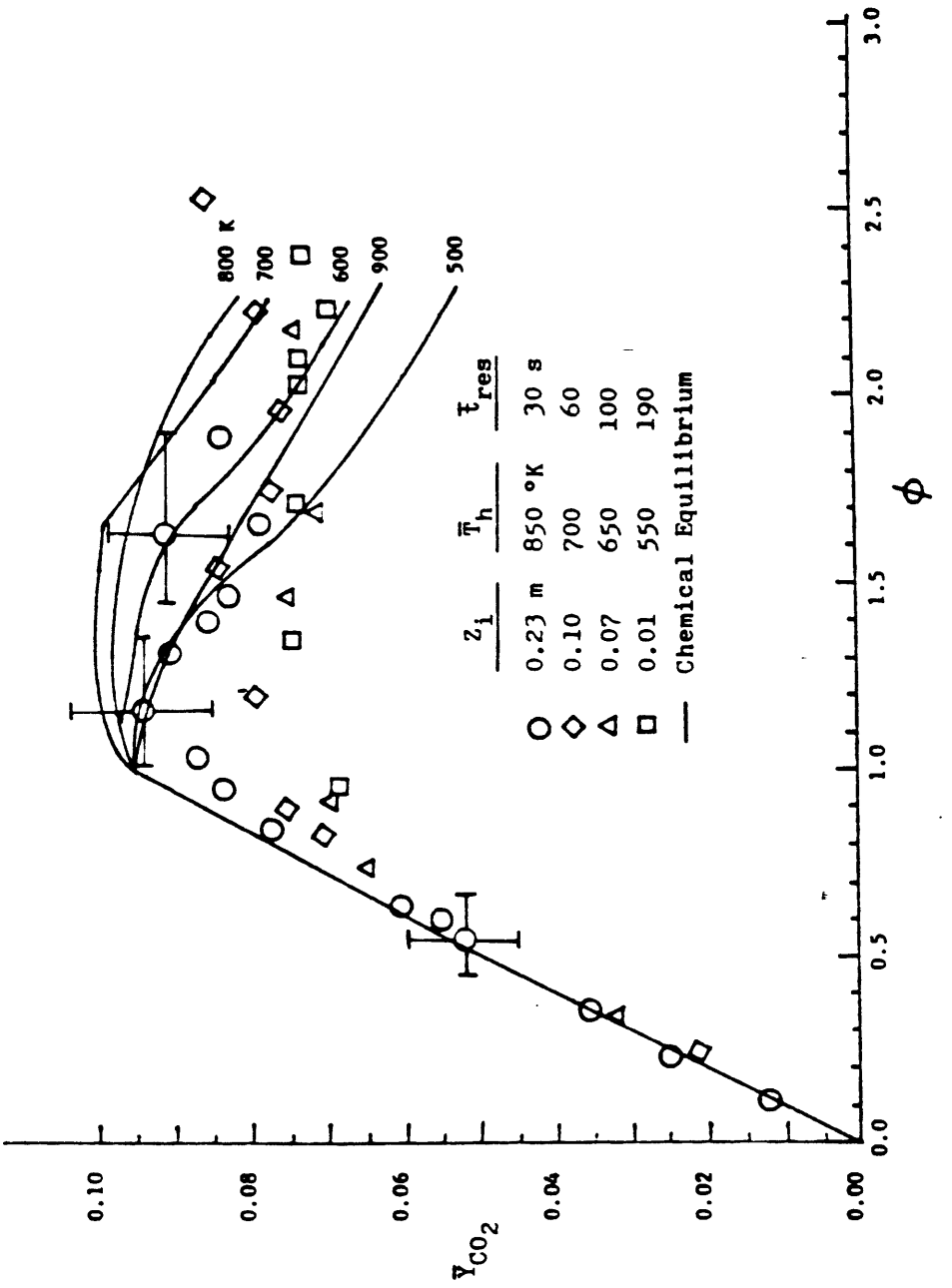
0.10
0.08
0.06
0.04
0.02
0.00
Y_{CO_2}
0.0
0.5
1.0
1.5
2.0
2.5
3.0
ϕ
800 K
700
600
900
500
z_i
$\bar{T}_h$
$\bar{\tau}_{res}$
0.23 m 850 °K 30 s
0.10 700 60
0.07 650 100
0.01 550 190
Chemical Equilibrium

Figure 5.3

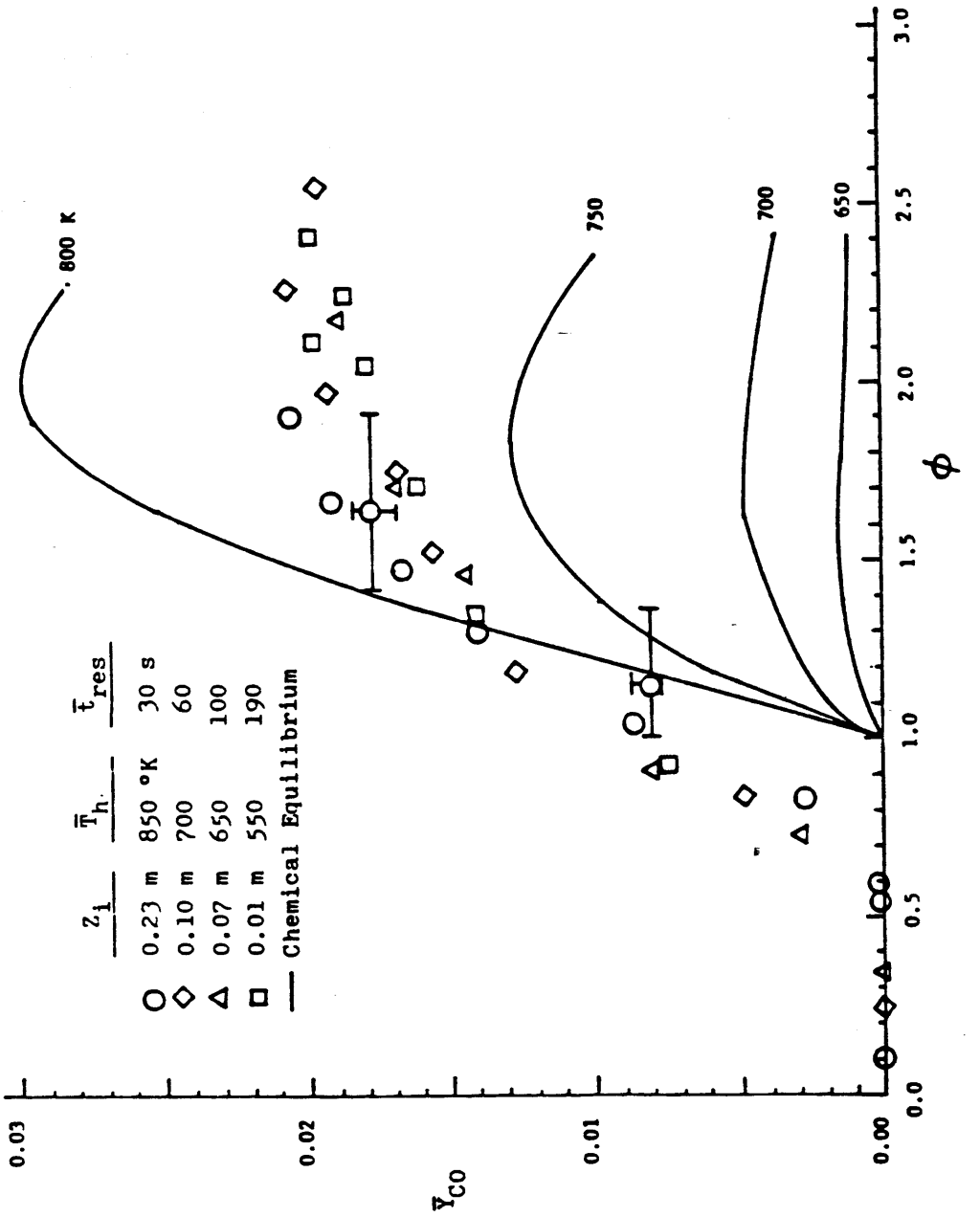
z_i $\bar{T}_h$ $\bar{t}_{res}$
0.23 m 850 °K 30 s
0.10 m 700 60
0.07 m 650 100
0.01 m 550 190
Chemical Equilibrium
800 K
750
700
650
$\bar{Y}_{CO}$
ϕ
0.00
0.01
0.02
0.03
0.0
0.5
1.0
1.5
2.0
2.5
3.0

Figure 5.4

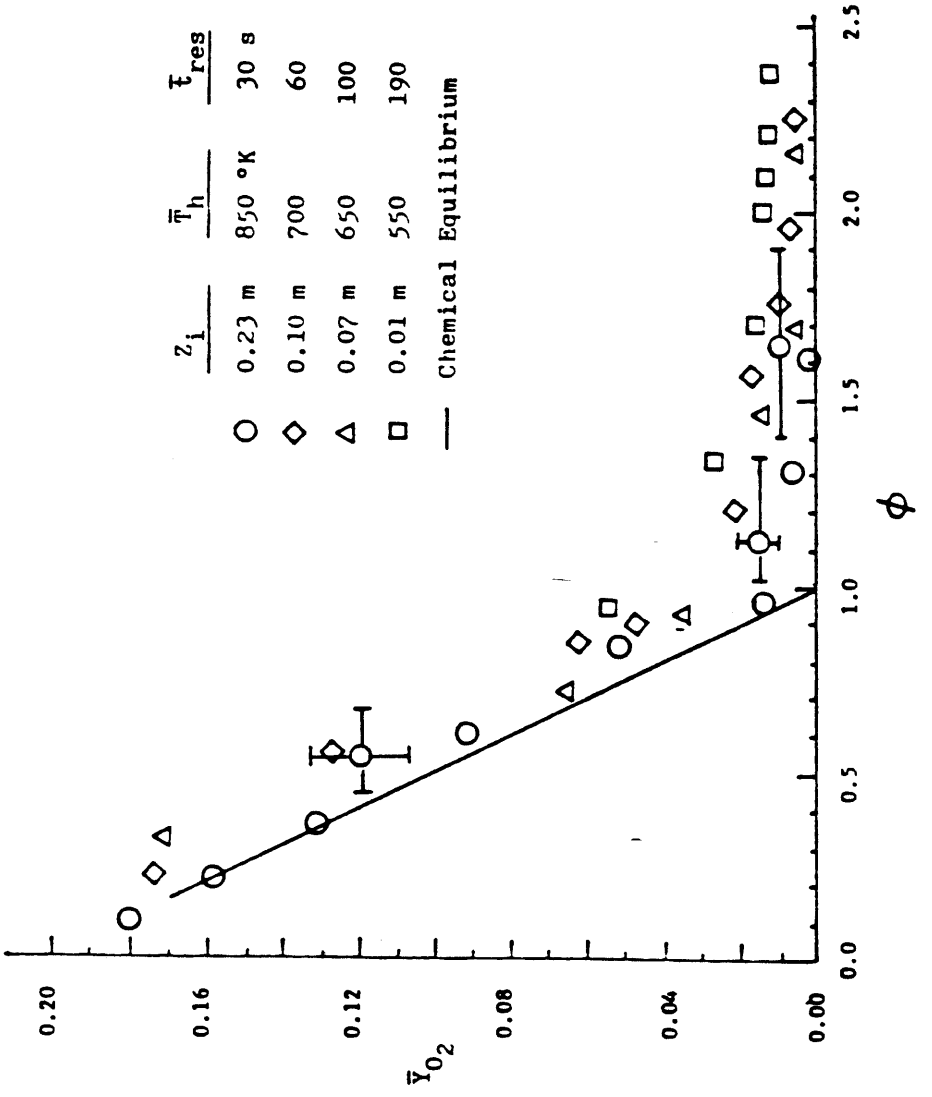
z_i
$\bar{T}_h$
$\bar{t}_{res}$
0.23 m 850 °K 30 s
0.10 m 700 60
0.07 m 650 100
0.01 m 550 190
Chemical Equilibrium
$\bar{Y}_{O_2}$
0.20
0.16
0.12
0.08
0.04
0.00
0.0
0.5
1.0
1.5
2.0
2.5
ϕ

Figure 5.5

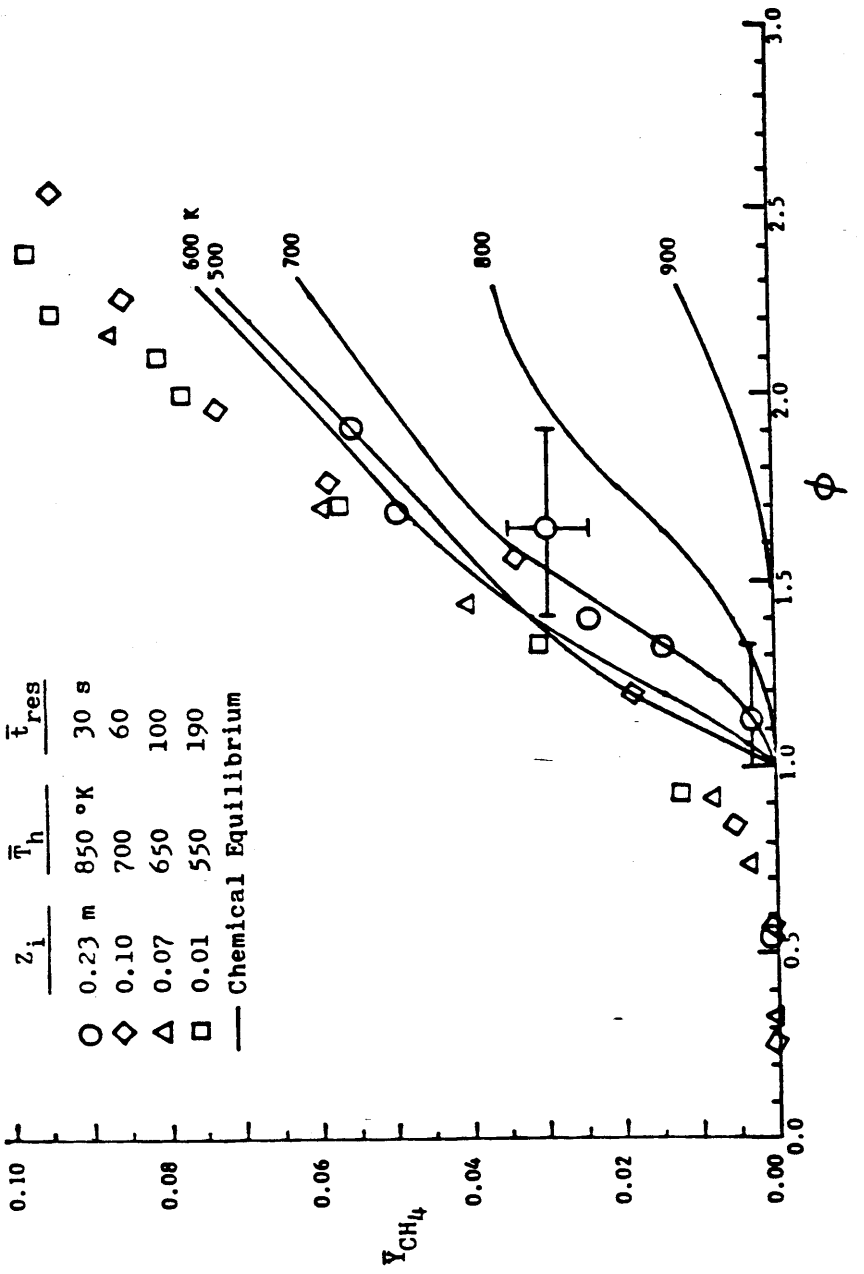
z_i
$\bar{T}_h$
$\bar{t}_{res}$
0.23 m 850 °K 30 s
0.10 700 60
0.07 650 100
0.01 550 190
Chemical Equilibrium
600 K
500
700
800
900
Y_{CH_4}
ϕ
0.00
0.02
0.04
0.06
0.08
0.10
0.0
0.5
1.0
1.5
2.0
2.5
3.0

Figure 5.6

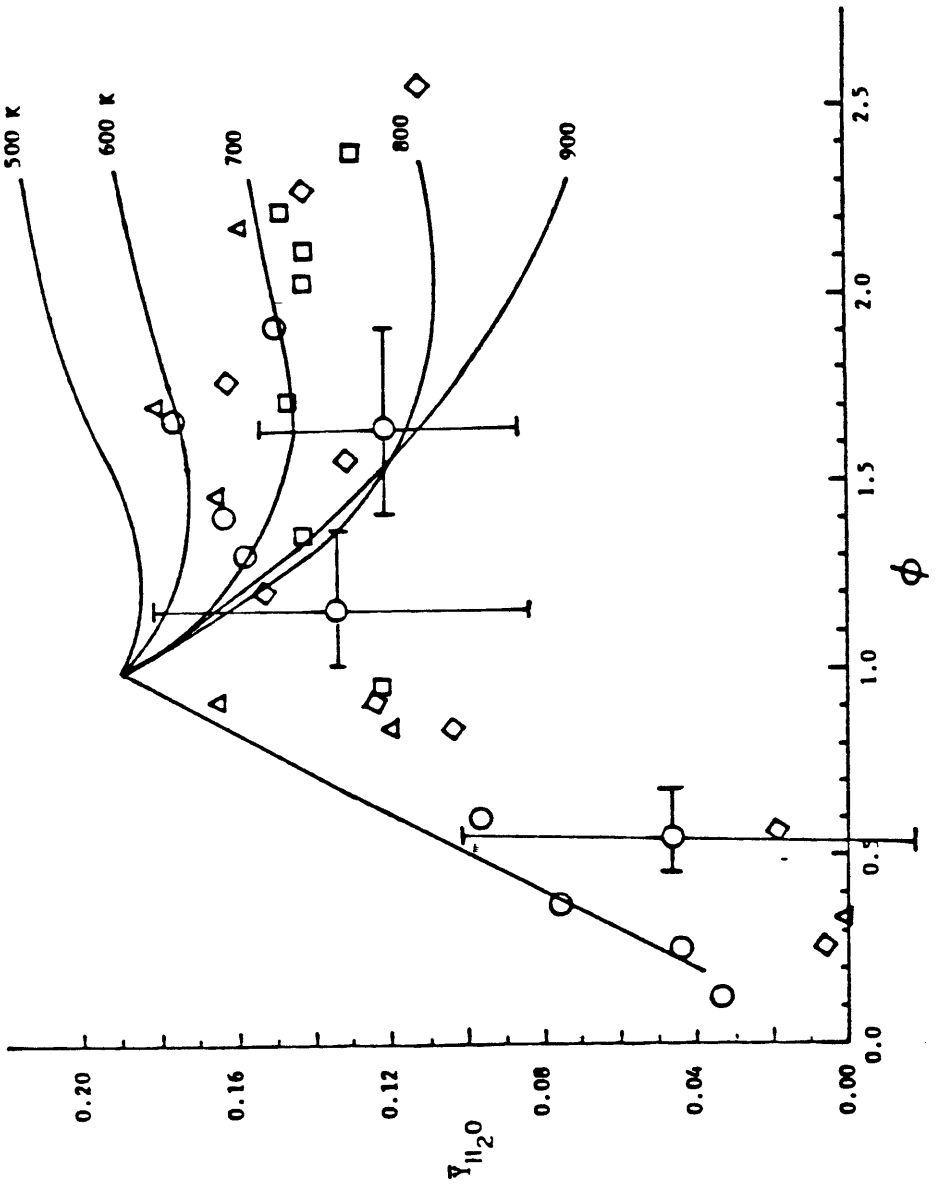
500 K
600 K
700
800
900
0.20
0.16
0.12
0.08
0.04
0.00
Y_{H_2O}
0.0
0.5
1.0
1.5
2.0
2.5
ϕ

Figure 5.7

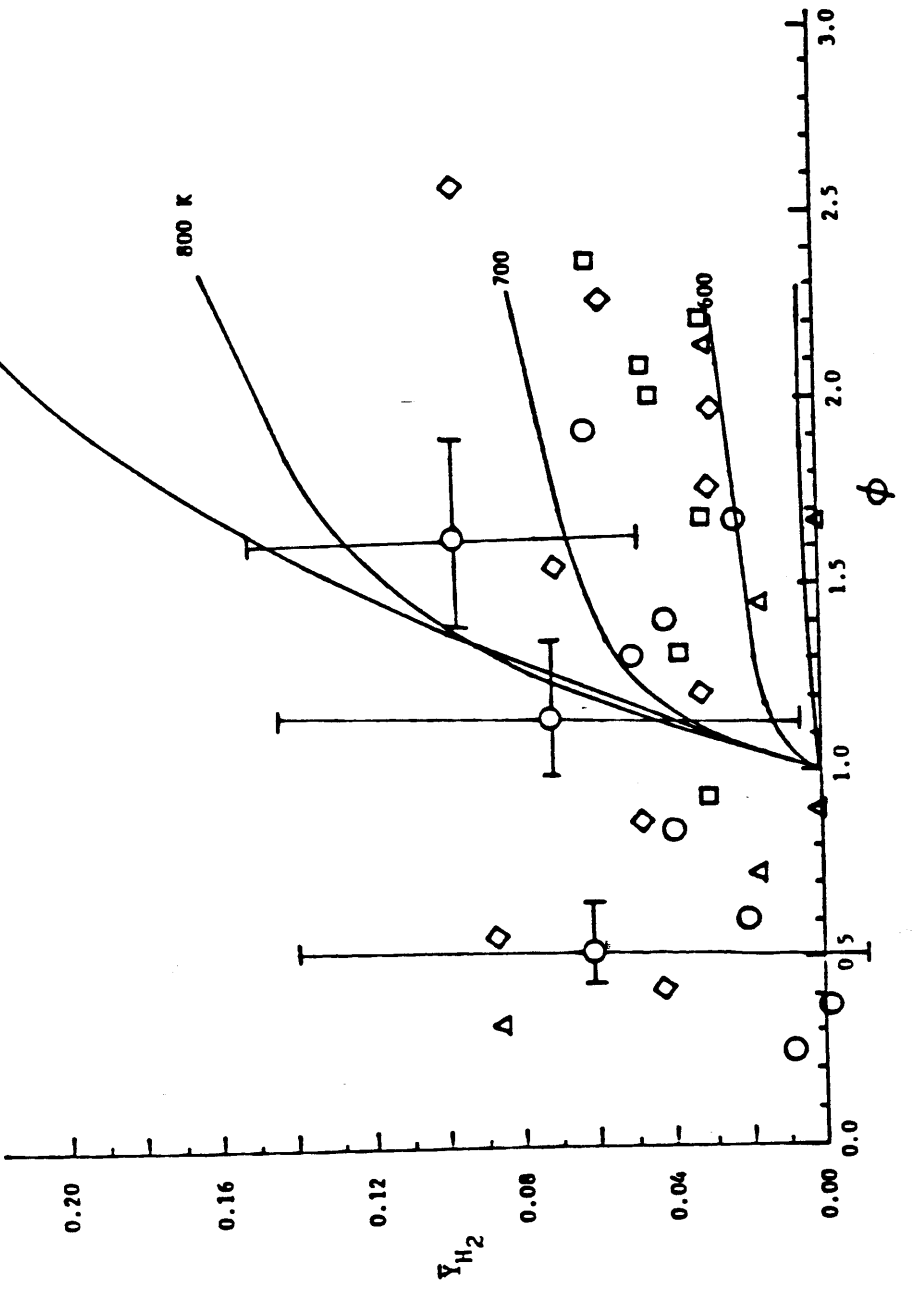
900 K
800 K
700
600
Y_{H_2}
0.20
0.16
0.12
0.08
0.04
0.00
0.0
0.5
1.0
1.5
2.0
2.5
3.0
ϕ

Figure 5.8

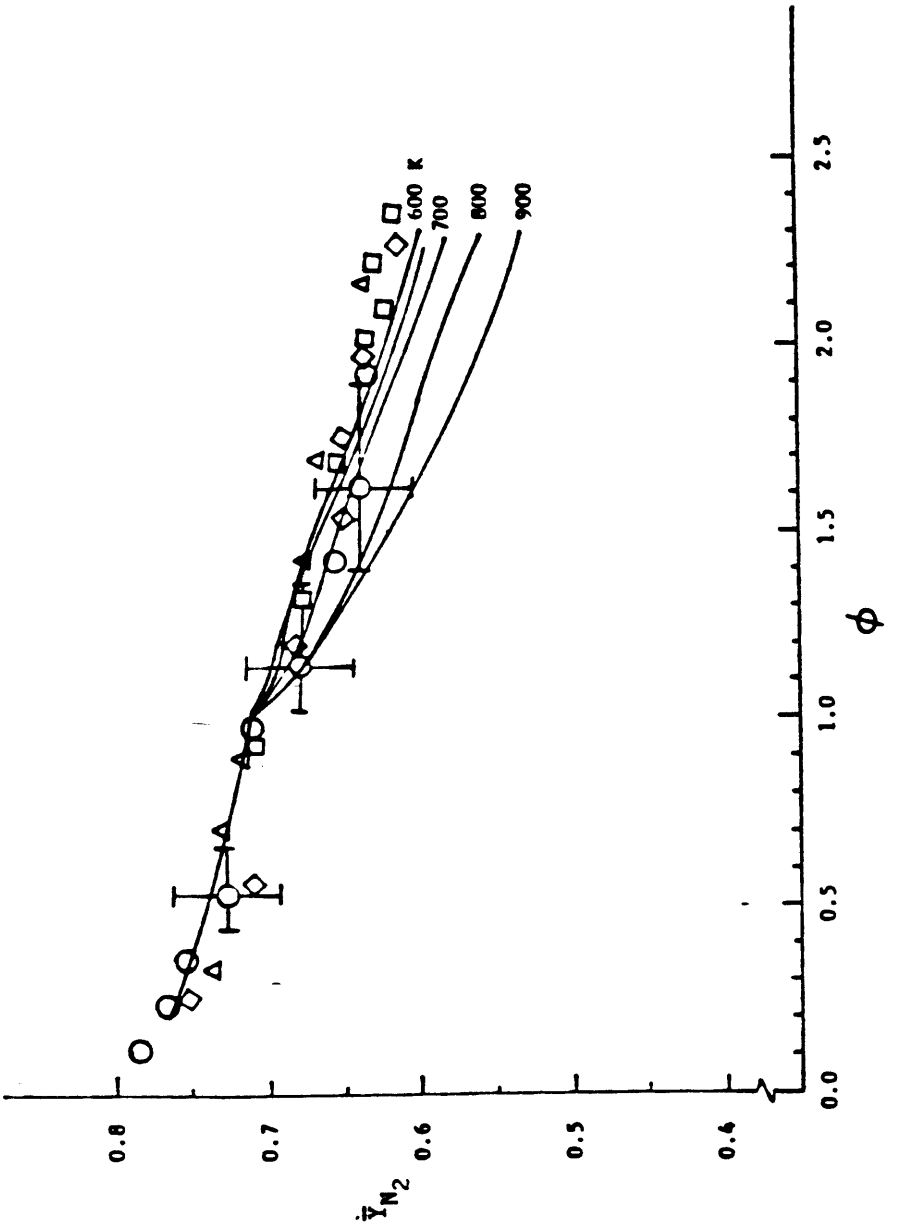

Figure 5.9

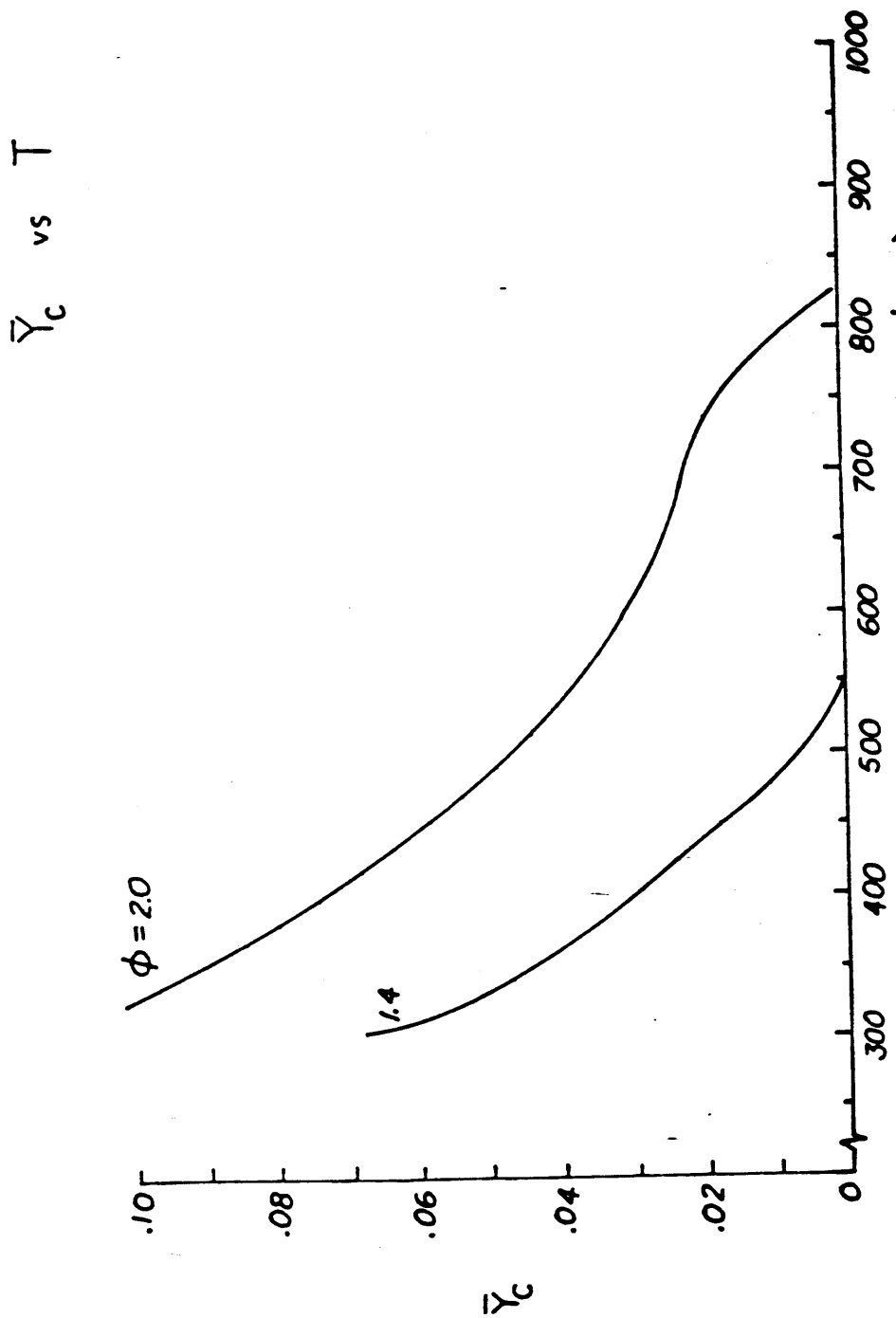
$\bar{Y}_c$ vs T
ϕ=2.0
1.4
$\bar{Y}_c$
.10
.08
.06
.04
.02
0
300
400
500
600
700
800
900
1000
EQUILIBRIUM TEMPERATURE (°K)

Figure 5.10

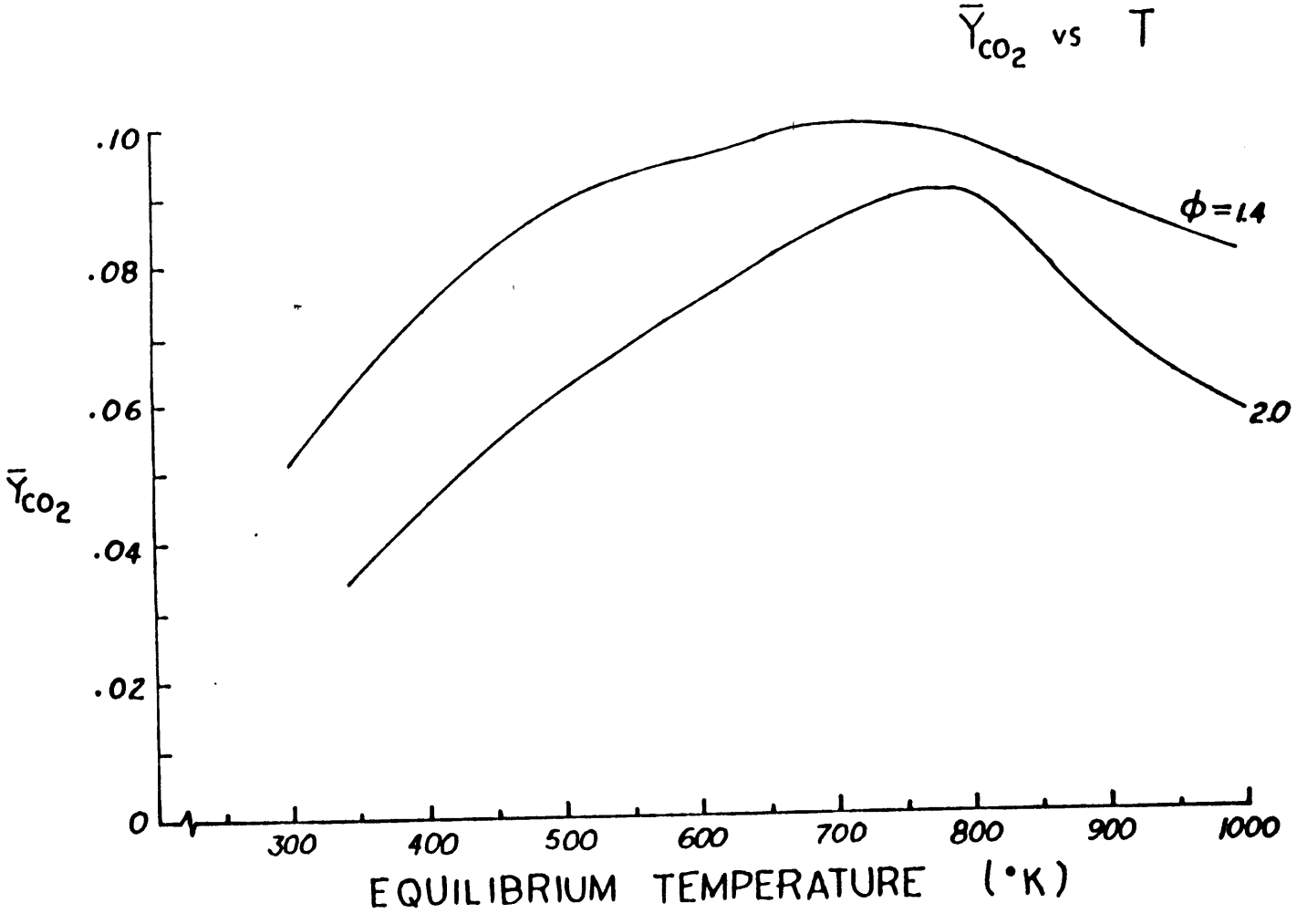
$\bar{Y}_{CO_2}$ vs T
.10
.08
.06
.04
.02
0
$\bar{Y}_{CO_2}$
$\phi = 1.4$
2.0
300
400
500
600
700
800
900
1000
EQUILIBRIUM TEMPERATURE (°K)

Figure 5.11

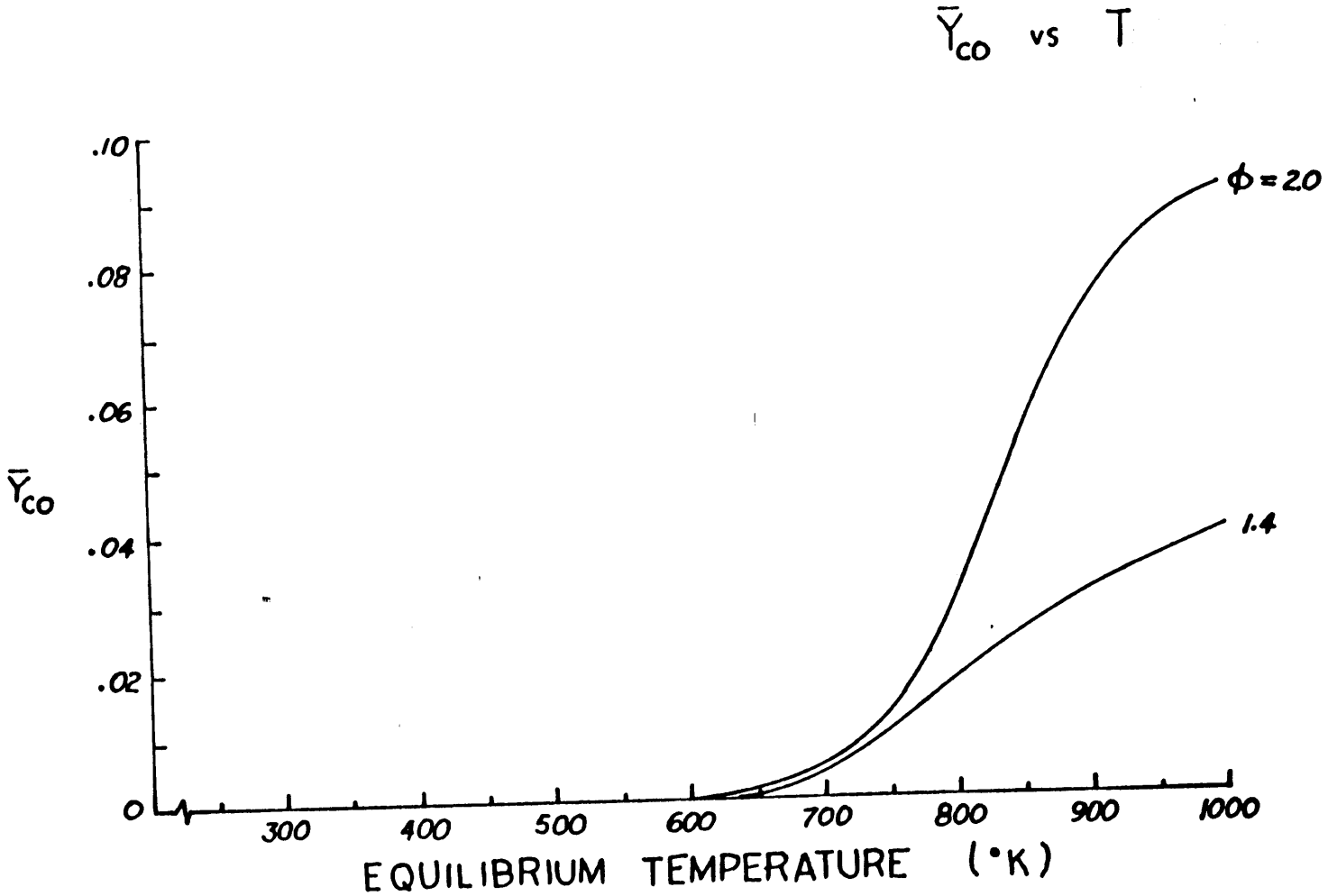
$\bar{Y}_{CO}$ vs T
.10
.08
.06
.04
.02
0
$\bar{Y}_{CO}$
$\phi = 2.0$
1.4
300
400
500
600
700
800
900
1000
EQUILIBRIUM TEMPERATURE (°K)

Figure 5.12

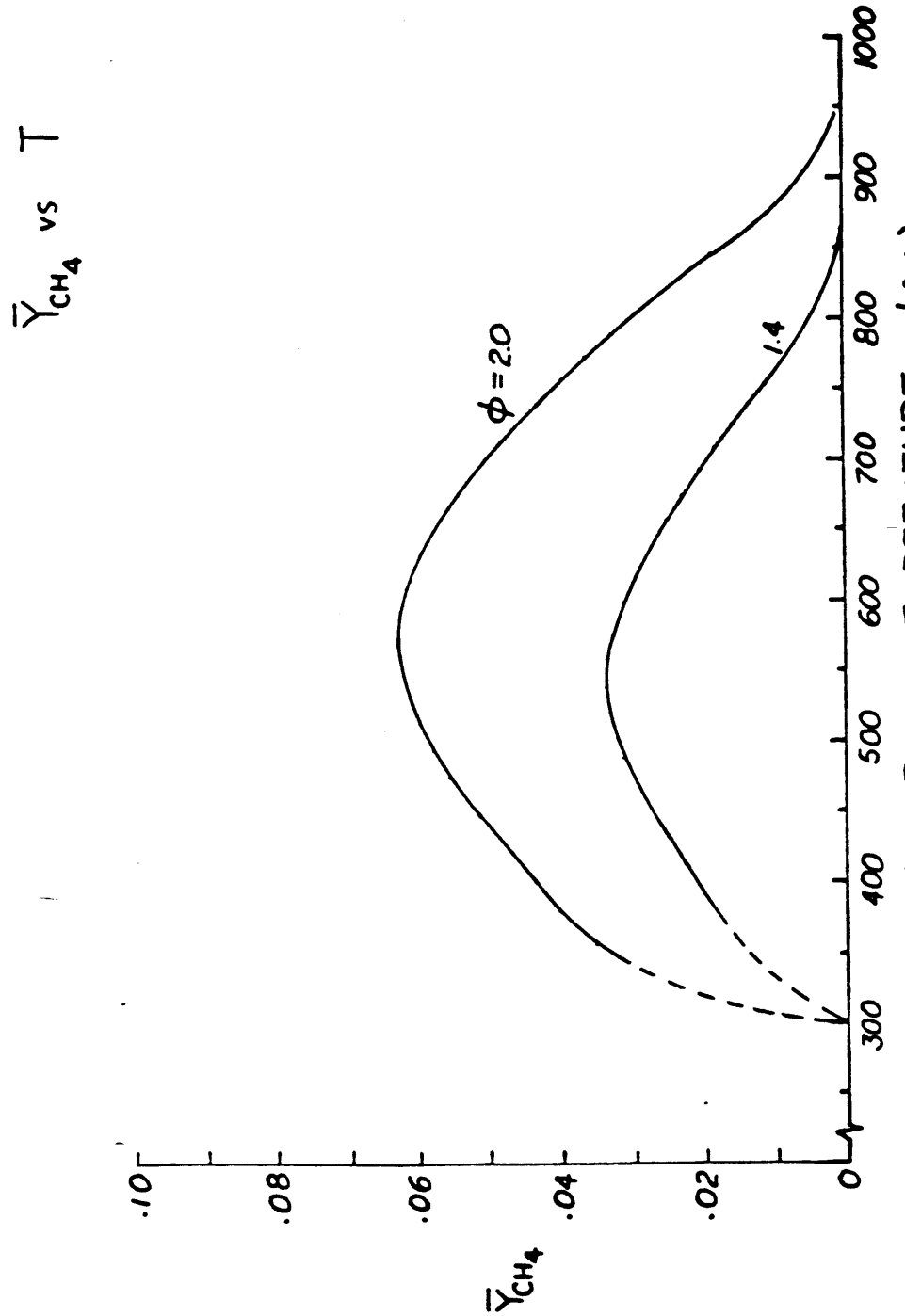
$\bar{Y}_{CH_4}$ vs T
$\bar{Y}_{CH_4}$
.10
.08
.06
.04
.02
0
300
400
500
600
700
800
900
1000
EQUILIBRIUM TEMPERATURE (°K)
ϕ=2.0
1.4

Figure 5.13

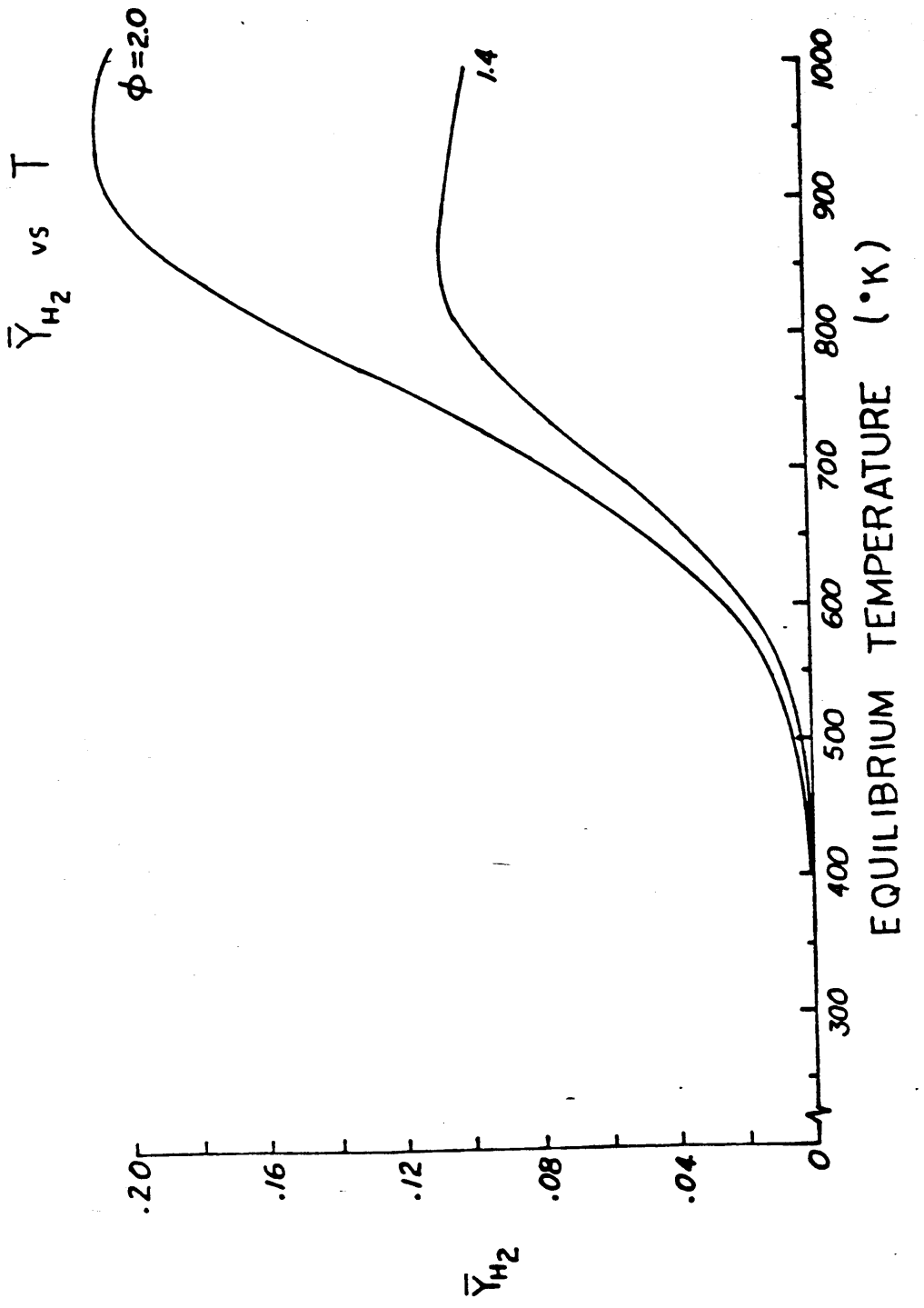
$\bar{Y}_{H_2}$ vs T
ϕ=2.0
1.4
.20
.16
.12
.08
.04
0
$\bar{Y}_{H_2}$
300
400
500
600
700
800
900
1000
EQUILIBRIUM TEMPERATURE (°K)

Figure 5.14

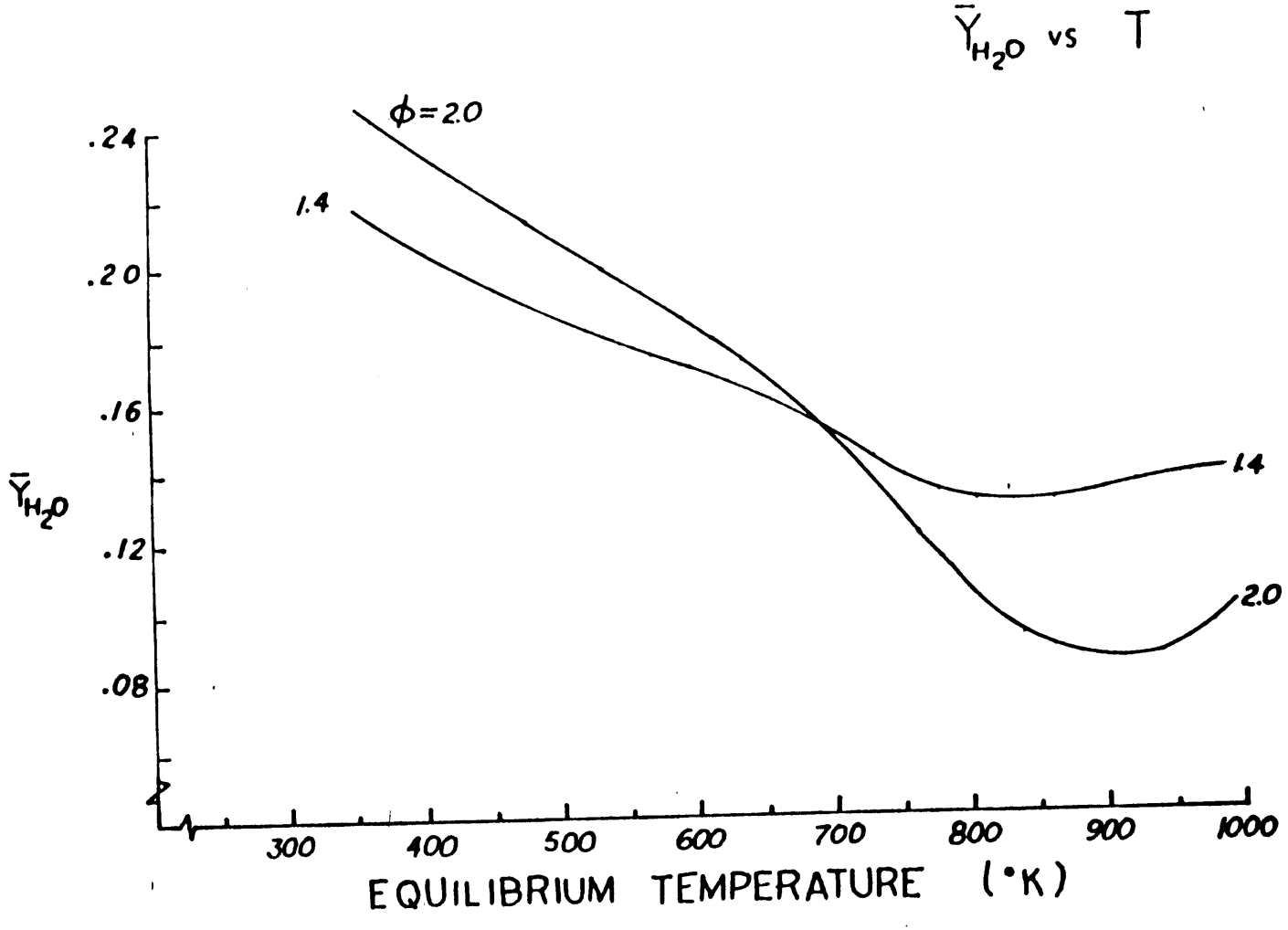
$\bar{Y}_{H_2O}$ vs T
ϕ=2.0
1.4
.24
.20
.16
.12
.08
$\bar{Y}_{H_2O}$
1.4
2.0
300
400
500
600
700
800
900
1000
EQUILIBRIUM TEMPERATURE (°K)

Figure 5.15

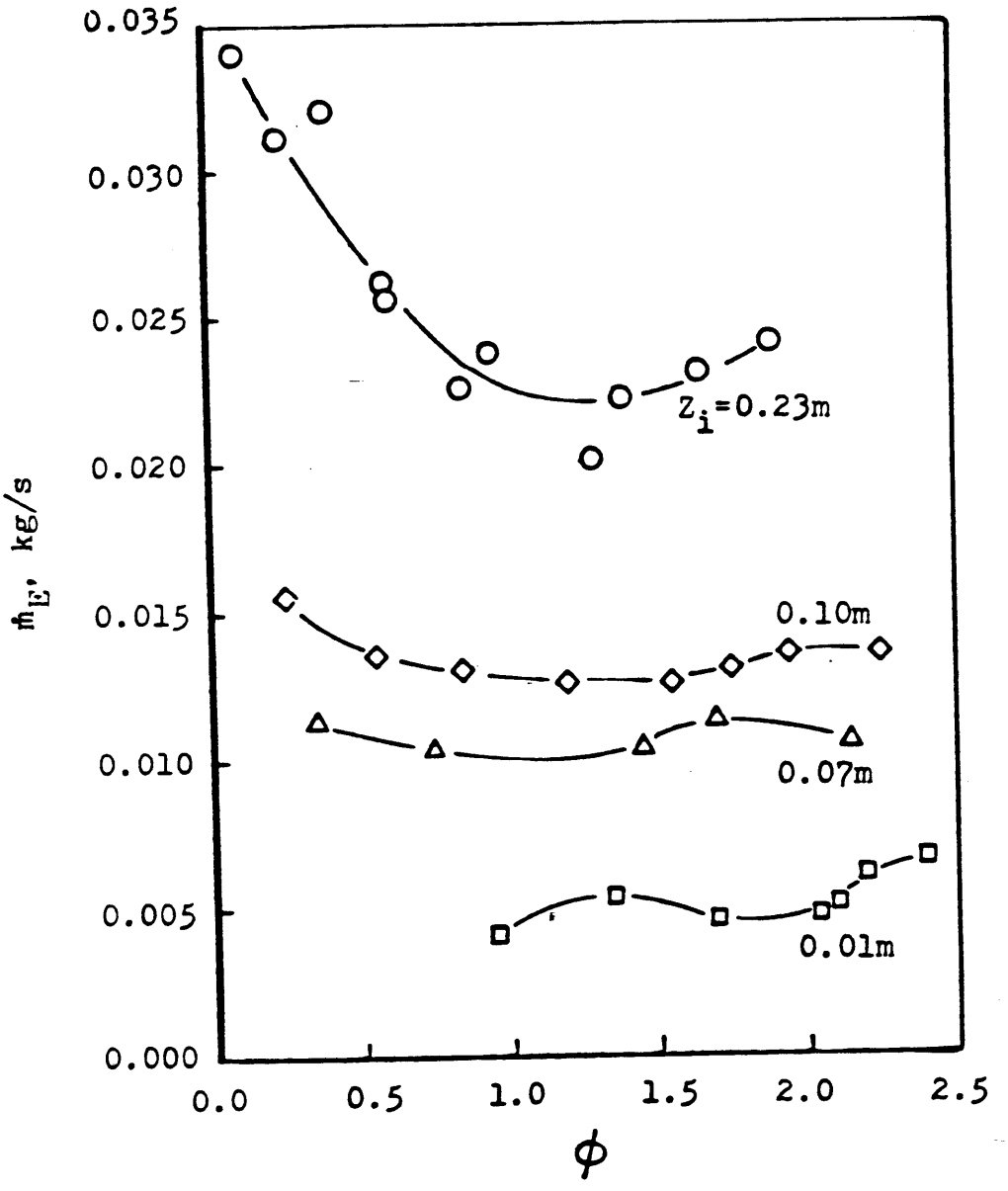
0.035
0.030
0.025
0.020
0.015
0.010
0.005
0.000
$\dot{m}_{L'}$, kg/s
Z_i=0.23m
0.10m
0.07m
0.01m
0.0
0.5
1.0
1.5
2.0
2.5
ϕ

Figure 5.16

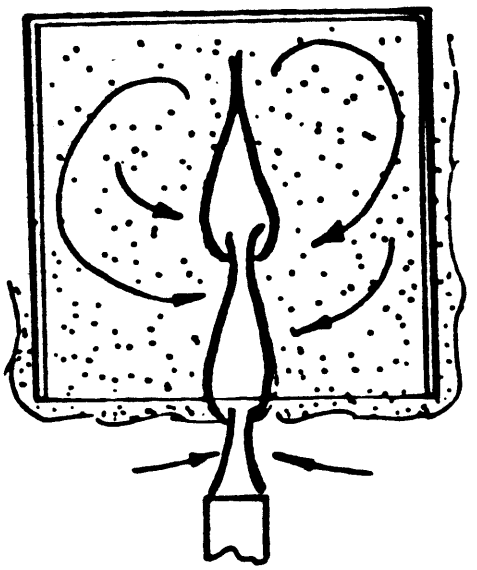

t = 0 sec:
- o Steady flame
- o Steady, low soot
- o 1.4% CO

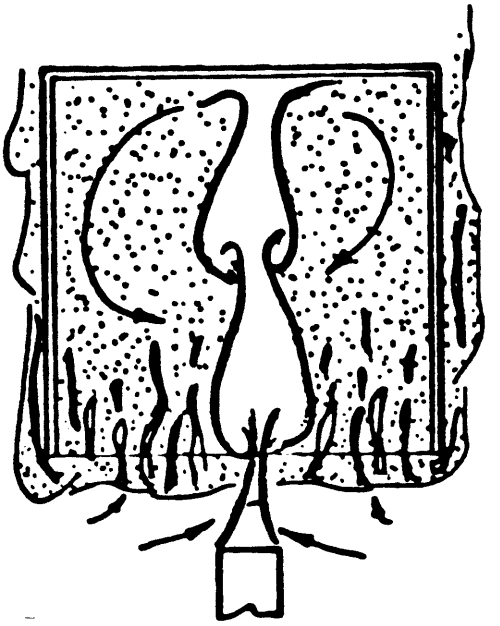

t = 40 sec:
- o Flamelets form
- o Taylor instability
- o More soot, 1.8% CO

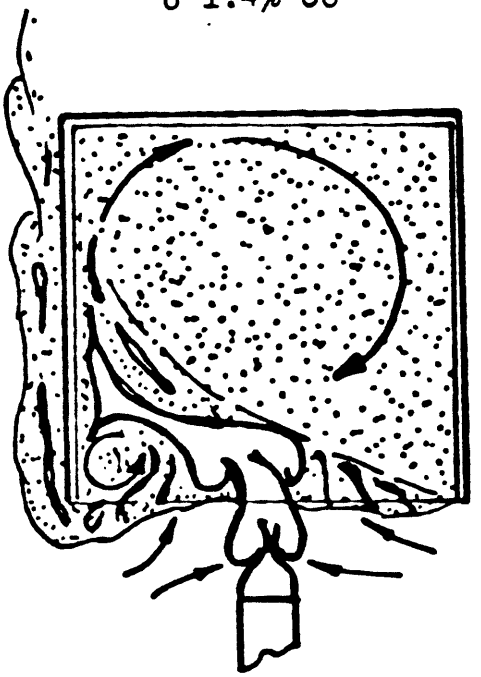

t = 47 sec:
- o Violent turnover
- o Flame strongly blown
- o Flamelets decay

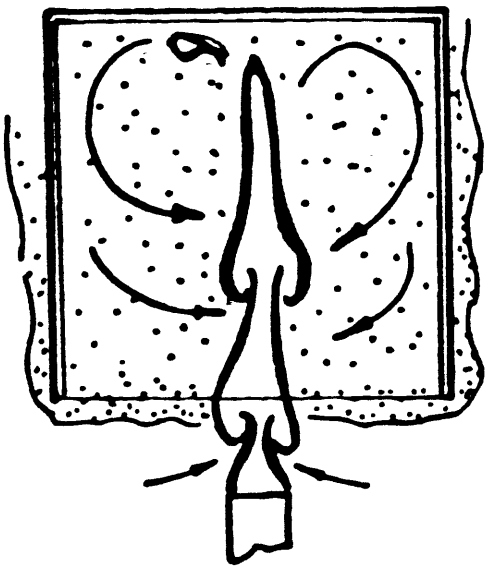

t = 62 sec:
- o Return to steady flame
- o Residence time about 100 sec.
- o Periodic cycle

Figure 5.17 (a)

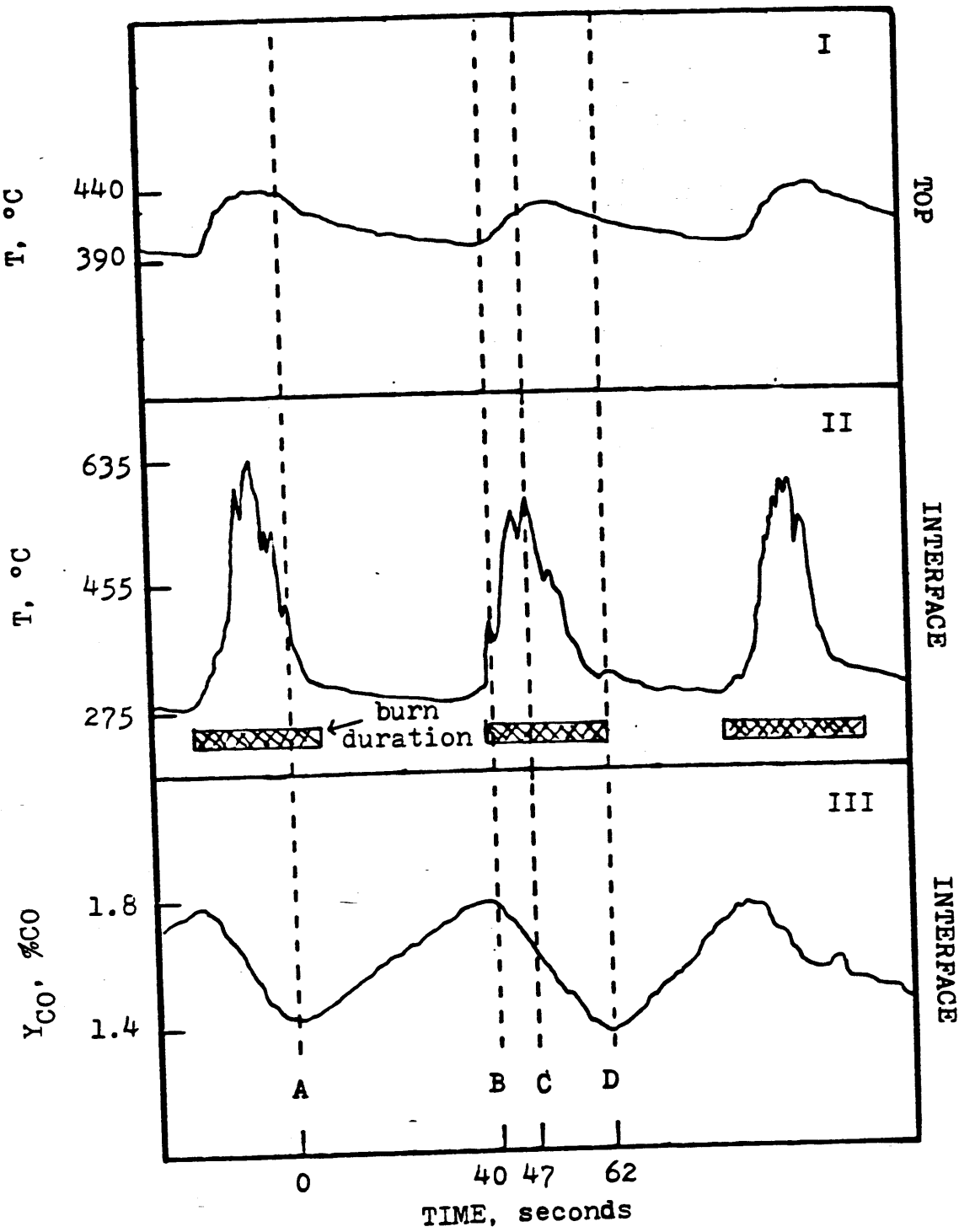
I
II
III
T, °C
440
390
635
455
275
Y_{CO}, %CO
1.8
1.4
TOP
INTERFACE
INTERFACE
burn
duration
A
B
C
D
0
40
47
62
TIME, seconds

Figure 5.17(b)

Chapter 6

SUMMARY AND CONCLUSIONS

6.1. Mixing in Doorway Flows

We have presented the results of experiments done in a half-scale room to investigate the mixing process near a doorway. No actual fire was present in the room; instead, a pump-furnace setup was used to simulate the entrainment and heating of fresh air by the fire plume. Four door geometries were used in the experiments. To estimate the mass transfer rates, it was assumed that the room and ambient air can be separated into four distinct regions with uniform thermodynamic properties: the hot ceiling layer, the cooler floor layer, the furnace, and the ambient or outside air regions.

The dimensionless temperature profiles (gas temperature normalized by the furnace and ambient air temperatures) were plotted as a function of distance from the interface for different floor suction rates. It was found that, for certain door geometries, the profile shapes were independent of the floor suction rate.

It was observed that the furnace temperature and the floor suction rate have a very strong influence on the interface height and the mixing rates. The mixing rates (expressed as the entrainment rate into the cold layer divided by the floor suction rate) were found to be a function of a Richardson number that uses the interface height as the characteristic length. The average inflow velocity, U_{1c}, was estimated with the use of the door width and the interface height. For a given value of $\dot{m}_2$, the effect of reducing the door area is to reduce the value of Ri_0 and hence increase the mixing rate. The door height was found to be a

much stronger influence on the mixing rate and interface height than the door width.

With the use of Taylor's entrainment hypothesis and a velocity scale based on the initial momentum of the jet, we found that the relationship between $\dot{m}_d/\dot{m}_{1c}$ and Ri_o is:

$$\left[\frac{1}{2}\left[\frac{\dot{m}_d}{\dot{m}_{1c}}\right]^2 + \frac{\dot{m}_d}{\dot{m}_{1c}}\right]\left[1 + \frac{\dot{m}_d}{\dot{m}_{1c}}\right]^2 = 11.7\left[\frac{\rho_h}{\rho_\infty}\frac{b}{W}\frac{1}{\sqrt{Ri_o}}\right]^2. \qquad (3.16a)$$

This correlation was derived from data obtained from a rectangular room with a door; it should not be applied to other room geometries which are radically different from the one used in our experiments.

6.2. Entrainment in Fire Plumes

We have made entrainment measurements in the near field of a buoyant diffusion flame where the interface height was well below the top of the flames. The entrainment rates were estimated by analyzing the composition of the hot combustion products in the ceiling layer. It was found that the temperature and species concentrations did not vary significantly within the ceiling layer.

For a given interface height, it was observed that the gas temperature reaches a maximum when the fuel-air ratio was increased above the stoichiometric value. This maximum temperature was found to decrease with interface height and is a result of changes in the relative magnitude of the heat released by the fire and heat loss from the system to the surrounding environment.

The measured species concentrations were compared with the theoretical equilibrium composition values obtained from a computer program written by

Gordon and McBride (1976). It was found that the measured species concentrations were almost independent of the gas temperature. The error resulting from the assumption of negligible soot concentration was found to be large enough to affect the accuracies of the calculated water and hydrogen concentrations.

The mass entrainment rates of air into the fire plume were measured for four interface heights. The entrainment data correlated well with the values reported by Cetegen (1982). As was also observed by Cetegen (1982), the entrainment rates were found to be a very weak function of the fuel-air ratio and at very low elevations of the interface.

In our study of fuel rich ceiling layers, it was observed that there was a critical fire size for a given interface height in which flamelets started to form in the interface and spread until the entire interface was set on fire. The burning of the interface caused an inversion process to occur in the ceiling layer. It was observed that the inversion process occurred in regular cycles with the period being inversely proportional to the fire size.

Some preliminary experiments were made to investigate the effect of injecting fuel into an oxygen rich ceiling layer. Fuel and oxygen mass models were set up to estimate the amount of added fuel that reacts in the fire plume. For a ceiling layer with an oxygen content of about 12% by volume, it was found that more than 50% of the fuel injected into the ceiling layer reacted with the oxygen. Since it was assumed that the plume entrainment rates were independent of the flowrate of added fuel, the models were found to be inaccurate when a large amount of fuel was added to the ceiling layer.

In another experiment to determine if the added fuel will react in an oxygen rich ceiling layer, the pipe used to inject the fuel was lighted and then placed inside the ceiling layer. It was found that the critical mole fraction of oxygen is

about 0.13 for the flame on the pipe to keep burning. These findings are the results of preliminary experiments; more refined methods must be used to accurately determine the effect of adding fuel to an oxygen rich ceiling layer.

7. References

G.N. ABRAMOVICH, Theory of turbulent jets. M.I.T. Press, Cambridge, Mass. (1963).

G.L. BROWN and A. ROSHKO, On density effects and large structures in turbulent mixing layers. *Journal of Fluid Mechanics*, **64**, 775-815 (1974).

B. CETEGEN, E.E. ZUKOSKI and T. KUBOTA, Entrainment and flame geometry of fire plumes. California Institute of Technology (August 1982).

V. CHU and M.R. VANVARI, Experimental study of turbulent stratified shearing flow. *Journal of the Hydraulics Division*, ASCE, **102**, no. HY6, 691-705 (1976).

T.H. ELLISON & J.S. TURNER, Turbulent entrainment in stratified flows. *Journal of Fluid Mechanics*, **6**, 423-448 (1959).

H.B. FISCHER, E.J. LIST, R.C. KOH, J. IMBERGER & N.H. BROOKS, Mixing in inland and coastal waters. Academic Press, New York (1979).

S. GORDON and B.J. McBRIDE, Computer program for calculation of complex chemical equilibrium compositions, rocket performance, incident and reflected shocks, and Chapman-Jouguet detonations. NASA SP-273 (March 1976).

K. KAWAGOE, Fire behavior in rooms. Report No. 27. Building Research Institute, Japan (1958).

B. LEWIS and G. VON ELBE, Combustion, flames and explosion of gases. Academic Press, New York (1963).

B.R. MORTON, G.I. TAYLOR & J.S. TURNER. *Proc. Roy. Soc.* A, **234**, 1-23 (1956).

W.S. SARGENT, Natural convection and associated heat transfer processes in room fires. Ph.D. Thesis, California Institute of Technology (1983).

R.S. SCOTTI and G.M. CORCOS, An experiment on the stability of small disturbances in a stratified free shear layer. *Journal of Fluid Mechanics*, **52**, 499-528 (1972).

P.M. SFORZA and G. HERBST, A study of three dimensional, incompressible, turbulent wall jets. *AIAA*, **8**, 276 (1970).

F.S. SHERMAN, J. IMBERGER & G.M. CORCOS, Turbulence and mixing in stably stratified waters, *Annual Review of Fluid Mechanics*, **10**, 267-288 (1978).

A. SIGALLA, Experimental data on turbulent wall jets. *Aircraft Eng.*, **30**, 131-134 (1958).

E.N. TANGREN, W.S. SARGENT and E.E. ZUKOSKI, Hydraulic and numerical modeling of room fires. California Institute of Technology. NSF Grant No. ENV 76-06660 (June 1978).

P.H. THOMAS, P.L. HINKLEY, C.R. THEOBALD and D.L. SIMMS, Investigations into the flow of hot gases in roof venting. Fire Research Technical Paper No. 7. Department of Scientific and Industrial Research and Fire Offices' Committee Joint Fire Research Organization, Borehamwood (1963).

J.S. TURNER, Buoyancy effects in fluids. Cambridge Univ. Press (1973).

E.E. ZUKOSKI, Convective flows associated with room fires. California Institute of Technology, NSF Grant No. GI 31892X1. NSF RANN Conference on Fire Research, Harvard University (June 1975).

E.E. ZUKOSKI, Development of a stratified ceiling layer in the early stages of a closed-room fire. *Fire Mater.*, **2**, 54-62 (1978).

E.E. ZUKOSKI and T. KUBOTA, A computer model for fluid dynamic aspects of a transient fire in a two-room structure. California Institute of Technology (January 1978).

E.E. ZUKOSKI and T. KUBOTA, Two-layer modeling of smoke movement in building fires. *Fire Mater.*, **4**, 17-27 (1980).

E.E. ZUKOSKI and D.L. PETERKA, Measurements of entrainment in a doorway flow. California Institute of Technology (October 1979).

Appendix A

THE TWO-LAYER ROOM MODEL

A.1. Mass Transfer Model

The two-layer room model assumes that the room may be divided into two homogeneous regions with uniform properties: the ceiling (or hot) layer which contains the combustion products, and the floor (or cold) layer which contains fresh air. In addition to the two layers, the furnace and the ambient air region are also assumed to have uniform properties. Figure 2.2(b) is a schematic diagram of the model used in the calculation of the mass flows between each region. The thermodynamic properties in each region are assumed to be uniform throughout the region and independent of time.

Given the quantities $\dot{m}_2$, $\dot{m}_f$, K_h, K_c, and K_∞, the mass flowrates $\dot{m}_{1h}$, $\dot{m}_{1c}$, $\dot{m}_d$, and $\dot{m}_u$ may be calculated by balancing the total mass flows and the carbon dioxide mass flows in each region.

For the floor layer: $$\dot{m}_{1c} + \dot{m}_d - \dot{m}_u - \dot{m}_2 = 0 \qquad \text{(A.1)}$$

$$C_\infty \dot{m}_{1c} + C_h \dot{m}_d - C_c \dot{m}_u - C_c \dot{m}_2 = 0 \qquad \text{(A.2)}$$

For the ceiling layer: $$\dot{m}_3 + \dot{m}_u - \dot{m}_{1h} - \dot{m}_d = 0 \qquad \text{(A.3)}$$

$$C_3 \dot{m}_3 + C_c \dot{m}_u - C_h \dot{m}_{1h} - C_h \dot{m}_d = 0 \qquad \text{(A.4)}$$

For the furnace: $\dot{m}_3 = \dot{m}_2 + \dot{m}_f$ (A.5)

where C_i is the mass fraction of CO_2 in region i. In our experiment the fuel flow rate, $\dot{m}_f$, was found to be negligible compared to the total mass flow $\dot{m}_2$. $\dot{m}_3$ may then be approximated by

$$\dot{m}_3 \approx \dot{m}_2 . \tag{A.6}$$

The equations must now be manipulated to solve for the unknown mass flows. $\dot{m}_u$ may be eliminated from Eq. A.1 with the use of Eq. A.3.

$$\dot{m}_{1c} - \dot{m}_{1h} = \dot{m}_2 - \dot{m}_3 \tag{A.7}$$

Similarly, Eq. A.4 may be used to eliminate the term $\dot{m}_u$ in Eq. A.2.

$$C_a\dot{m}_{1c} - C_h\dot{m}_{1h} = C_c\dot{m}_2 - C_3\dot{m}_3 \tag{A.8}$$

The equation for $\dot{m}_{1h}$ is found by multiplying K_a to both sides of Eq. A.7 and subtracting the result from Eq. A.8 to eliminate the term $K_a\dot{m}_{1c}$.

$$\dot{m}_{1h} = \frac{(C_a - C_c)\dot{m}_2 + (C_3 - C_a)\dot{m}_3}{C_h - C_a} \tag{A.9}$$

Eq. A.7 gives $\dot{m}_{1c}$ in terms of $\dot{m}_2$, $\dot{m}_3$, and $\dot{m}_{1h}$:

$$\dot{m}_{1c} = \dot{m}_2 - \dot{m}_3 + \dot{m}_{1h} \tag{A.10}$$

$\dot{m}_u$ is found by combining Eqs.A.3 and A.4 to eliminate the term $\dot{m}_d$.

$$\dot{m}_u = \frac{\dot{m}_3(C_3 - C_h)}{C_h - C_c} \tag{A.11}$$

and, finally, Eq. A.1 is used to find $\dot{m}_d$.

$$\dot{m}_d = \dot{m}_u + \dot{m}_2 - \dot{m}_{1c} \tag{A.12}$$

If $\dot{m}_3 \approx \dot{m}_2$, Eq. A.12 may be combined with Eqs. A.9, A.10, and A.11 to give

$$\dot{m}_d = \dot{m}_2 \left[\frac{(C_3 - C_c)(C_c - C_\infty)}{(C_h - C_c)(C_h - C_\infty)} \right]. \tag{A.13}$$

If we assume that the molecular weight of the gas in the room is approximately the ambient value, then the above equations may be rewritten in terms of the mole fractions K_i.

$$\dot{m}_{1h} = \frac{(K_\infty - K_c)\dot{m}_2 + (K_3 - K_\infty)\dot{m}_3}{K_h - K_\infty} \tag{A.14}$$

$$\dot{m}_{1c} = \dot{m}_2 - \dot{m}_3 + \dot{m}_{1h} \tag{A.15}$$

$$\dot{m}_u = \frac{\dot{m}_3(K_3 - K_h)}{K_h - K_c} \tag{A.16}$$

$$\dot{m}_d = \dot{m}_2 \left[\frac{(K_3 - K_c)(K_c - K_\infty)}{(K_h - K_c)(K_h - K_\infty)} \right] \tag{A.17}$$

A.2. Definition of U^*

Taylor's entrainment hypothesis states that local entrainment rate is proportional to the local maximum velocity and the local entrainment coefficient (see Sec. 3.1.3). Since we have no knowledge of the velocity profiles in the room, we were forced to look for another velocity scale. From previous experimental work (Chu & Vanvari 1976), it is known that the entrainment process takes place primarily in the so-called "supercritical" (i.e., momentum-dominated) region of a stratified wall jet. In this supercritical region, the flow is influenced by the upstream condition only and has similar characteristics to a neutral jet (Chu & Vanvari 1976). For our range of experiments, it follows that we may ignore the momentum losses due to wall friction and changes in hydrostatic pressure and define a new velocity scale based on the initial momentum of the jet. The velocity scale, U^*, is defined to be:

$$U^*(x) \equiv \frac{\int_0^\infty \rho U^2 dy}{\int_0^\infty \rho U\, dy}. \tag{A.18}$$

A mass balance of the cold layer jet gives ($\dot{m}_u = 0$):

$$\int_0^\infty \rho U\, dy \equiv \dot{m}(x) = \dot{m}_d(x) + \dot{m}_{1c} \tag{A.19}$$

where $\dot{m}_d(x)$ is the mass flux of entrained hot layer gas, and $\dot{m}_{1c}$ is the mass flowrate of fresh air entering the room.

A momentum balance of the cold layer jet gives:

$$\int_0^\infty \rho U^2 dy = \dot{m}_{1c} U_{1c} - \dot{m}_{1c} U_{1c} \left[1 - \frac{b}{W}\right] - \left[C_F(x)\right] - \left[C_P(x)\right] \qquad (A.20)$$

where $\dot{m}_{1c} U_{1c}$ is the initial jet momentum; $(\dot{m}_{1c} U_{1c})(1 - b/W)$ is the loss due to the sudden expansion of the jet width (from b to W); $C_F(x)$ represents the frictional drag of the walls; and $C_P(x)$ represents the pressure force on the layer due to its changing depth and density (see Ellison & Turner 1959). If we now assume that the losses due to the presence of pressure gradients and wall friction are negligible compared to $(\dot{m}_{1c} U_{1c})(b/W)$, Eq. A.18 may be combined with Eqs. A.19 and A.20:

$$U^*(x) \approx \frac{\dot{m}_{1c} U_{1c}}{\dot{m}(x)} \frac{b}{W}. \qquad (A.21)$$

A.3. Relationship between U^* and U_{max}

From Eq. A.18:

$$U^*(x) = \frac{x\, U_{max}^2(x) \int_0^\infty \rho \left[\frac{U}{U_{max}}\right]^2 d(y/x)}{x\, U_{max}(x) \int_0^\infty \rho \frac{U}{U_{max}} d(y/x)}. \qquad (A.22)$$

For self-preserving jets with small density variations in the streamwise direction ($\rho \approx \rho_\infty$), Eq. A.22 reduces to:

$$U^*(x) = \frac{U_{max}(x)}{A_1} \qquad (A.23)$$

where

$$A_1 = \frac{\int_0^\infty \rho \frac{U}{U_{max}} d(y/x)}{\int_0^\infty \rho \left[\frac{U}{U_{max}}\right]^2 d(y/x)} = \text{constant} . \qquad (A.24)$$

A_1 is an empirical constant whose value depends on the shape of the velocity profile. For Gaussian velocity profiles ($U/U_{max} = e^{-[\gamma y/x]^2}$), A_1 is approximately 1.4.

Appendix B

CALCULATION OF SPECIES CONCENTRATIONS IN A FIRE PLUME

For one mole of methane fuel burning in x moles of excess air:

$$\left[CH_4 + (2 + x)(O_2 + 3.76N_2) \rightarrow n_{CO_2}CO_2 + n_{CO}CO + \right.$$
$$\left. + n_{CH_4}CH_4 + n_{O_2}O_2 + n_{H_2O}H_2O + n_{H_2}H_2 + n_{N_2}N_2\right]$$

where n_i is the number of moles of species i. We can now write four equations to balance the number of moles of the elements C, H, O, and N.

$$C: \quad 1 = n_{CO_2} + n_{CO} + n_{CH_4} \tag{B.1}$$

$$H: \quad 2 = 2n_{CH_4} + n_{H_2O} + n_{H_2} \tag{B.2}$$

$$O: \quad 2 + x = n_{CO_2} + n_{O_2} + \frac{1}{2}(n_{H_2O} + n_{CO}) \tag{B.3}$$

$$N: \quad 3.76(2 + x) = n_{N_2} \tag{B.4}$$

Using our analyzers, we are able to measure the mole fraction of CH_4, CO_2, CO, and O_2 in a *dried* sample. Using this data we wish to find: (1) the actual mole fractions of the seven species in the hood; (2) the equivalence ratio; (3) the mass of air entrained into the plume; and (4) the molecular weight of the mixture.

B.1. Species Concentrations

Let N_{sample} be the total number of moles in the dried sample, i.e.,

$$N_{sample} = n_{CO_2} + n_{CO} + n_{CH_4} + n_{O_2} + n_{N_2} + n_{H_2} . \tag{B.5}$$

Now define

$$Y_{CO_2} \equiv \frac{n_{CO_2}}{N_{sample}}; \; Y_{CO} \equiv \frac{n_{CO}}{N_{sample}}; \; Y_{H_2O} \equiv \frac{n_{H_2O}}{N_{sample}}; \; etc.$$

or, in general, for species i:

$$Y_i \equiv \frac{n_i}{N_{sample}} \tag{B.6}$$

Note that Y_i is the mole fraction of species i in the dried sample with the exception of Y_{H_2O} which has no physical significance. Dividing Eqs. B.1, B.2, B.3, B.4, and B.5 by N_{sample} yields

$$\frac{1}{N_{sample}} = Y_{CO_2} + Y_{CO} + Y_{CH_4} \tag{B.7}$$

$$\frac{2}{N_{sample}} = 2Y_{CH_4} + Y_{H_2O} + Y_{H_2} \tag{B.8}$$

$$\frac{Y_{N_2}}{3.76} = Y_{CO_2} + Y_{O_2} + \frac{1}{2}(Y_{H_2O} + Y_{CO}) \tag{B.9}$$

$$1 = Y_{CO_2} + Y_{CO} + Y_{CH_4} + Y_{O_2} + Y_{N_2} + Y_{H_2} . \qquad \text{(B.10)}$$

where Eq. B.9 was obtained by combining Eqs. B.3 and B.4. The value of N_{sample} is given explicitly by Eq. B.7 since Y_{CO_2}, Y_{CO}, and Y_{CH_4} are known.

We now have to manipulate the equations to find the unknown terms. Subtracting Eq. B.10 from B.8 eliminates the term Y_{H_2}.

$$\frac{2}{N_{sample}} - 1 = Y_{CH_4} + Y_{H_2O} - Y_{CO_2} - Y_{CO} - Y_{O_2} - Y_{N_2} \qquad \text{(B.11)}$$

Multiplying Eq. B.9 by 2 then subtracting the result from Eq. B.11 eliminates the term Y_{H_2O}:

$$\frac{2}{N_{sample}} - 1 = Y_{CH_4} - 3Y_{CO_2} - 2Y_{CO} - 3Y_{O_2} - 0.4681\,Y_{N_2} \qquad \text{(B.12)}$$

Y_{N_2} is calculated from Eq.B.12:

$$Y_{N_2} = \frac{1}{0.4681}\left[Y_{CH_4} - 3Y_{CO_2} - 2Y_{CO} - 3Y_{O_2} - \frac{2}{N_{sample}} + 1\right] \qquad \text{(B.13)}$$

Eq. B.9 gives Y_{H_2O}:

$$Y_{H_2O} = 2\left[\frac{Y_{N_2}}{3.76} - Y_{CO_2} - Y_{O_2}\right] - Y_{CO} \qquad \text{(B.14)}$$

and Eq. B.8 yields Y_{H_2}:

$$Y_{H_2} = \frac{2}{N_{sample}} - 2Y_{CH_4} - Y_{H_2O} \tag{B.15}$$

The next step is to find the actual mole fractions of each species in the hood. Let N_{hood} be the total number of moles in the hood, i.e.,

$$\begin{aligned} N_{hood} &= n_{CO_2} + n_{CO} + n_{CH_4} + n_{O_2} + n_{H_2O} + n_{H_2} + n_{N_2} \\ &= N_{sample}\left[Y_{CO_2} + Y_{CO} + Y_{CH_4} + Y_{O_2} + Y_{H_2O} + Y_{H_2} + Y_{N_2}\right] \\ &= N_{sample}\left[1 + Y_{H_2O}\right] \end{aligned}$$

where the last result came from using (B.10). Now define $\overline{Y}_i$ as the actual mole fraction of species i, i.e.,

$$\begin{aligned} \overline{Y}_i &= \frac{n_i}{N_{hood}} \\ &= \frac{Y_i N_{sample}}{N_{hood}} \\ &= \frac{Y_i}{1 + Y_{H_2O}}. \end{aligned} \tag{B.16}$$

Therefore,

$$\overline{Y}_{CO_2} = \frac{Y_{CO_2}}{1 + Y_{H_2O}}; \quad \overline{Y}_{H_2O} = \frac{Y_{H_2O}}{1 + Y_{H_2O}}; \quad etc.$$

B.2. The Equivalence Ratio

The equivalence ratio is defined to be the fuel-air ratio divided by the stoichiometric fuel-air ratio.

$$\varphi = \frac{2}{2 + x} \tag{B.17}$$

Eq. B.4 may be used to calculate x.

$$n_{N_2} = (2 + x)3.76 = Y_{N_2} N_{sample}$$

Therefore,

$$\varphi = \frac{2}{2 + x} = \frac{7.52}{Y_{N_2} N_{sample}} \tag{B.18}$$

where Y_{N_2} and N_{sample} can be calculated from Eqs. B.7 and B.13, respectively.

B.3. Air Entrainment Rate

The mass entrainment of air, $\dot{m}_E$, can be calculated if the mass flowrate of fuel, $\dot{m}_f$, is given.

$$\dot{m}_E = (2 + x)(4.76)\left[\frac{\dot{m}_f}{16}\right](28.8)$$

$$= 8.58(2 + x)\dot{m}_f = 8.58\left[\frac{2}{\varphi}\right]\dot{m}_f \tag{B.19}$$

where $(2 + x)(4.76)$ is the number of moles of air per mole of fuel; 16 is the

molecular weight of the fuel; and 28.8 is the molecular weight of air.

B.4. Molecular Weight

The molecular weight, MW, of the mixture is

$$MW = \frac{\text{total mass in hood}}{\text{total moles in hood}}$$

$$= \sum_i \bar{Y}_i \times MW_i \qquad \text{(B.20)}$$

where $\bar{Y}_i$ and MW_i are the mole fraction and molecular weight of species i.

Appendix C

TABULATED DATA FROM THE ROOM EXPERIMENTS

The experimental data obtained from the room experiments are tabulated on the following pages. The symbols are defined in the List of Symbols. The units of the symbols are as follows:

Symbol	Units
K_∞, K_h, K_3, K_c	$\%CO_2$ by volume
$\dot{m}_2$, $\dot{m}_{1h}$, $\dot{m}_{1c}$, $\dot{m}_u$, $\dot{m}_d$	kilograms per second
$\dot{Q}_f$	kilowatts
F, Ri_o	dimensionless
T_∞, T_h, T_3, T_c	degrees Celsius
t_{res}	seconds
U_{1c}	meters per second
Y_i, δ_C	inches

DOOR GEOMETRY: 18" by 39" high							
Run	24	25	26	28	29	30	31
$\dot{m}_2$	0.076	0.146	0.176	0.186	0.037	0.165	0.200
$\dot{Q}_f$	13.7	26.5	26.5	29.2	7.7	23.7	24.3
K_∞	0.05	0.05	0.03	0.04	0.05	0.05	0.05
K_h	0.72	0.63	0.61	0.63	0.83	0.63	0.65
K_3	0.73	0.68	0.66	0.66	0.85	0.67	0.63
K_c	0.06	0.11	0.17	0.18	0.05	0.12	0.21
T_∞	25	25	24	23	22	23	24
T_h	147	150	147	148	128	147	147
T_3	166	166	159	162	155	163	159
T_c	33	38	48	50	32	41	56
$\dot{m}_{1h}$	0.076	0.143	0.149	0.151	0.038	0.156	0.140
$\dot{m}_{1c}$	0.076	0.143	0.149	0.151	0.038	0.156	0.140
$\dot{m}_u$	.0012	.0140	.0200	.0124	.0009	.0129	-.009
$\dot{m}_d$	.0012	.0166	.0473	.0471	.0000	.0215	.0509
Y_i	27.6	19.7	14.9	14.0	34.3	17.3	11.5
U_{1c}	0.200	0.529	0.723	0.780	0.080	0.653	0.880
Ri_0	45.38	4.44	1.55	1.22	312.3	2.41	0.72
δ_C	8.0	8.0	8.0	8.8	5.6	8.0	11.2
t_{res}	17.04	12.22	11.94	11.58	24.63	11.81	11.59
$\frac{\dot{m}_d}{\dot{m}_{1c}}$	0.0152	0.115	0.318	0.3111	0.000	0.137	0.364
F	0.040	0.125	0.213	0.239	0.016	0.170	0.312

DOOR GEOMETRY: 18" by 24" high						
Run	32	33	34	35	36	37
$\dot{m}_g$	0.067	0.030	0.208	0.067	0.146	0.050
$\dot{Q}_f$	12.1	7.7	20.1	12.8	20.1	10.4
K_a	0.09	0.05	0.05	0.05	0.06	0.04
K_h	0.78	1.03	0.89	0.82	0.88	0.83
K_s	0.79	1.05	0.89	0.82	0.89	0.84
K_c	0.17	0.05	0.51	0.13	0.36	0.08
T_a	23	24	21	21	21	21
T_h	131	115	142	125	154	125
T_s	162	153	157	160	164	160
T_c	38	35	102	40	72	33
$\dot{m}_{1h}$	0.060	0.031	0.094	0.060	0.094	0.048
$\dot{m}_{1c}$	0.060	0.031	0.094	0.060	0.094	0.048
$\dot{m}_u$	.0011	.0006	.0000	.0000	.0028	.0007
$\dot{m}_d$	.0079	.0000	.1139	.0070	.0544	.0026
Y_i	11.0	18.2	4.3	13.2	6.5	15.8
U_{1c}	0.395	0.122	1.568	0.326	1.041	0.218
Ri_o	3.85	60.83	0.03	6.20	0.24	18.35
δ_C	4.0	6.0	9.6	4.0	10.4	4.0
t_{res}	36.46	68.28	13.50	34.81	17.75	43.15
$\frac{\dot{m}_d}{\dot{m}_{1c}}$	0.131	0.000	1.211	0.116	0.577	0.053
F	0.140	0.037	1.465	0.111	0.522	0.065

DOOR GEOMETRY: 12" by 39" high						
Run	38	39	40	41	42	43
$\dot{m}_2$	0.068	0.147	0.044	0.196	0.112	0.100
$\dot{Q}_f$	12.4	20.1	9.6	26.5	19.2	17.2
K_∞	0.04	0.04	0.04	0.04	0.05	0.05
K_h	0.63	0.73	0.84	0.77	0.72	0.69
K_s	0.63	0.75	0.84	0.79	0.72	0.70
K_c	0.05	0.16	0.05	0.31	0.10	0.08
T_∞	22	22	22	20	21	21
T_h	124	146	132	148	150	149
T_s	158	161	160	164	161	161
T_c	32	45	33	65	40	39
$\dot{m}_{1h}$	0.067	0.126	0.044	0.128	0.103	0.096
$\dot{m}_{1c}$	0.067	0.126	0.044	0.128	0.103	0.096
$\dot{m}_u$	.0006	.0052	.0000	.0063	.0000	.0008
$\dot{m}_d$	.0012	.0265	.0003	.0743	.0087	.0049
Y_i	25.4	13.7	31.2	7.0	17.8	21.1
U_{1c}	0.286	0.988	0.151	1.959	0.624	0.489
Ri_g	17.28	0.78	80.21	0.08	2.78	5.40
δ_C	4.0	6.4	4.0	14.4	4.0	4.8
t_{res}	22.33	14.85	25.14	13.25	17.00	17.00
$\frac{\dot{m}_d}{\dot{m}_{1c}}$	0.017	0.211	0.006	0.581	0.084	0.051
F	0.045	0.199	0.020	0.625	0.104	0.075

DOOR GEOMETRY: 12" by 26" high						
Run	44	45	46	47	48	49
$\dot{m}_2$	0.067	0.044	0.033	0.078	0.057	0.094
$\dot{Q}_f$	13.7	10.0	9.3	13.1	11.0	13.9
K_-	0.05	0.05	0.05	0.05	0.05	0.05
K_h	0.89	0.83	1.06	0.87	0.97	0.97
K_s	0.89	0.83	1.06	0.87	0.97	0.97
K_c	0.20	0.08	0.06	0.18	0.16	0.32
T_-	21	22	22	22	20	21
T_h	135	129	119	141	126	144
T_s	168	164	158	160	166	165
T_c	37	36	33	50	35	54
$\dot{m}_{1h}$	0.055	0.042	0.033	0.066	0.050	0.066
$\dot{m}_{1c}$	0.055	0.042	0.033	0.066	0.050	0.066
$\dot{m}_u$	.0000	.0000	.0000	.0000	.0000	.0000
$\dot{m}_d$	.0120	.0017	.0003	.0124	.0068	.0276
Y_i	11.0	15.4	18.7	9.1	13.4	7.2
U_{1c}	0.538	0.296	0.188	0.777	0.401	0.990
Ri_o	2.16	9.64	27.71	0.75	4.49	0.35
δ_C	4.0	4.8	5.6	11.2	3.2	8.8
t_{res}	36.10	49.15	60.41	32.13	40.57	27.76
$\frac{\dot{m}_d}{\dot{m}_{1c}}$	0.217	0.040	0.010	0.188	0.136	0.415
F	0.123	0.059	0.036	0.205	0.087	0.296

DOOR GEOMETRY: 12" by 26" high (variable T_s)				
Run	50	51	52	53
$\dot{m}_g$	0.057	0.093	0.057	0.057
$\dot{Q}_f$	8.6	11.1	5.8	3.1
K_∞	0.05	0.05	0.05	0.05
K_h	0.75	0.76	0.52	0.31
K_s	0.75	0.76	0.52	0.31
K_c	0.16	0.29	0.15	0.12
T_∞	20	20	21	21
T_h	103	120	79	62
T_s	131	133	98	67
T_c	33	55	32	32
$\dot{m}_{1h}$	0.048	0.062	0.045	0.042
$\dot{m}_{1c}$	0.048	0.062	0.045	0.042
$\dot{m}_u$	.0000	.0000	.0000	.0000
$\dot{m}_d$	.0090	.0314	.0121	.0153
Y_i	12.0	7.0	10.3	9.0
U_{1c}	0.429	0.942	0.468	0.498
Ri_o	2.89	0.29	1.51	0.78
δ_C	5.2	10.4	3.2	3.2
t_{res}	44.80	29.92	50.11	54.47
$\frac{\dot{m}_d}{\dot{m}_{1c}}$	0.186	0.511	0.270	0.368
F	0.115	0.346	0.170	0.248

Appendix D

TABULATED DATA FROM THE FIRE PLUME EXPERIMENTS

The experimental data obtained from the plume experiments are tabulated on the following pages. The symbols are defined in the List of Symbols. Y_i is the measured mole fraction of species i in the dried sample, and $\bar{Y}_i$ is the estimated mole fraction of species i in the ceiling layer. The units of the other symbols are as follows:

Symbol	Units
$\dot{Q}_f$	kilowatts
T_h, T_∞	degrees Kelvin
$\dot{m}_E$, $\dot{m}_{p_{in}}$	kilograms per second

0.19 m. Burner $Z_1 = 0.23\ m$							
$\dot{Q}_f$	10.5	21.1	31.6	42.1	52.6	63.2	73.7
$T_h\ ^\circ K$	448	539	614	692	800	826	838
$T_\infty\ ^\circ K$	293	293	293	293	293	293	293
Y_{O_2}	0.187	0.165	0.140	0.099	0.58	0.015	0.005
Y_{CO_2}	0.012	0.026	0.039	0.064	0.087	0.101	0.106
Y_{CO}	.0000	.0000	.0000	.0006	.0031	.0095	.0166
Y_{CH_4}	.0000	.0000	.0000	.0000	.0004	.0016	.0162
$\bar{Y}_{O_2}$	0.181	0.158	0.130	0.090	0.051	0.012	0.004
$\bar{Y}_{CO_2}$	0.012	0.025	0.036	0.058	0.077	0.083	0.090
$\bar{Y}_{CO}$	.0000	.0000	.0000	.0005	.0027	.0078	.0140
$\bar{Y}_{CH_4}$	.0000	.0000	.0000	.0000	.0004	.0013	.0137
$\bar{Y}_{N_2}$	0.784	0.767	0.762	0.735	0.711	0.716	0.672
$\bar{Y}_{H_2}$	-.008	.0075	-.001	.0211	.0383	-.003	.0512
$\bar{Y}_{H_2O}$	0.032	0.042	0.074	0.096	0.120	0.184	0.156
φ	0.111	0.244	0.357	0.597	0.842	0.962	1.312
$\dot{m}_E$	.0340	.0311	.0319	.0254	.0225	.0237	.0202
$\dot{m}_{P_{in}}$	.0342	.0316	.0326	.0263	.0236	.0251	.0217

0.19 m. Burner $Z_1 = 0.23\ m$							
$\dot{Q}_f$	84.2	105.2	126.3	42.1	73.7	105.2	29.2
T_h °K	847	827	830	680	852	821	618
T_∞ °K	293	293	293	298	298	298	295
Y_{O_2}	0.005	0.000	0.002	0.135	0.016	0.003	0.140
Y_{CO_2}	0.101	0.095	0.097	0.054	0.104	0.100	0.036
Y_{CO}	.0196	.0230	.0240	.0000	.0100	.0200	.0000
Y_{CH_4}	.0270	.0590	.0660	.0000	.0010	.0375	.0000
$\bar{Y}_{O_2}$	0.004	0.000	0.002	0.136	0.013	0.002	0.127
$\bar{Y}_{CO_2}$	0.085	0.078	0.083	0.055	0.087	0.083	0.033
$\bar{Y}_{CO}$	.0164	.0190	.0205	.0000	.0084	.0167	.0000
$\bar{Y}_{CH_4}$	.0226	.0487	.0563	.0000	.0008	.0312	.0000
$\bar{Y}_{N_2}$	0.670	0.659	0.632	0.700	0.699	0.667	0.775
$\bar{Y}_{H_2}$	.0395	.0198	.0595	.1177	.0282	.0324	-.028
$\bar{Y}_{H_2O}$	0.163	0.175	0.147	-.009	0.163	0.167	0.093
φ	1.387	1.666	1.897	0.585	1.035	1.478	0.317
$\dot{m}_F$	.0219	.0228	.0240	.0259	.0256	.0257	.0332
$\dot{m}_{p_{in}}$	.0237	.0250	.0267	.0268	.0271	.0279	.0339

0.19 m. Burner Z_i = 0.10 m						
$\dot{Q}_f$	10.5	21.1	31.6	42.1	52.6	63.2
T_h °K	480	567	625	670	691	687
T_∞ °K	296	296	296	296	296	296
Y_{O_2}	0.175	0.130	0.070	0.025	0.020	0.011
Y_{CO_2}	0.024	0.054	0.079	0.093	0.096	0.091
Y_{CO}	.0000	.0000	.0054	.0150	.0178	.0200
Y_{CH_4}	.0000	.0000	.0050	.0215	.0390	.0690
$\bar{Y}_{O_2}$	0.174	0.128	0.063	0.021	0.017	0.009
$\bar{Y}_{CO_2}$	0.024	0.053	0.071	0.079	0.084	0.077
$\bar{Y}_{CO}$	.0000	.0000	.0048	.0127	.0155	.0168
$\bar{Y}_{CH_4}$	.0000	.0000	.0045	.0182	.0340	.0581
$\bar{Y}_{N_2}$	0.754	0.713	0.706	0.686	0.651	0.653
$\bar{Y}_{H_2}$	.0424	.0880	.0480	.0313	.0696	.0282
$\bar{Y}_{H_2O}$	0.005	0.018	0.103	0.152	0.129	0.159
φ	0.238	0.559	0.854	0.911	1.204	1.538
$\dot{m}_E$	.0159	.0136	.0133	.0126	.0123	.0130
$\dot{m}_{p_{th}}$	.0161	.0140	.0140	.0135	.0134	.0143

0.19 m. Burner $Z_i = 0.10\ m$						
$\dot{Q}_f$	73.7	84.2	105.2	84.2	52.6	31.6
$T_h\ °K$	681	703	728	716	697	669
$T_\infty\ °K$	296	296	296	296	296	296
Y_{O_2}	0.007	0.005	0.005	0.006	0.016	0.070
Y_{CO_2}	0.089	0.091	0.096	0.093	0.096	0.085
Y_{CO}	.0230	.0240	.0220	.0230	.0196	.0060
Y_{CH_4}	.0870	.0990	.1070	.0960	.0400	.0030
$\bar{Y}_{O_2}$	0.006	0.004	0.004	0.005	0.014	0.066
$\bar{Y}_{CO_2}$	0.075	0.078	0.085	0.081	0.083	0.080
$\bar{Y}_{CO}$	.0193	.0206	.0195	.0200	.0169	.0056
$\bar{Y}_{CH_4}$	.0730	.0850	.0948	.0833	.0345	.0031
$\bar{Y}_{N_2}$	0.639	0.615	0.587	0.610	0.652	0.676
$\bar{Y}_{H_2}$	.0276	.0561	.0955	.0687	.0630	.1070
$\bar{Y}_{H_2O}$	0.160	0.141	0.114	0.133	0.137	0.063
φ	1.965	2.249	2.555	2.268	1.549	0.983
$\dot{m}_E$	.0135	.0135	.0148	.0134	.0122	.0116
$\dot{m}_{P_{in}}$	.0150	.0153	.0170	.0152	.0133	.0123

0.19 m. Burner $Z_1 = 0.07\ m$						
$\dot{Q}_f$	21.1	42.1	52.6	63.2	10.5	31.6
$T_h\ ^\circ K$	604	642	649	654	500	642
$T_\infty\ ^\circ K$	298	298	298	298	298	298
Y_{O_2}	0.076	0.018	0.008	0.006	0.170	0.043
Y_{CO_2}	0.074	0.090	0.088	0.088	0.031	0.084
Y_{CO}	.0033	.0174	.0208	.0224	.0000	.0096
Y_{CH_4}	.0030	.0486	.0730	.1038	.0000	.0097
$\bar{Y}_{O_2}$	0.067	0.015	0.007	0.005	0.174	0.036
$\bar{Y}_{CO_2}$	0.065	0.075	0.072	0.074	0.032	0.070
$\bar{Y}_{CO}$	.0029	.0145	.0171	.0189	.0000	.0080
$\bar{Y}_{CH_4}$	.0026	.0406	.0599	.0875	.0000	.0081
$\bar{Y}_{N_2}$	0.726	0.675	0.666	0.628	0.731	0.721
$\bar{Y}_{H_2}$	.0172	.0158	-.001	.0296	.0851	-.006
$\bar{Y}_{H_2O}$	0.119	0.164	0.180	0.157	-.022	0.163
φ	0.733	1.454	1.685	2.163	0.326	0.903
$\dot{m}_E$	.0104	.0104	.0113	.0105	.0116	.0126
$\dot{m}_{P_{in}}$	.0108	.0113	.0124	.0118	.0118	.0133

0.19 m. Burner $Z_1 = 0.01\ m$							
$\dot{Q}_f$	31.6	21.1	42.1	10.5	21.1	26.3	36.9
$T_h\ °K$	549	556	563	507	532	539	568
$T_\infty\ °K$	298	298	298	298	298	298	298
Y_{O_2}	0.016	0.032	0.015	0.062	0.023	0.017	0.016
Y_{CO_2}	0.085	0.087	0.085	0.078	0.086	0.086	0.082
Y_{CO}	.0230	.0164	.0230	.0087	.0186	.0210	.0218
Y_{CH_4}	.0944	.0358	.1122	.0136	.0681	.0912	.1119
$\bar{Y}_{O_2}$	0.014	0.028	0.013	0.055	0.020	0.015	0.014
$\bar{Y}_{CO_2}$	0.073	0.075	0.074	0.069	0.074	0.074	0.070
$\bar{Y}_{CO}$	.0198	.0141	.0200	.0076	.0159	.0180	.0186
$\bar{Y}_{CH_4}$	.0812	.0308	.0978	.0119	.0582	.0784	.0955
$\bar{Y}_{N_2}$	0.626	0.675	0.607	0.705	0.654	0.631	0.625
$\bar{Y}_{H_2}$	.0464	.0374	.0600	.0310	.0328	.0433	.0305
$\bar{Y}_{H_2O}$	0.139	0.140	0.128	0.121	0.146	0.141	0.147
φ	2.092	1.333	2.379	0.940	1.696	2.029	2.214
$\dot{m}_E$	.0054	.0057	.0064	.0040	.0045	.0047	.0060
$\dot{m}_{p_{in}}$	.0061	.0061	.0073	.0042	.0049	.0053	.0068

NBS-114A (REV. 2-8C)

U.S. DEPT. OF COMM. BIBLIOGRAPHIC DATA SHEET (See instructions)	1. PUBLICATION OR REPORT NO. NBS/GCR-85/493	2. Performing Organ. Report No.	3. Publication Date May 1985

4. TITLE AND SUBTITLE

Experimental Study of Environment and Heat Transfer in a Room Fire. Mixing in Doorway Flows and Entrainment in Fire Plumes.

5. AUTHOR(S)

E.E. Zukoski, T. Kubota, and C.S. Lim

6. PERFORMING ORGANIZATION (If joint or other than NBS, see instructions)

California Institute of Technology
Div. of Engineering & Applied Science
Pasadena, CA 91125

7. Contract/Grant No.

NB82NADA3033

8. Type of Report & Period Covered

1982-1984

9. SPONSORING ORGANIZATION NAME AND COMPLETE ADDRESS (Street, City, State, ZIP)

National Bureau of Standards
Department of Commerce
Gaithersburg, MD 20899

10. SUPPLEMENTARY NOTES

This is a two-part report. The first is a general summary and the second is a detailed description of the experimental results.

☐ Document describes a computer program; SF-185, FIPS Software Summary, is attached.

11. ABSTRACT (A 200-word or less factual summary of most significant information. If document includes a significant bibliography or literature survey, mention it here)

This report contains a description of an ongoing study of gravity currents for conditions which match those we expect to find in unwanted fires in buildings. A review is made of the pertinent literature and a description is given of the flow regimes which can exist for ideal gravity currents when viscous effects, heat transfer, and mixing are ignored. The influence of boundary conditions fixed by the method used to withdraw the fluid displaced by the current is given. Algebraic equations for the thickness of the current and the velocity of the head are derived for these ideal flows. The influences of viscosity and mixing are briefly discussed and the status of salt water and gas modeling experiments is given.

12. KEY WORDS (Six to twelve entries; alphabetical order; capitalize only proper names; and separate key words by semicolons)

bibliographies; building fires; ceilings; doors; gas flow; gravity; heat transfer; room fires

13. AVAILABILITY

☒ Unlimited

☐ For Official Distribution. Do Not Release to NTIS

☐ Order From Superintendent of Documents, U.S. Government Printing Office, Washington, D.C. 20402.

☒ Order From National Technical Information Service (NTIS), Springfield, VA. 22161

14. NO. OF PRINTED PAGES

173

15. Price

$16.00